2017-12

The Potential of Raman Spectroscopy in the Diagnosis of Premalignant Oral Lesions

Ola Ibrahim
Technological University Dublin

The Potential of Raman Spectroscopy in the Diagnosis of Premalignant Oral Lesions

Ola Ibrahim BDS MSc

Thesis submitted in partial fulfilment for the degree of Doctor of Philosophy (PhD)

Dublin Institute of Technology, School of Physics

December 2017

Supervised by:

Prof. Fiona M. Lyng

Prof. Hugh J. Byrne

Declaration

I certify that this thesis which I now submit for examination for the award of Doctor of Philosophy is entirely my own work and has not been taken from the work of others, save and to the extent that such work has been cited and acknowledged within the text of my work.

This thesis was prepared according to the regulations for graduate study by research of the Dublin Institute of Technology and has not been submitted in whole or in part for another award in any other third level institution.

The work reported on in this thesis conforms to the principles and requirements of the Institute's guidelines for ethics in research.

The Institute has permission to keep, lend or copy this thesis in whole or in part, on condition that any such use of the material of the thesis be duly acknowledged.

Signature _____ Date _____

(Ola Ibrahim)

Abstract

Oral squamous cell carcinoma is commonly preceded by a range of cell and tissue alterations termed dysplasia, which indicate an increased risk of malignant transformation. Dysplasia is classified according to severity into mild, moderate, severe and carcinoma in situ. The early diagnosis, treatment and/or surveillance of these premalignant lesions are important factors in preventing progression to oral cancer. The current gold standard for screening and diagnosis of oral cancer and premalignant lesions is through histopathological diagnosis, which is limited by inter and intra observer and sampling errors. Although other methods are available for screening, most are not sensitive enough or do not provide enough information. Hence, there is a requirement for a sensitive, non-invasive method that can provide real time information. Raman spectroscopy fulfils these criteria, as it can provide detailed information on the biological content of a sample, through the unique vibrations of its constituent molecules. By analysing mild, moderate, and severely dysplastic formalin fixed paraffin preserved archival tissue samples; first within the same patient (intra-patient study), then between patients (inter-patient study), it was found that Raman spectroscopy could classify mild, moderate and severe dysplasia in the same patient with an accuracy of over 90% in epithelium and over 80% in connective tissue. The findings of the inter-patient study were that the different degrees of dysplasia could be identified with an accuracy of 60%, while oral squamous cell carcinoma could be differentiated from dysplasia and benign lesions with an accuracy of 70% in epithelium and 80% in connective tissue. Confounding factors of the Raman classification of pathology, such as smoking and inflammation, were also evaluated. In addition, protocols for the processing of the Raman spectra of the oral tissues, including the subtraction of the wax and substrate were developed.

"Everything that living things do can be understood in terms of the jiggling and wiggling of atoms”

-Richard Feynman, The Feynman Lectures on Physics, 1963

Acknowledgments

I would like to thank my supervisors Prof Fiona M. Lyng and Prof Hugh J. Byrne for their incredible support and advice throughout.

I would also like to thank everyone in the RESC for their help particularly Dr Adrian Maguire for his help with the data analysis and Damien Traynor for his help with the lab work.

FOCAS institute has been such a pleasure to work in; I would like to thank everyone there for creating such a friendly and supportive work environment.

This would not have been possible without our collaborators Prof Stephen Flint from the Dublin Dental University Hospital and Dr Mary Toner from St James Hospital. So, my sincerest thanks to them both.

To my family; my Mum, Dad, and my brother Hisham, I could not thank you enough for your support and encouragement, for believing in me when I was finding it hard to believe in myself. I know I would not have made it this far without you.

Finally, my grandfather, Sheikh-Idris Ibrahim, thank you for inspiring and encouraging me throughout my life.

List of Abbreviations

AUC	Area under curve
CaF2	Calcium fluoride
CCD	Charge coupled device
COE	Conventional oral exam
cpd	Cigarettes per day
cpw	Cigarettes per week
DLE	Discoid Lupus Erythematoses
DNA	Deoxyribonucleotidic acid
EGFR	Epidermal Growth Factor Receptor
EMSC	Extended multiplicative signal correction
FAD	Flavin adenine dinucleotide
FFPP	Formalin Fixed Paraffin Preserved
FITC	Fluorescein isothiocyanate
FTIR	Fourier Transform Infrared Spectroscopy
HPLC	High performance liquid chromatography
HPV	Human Papilloma virus
IR	Infrared
LDA	Linear discriminate analysis
LOH	Loss of Heterozygosity
LOOCV	Leave one out cross validation
LOPOCV	Leave one patient out cross validation

LV	Latent Variable
NADH	Nicotineamide dinucleotide
NNLS	Non Negatively Constrained Least Squares
OSCC	Oral squamous cell carcinoma
PC	Principal component
PCA	Principal component analysis
PCNA	Proliferating cell nuclear antigen
PI	Propidium Iodide
PLS	Partial Least Squares
PLSDA	Partial Least Squares Discriminate Analysis
PSA	Prostate specific antigen
RB	Retinoblastoma protein
RNA	Ribonucleic acid
SCC	Squamous cell carcinoma
SERS	Surface enhanced Raman spectroscopy
SELDI TOF	Surface enhanced laser desorption and ionization time of flight
SORS	Spacially offset Raman spectroscopy
SVM	Support vector machine
TB	Toludine blue
WHO	World Health Organisation

Table of Contents

List of Figures

List of Tables

Chapter 1: Introduction

1.1 Thesis Outline

This study addresses the potential of Raman spectroscopy for applications in the diagnosis of dysplastic and malignant oral disease, based on tissue biopsies. Patients with benign oral lesions, mild, moderate and severe dysplasia and oral squamous cell carcinoma (OSCC) were consented during their check-ups at the Dysplasia Clinic of the Dublin Dental Hospital. The archival formalin fixed paraffin preserved (FFPP) samples from the patients with benign lesions, different levels of dysplasia and OSCC were collected from the Central Pathology Laboratory, St James' Hospital, Dublin where all the oral biopsies are stored. The FFPP tissue sections were assessed with Raman spectroscopy.

The broad objectives of the thesis were to;

1) investigate the Raman profiles of an oral squamous cell carcinoma (OSCC) cell line at different phases of the cell cycle and to correlate these with biomarker expression in the different phases of the cell cycle
2) optimise the processing of the Raman spectra from the FFPP tissue sections; which included removing the wax and glass background.
3) discriminate between different degrees of dysplasia from the FFPP biopsies of individual patients with serial biopsies (intra-patient study).
4) discriminate between benign, different degrees of dysplasia and OSCC from the FFPP tissues in a cohort of patients (inter-patient study).
5) evaluate the influence of patient factors and clinical features on the Raman spectra of the FFPP tissues

Chapter 1 of the thesis is a general introduction to oral cancer, dysplasia and Raman spectroscopy.

Chapter 2 of the thesis is a review paper on the optical diagnosis of oral cancers, published in the journal, Head & Neck.

The subsequent chapters address the aims/objectives of the thesis, chapters 3, 4, 5, 6 and 7 addressing the objectives 1, 2, 3, 4 and 5, respectively.

Chapter 8 presents a summary of the work, its clinical relevance and future perspectives.

1.2 Oral Squamous cell carcinoma

1.2.1 Overview/epidemiology

Oral cancers are prevalent worldwide, having an estimated incidence of 300,400 new cases and 145,400 deaths in 2012[1]. Incidence is highest in South Central Asia, Eastern Europe and some regions of Oceania[1]. Oral squamous cell carcinoma (OSCC) is the predominant malignancy in most cases. It is more common in males than females, having a ratio of 1.5:1, and more common in older persons (aged 50 or over)[2]. Nevertheless, there are currently changes in the trend, manifest as an increase in incidence in young persons, which may be due to HPV infection as opposed to the traditional risk factors such as smoking and tobacco[3]. In Ireland, oral and pharyngeal cancers make up 3% of all cancers in males and 1.5% in females[4].

1.2.2 Carcinogenesis

OSCC arises in the squamous epithelium and, like all cancers, is a multi-step process in which cells acquire mutations that allow them to evade immune surveillance and divide uncontrollably. Hanahan and Weinberg[5] described six biological capabilities that enable tumour growth and metastasis which are; sustaining proliferative signalling, evading growth suppressors, resisting cell death, enabling replicative immortality, inducing angiogenesis, and activating invasion and metastasis. There are three main phases in carcinogenesis; 1) Initiation, in which one or more mutations arise in the cells either spontaneously or as a result of exposure to carcinogens, which increases the susceptibility of the cells for malignant transformation. 2) Promotion, which involves the clonal expansion of initiated cells, producing a larger population

of cells at risk for malignant transformation. 3) Progression, in which successive changes in the transformed cells give rise to increasingly malignant sub-populations[6].

1.2.3 Causes/risk factors

1.2.3.1 Smoking

Smoking is implicated in the development of a number of cancers including; lung, oesophageal, pharyngeal and oral cancer. It is responsible for 71% of oral cancers in developed countries and 37% in developing countries[1]. Over 60 carcinogens have been identified in cigarette smoke, including; benzene, vinyl chloride, tobacco specific nitrosamines and aromatic hydrocarbons such as benzopyrene, which has been linked to damage to the tumour suppressor gene P53[7,8] . Smoking, independent of other risk factors such as alcohol consumption, has been associated with a likelihood ratio of 2.15 of developing oral cancer[9]. The risk increases with increased consumption and is higher in females compared to male smokers[10].

1.2.3.2 Alcohol

As with cigarette smoking, alcohol consumption has been linked to a number of cancers such as; oral, pharyngeal, oesophageal, and breast cancer[11]. It is estimated to be responsible for 3.5% of cancer deaths, although the mechanisms by which it causes cancer are poorly understood[12]. It is thought that acetaldehyde, the main metabolite of ethanol, may have a genotoxic effect. Moreover, alcohol is believed to act as a solvent for other carcinogens which would explain the synergistic relationship between smoking and alcohol consumption in the development of oral cancer[11,13]. The amount and duration of alcohol consumed has a direct effect on cancer risk and, in the oral cavity, the most frequently affected areas were found to be those most in contact with the alcohol, such as the tongue, oropharynx and larynx[9,11].

1.2.3.3 Smokeless tobacco and betel quid

Smokeless tobacco is used in either chewing or snuff form and is sometimes combined with other substances such as betel quid. Similar to smoked tobacco, the carcinogenicity of

smokeless tobacco is attributed to tobacco specific nitrosamines, although their concentrations are different to the smoked form[14]. Smokeless tobacco has been associated with a relative risk of 2.6% of developing oral cancer[15]. Betel quid chewing is prevalent in Taiwan, India, Papua New Guinea, South-Africa and other Southeast Asian countries. However, it is not commonly consumed in Ireland. Betel quid is prepared from the betel plant leaves and can be consumed with or without tobacco. The areca nut extract in betel quid has demonstrated mutagenicity and genotoxicity in animal models with areca alkaloids believed to be the major contributors[16,17] .

1.2.3.4 Human Papilloma Virus (HPV)

The human papilloma virus (HPV) is generally associated with warts, epithelial cysts and benign neoplasias. However, two subtypes, 16 and 18, have been linked to cancer development. 23% of oral squamous cell carcinomas (OSCC) were found to be positive for HPV and, of these, two thirds were positive for HPV-16 and a third was positive for HPV-18[18]. Remarkably, the survival of HPV positive cancer patients was higher than their HPV negative counterparts[19]. The carcinogenicity of HPV is due to the expression of E6 and E7; two viral oncoproteins which deregulate the cell cycle by interfering with the functions of PRB and P53, leading to cell immortalisation[20].

1.2.4 Anatomic site

The anatomic site at which oral cancer develops has been found to relate to its aetiology, as cigarette smoking was associated with cancers in the retromolar area and floor of the mouth, while alcohol was most associated with floor of the mouth cancers. The buccal mucosa was associated with the lowest relative risk in both alcohol and cigarette smokers[21]. On the other hand, HPV was associated with cancers in the oropharynx and base of the tongue. Anatomic site is also linked to prognosis, base of the tongue cancers having the lowest five year survival (41.6%) and labial mucosa the highest (81.5%)[22]. This may be related to the fact that

carcinogens tend to pool at the base of the tongue and, moreover, the area is not easily visible, so the condition is usually advanced by the time it is diagnosed.

1.2.5 Staging

As with most cancers, oral cancer is staged according to the TNM staging system, which is an anatomical classification whereby;

T: Extent (size) of primary tumour

N: Regional lymph node involvement (absence or presence and extent)

M: Distant metastasis (absence or presence)

Table 1-1 T staging based on the size of primary tumour[23]

Tx	Tumour could not be assessed
T0	No evidence of primary tumour
Tis	Carcinoma in situ (CIS)
T1	Tumour < 2cm
T2	Tumour 2- 4 cm
T3	Tumour > 4cm
T4a	Tumour has invaded local structures such as cortical bone, muscles of the tongue or skin of the face
T4b	Tumour has invaded into pterygoid plates, skull base or internal carotid artery

Table 1-2 N staging based on regional lymph node involvement[23]

Nx	Lymph nodes cannot be assessed
N0	Absence of regional metastasis
N1	Involvement of a single ipsilateral lymph node, no more than 3cm.
N2	Single ipsilateral lymph node more than 3cm in size, or multiple ipsilateral or contralateral lymph nodes, none more than 6cm
N3	Involvement of lymph node more than 6cm in diameter

Table 1-3 M staging based on distant metastasis[23]

Mx	Distant metastasis cannot be assessed
M0	No distant metastasis
M1	Distant metastasis

The TNM classification is used to determine cancer stage, which is important in making decisions in treatment choice and patient prognosis.

Table 1-4 TNM classification[23]

Stage	T stage	N stage	M stage
0	Tis	N0	M0
I	T1	N0	M0
II	T2	N0	M0
III	T3	N0	M0
	T1/2/3	N1	M0
IV	T4a	N0	M0
	T1/2/3	N2/3	M0
	T1/2/3	N1/2/3	M1

Another important classification is the histological grade, whereby the carcinoma is divided into 4 grades depending on the proportion of the tumour resembling the tissue of origin;

Table 1-5 Histological classification[24]

Grade I	Well differentiated (<25% undifferentiated cells)
Grade II	Moderately differentiated (<50% undifferentiated cells)
Grade III	Poorly differentiated (<75% undifferentiated cells)
Grade IV	Anaplastic or pleomorphic (>75% undifferentiated cells)

1.2.6 Oral Cancer Biomarkers

A number of biomarkers have been considered for the assessment of oral cancer risk, progression, and survival. Epidermal growth factor receptor (EGFR) expression has been studied in oral cancer, as EGF is involved in many cell signalling pathways such as proliferation, apoptosis and angiogenesis[25,26]. EGFR has been associated with a higher risk (1.18%) of oral cancer development[27], higher tumour grade[28], and poor survival[29]. P53, a

tumour suppressor gene, is commonly expressed in a mutated form in oral cancers[30,31]. Its expression increases according to the degree of dysplasia in premalignant lesions[32]. However, no distinct association was found between P53 expression and oral cancer patient outcome or survival[33,34]. Cyclin D1 is a protein required for the progression of the cell cycle from G1 to S phase[35]. Overexpression of cyclin D1 has been linked to recurrence and reduced overall survival in oral cancer patients[36,37]. Thus far, none of the aforementioned biomolecules has been established in routine clinical tests for oral cancer. There may be a need for studies with greater statistical power before it can be determined whether any of these biomolecules could serve as biomarkers for oral cancer.

1.2.7 Diagnosis

Oral cancer can manifest as an endophitic (inward growth) or exophytic (outward growth) that can be a white or red patch or an area of ulceration. Some are symptomless, while others may be associated with bleeding, pain and/or soreness. In the more advanced stages, patients may present with symptoms like difficulty swallowing and swollen/tender lymph nodes in the neck[38]. Especially at the early stages, oral cancer may resemble other benign oral lesions. Therefore, after eliminating the possibility of other benign conditions, a suspicious lesion is biopsied by the dentist and sent for histopathological examination, which is the gold standard for oral cancer diagnosis. Other diagnostic aids include toluidine blue staining and brush biopsy, which are discussed in more detail in chapter 2. Early diagnosis is very important in oral cancer as stage at diagnosis is the most important prognostic factor[39]. After the initial diagnosis of OSCC is made, the stage of the tumour and presence of lymph node or distant metastasis is determined by the use of imaging techniques such as MRI, CT, and chest X rays[40].

1.2.8 Management

Oral cancers are treated with surgery, radiation therapy and chemotherapy, either as single modalities or in combination (multimodality). Several factors affect the choice of management in oral cancer patients;

1. The extent of the disease; this depends on the TNM staging system as early small tumours are more amenable to radiation or surgery as a single modality therapy, while larger, more advanced tumours require more extensive surgical approaches and are more likely to have lymph node involvement. These are usually treated with multimodality therapy, in which surgery is coupled with pre or postoperative radiation and/or chemotherapy[40-42].
2. Patient factors; the age of the patient, compliance, and presence of comorbidities are all factors in determining the course of treatment in oral cancer[41].

Postoperative surveillance or follow up is crucial in oral cancer, as the tumour may recur or the patient can develop second primary tumours, which are tumours that develop in a different site in the oral cavity and are not metastasis from the primary tumour. Up to 30% of male and 20% of female patients develop second primary tumours[2]. The recommended follow up is every 2-3 months in the first year, every 3-4 months in the second year, every 4 months in the third year, and every 5 months in the fourth year. Thereafter, a yearly follow up is recommended[40].

1.3 Potentially Malignant Oral Disorders and Dysplasia

1.3.1 Potentially Malignant Oral Lesions

Potentially malignant lesions are defined as; 'a morphologically altered tissue in which cancer is more likely to occur than its apparently normal counterpart'[43]. The most commonly occurring potentially malignant lesion is leukoplakia, defined as; 'a predominantly white lesion of the oral mucosa that cannot be characterized as any other definable lesion'[43]. Leukoplakias are further classified, according to clinical appearance, into homogenous and non-homogenous

lesions. Homogenous lesions are usually flat and thin and have a reduced risk of malignant transformation compared to non-homogenous lesions. Non homogenous lesions carry an increased risk of malignant transformation and include; speckled, nodular and verrucous leukoplakia. Erythroplakia is defined as 'a fiery red patch that cannot be characterised clinically or pathologically as any other definable lesion'[43]. Erythroplakia may be smooth or nodular and has the highest potential for malignant transformation of any oral lesion[43].

1.3.2 Oral dysplasia

While leukoplakia and erythroplakia are clinical terms which describe the appearance of the lesions, dysplasia is a histological term which describes the cell morphology and tissue architecture. Depending on the degree of cellular atypia and architectural changes, dysplasia is classified into mild, moderate, severe and Carcinoma in situ CIN. Dysplasia indicates an increased risk of malignant transformation and has been reported to occur in 5-25% of oral leukoplakias, while almost all erythroplakias show some degree of dysplasia[44,45].

1.3.3 Potentially Malignant Oral Conditions

Potentially malignant oral conditions are described as; 'A generalized state associated with a significantly increased risk of cancer'[46]. A number of these conditions exist, such as; Plummer-Vinson syndrome, oral submucous fibrosis, syphilis, xeroderma pigmentosum and discoid lupus erythematosus (DLE), all of which are associated with epithelial atrophy[46].

1.3.4 Progression

It is hard to predict which potentially malignant oral lesions will progress to OSCC, but some factors have been associated with an increased risk, such as the presence of leukoplakia in non-smokers and dysplastic changes[47]. However, histological grade is not necessarily an indicator; severe dysplasia may not progress, while mild dysplasia can progress to OSCC[48]. Intra-oral site and size of the lesion were not found to be significant predictive factors either[49]. Molecular

markers such as loss of hetrozigosity (LOH) on chromosomes 3p/9p, DNA content and P53 expression levels have, however, shown promise in predicting OSCC development[49].

1.3.5 Diagnosis

The diagnosis of potentially malignant oral disorders is similar to that for OSCC, as it starts by exclusion of other differential diagnosis, followed by a biopsy and histopathological examination. The problem with this system is that it is subjective and prone to inter and intra observer errors[50]. Additionally, a biopsy may not be representative of the whole lesion, and studies looking at the histology of tumours post operatively and comparing them to the pre-operative biopsies have found that, in a significant number of cases, a neoplasia or carcinoma *in-situ* was misdiagnosed[48].

1.3.6 Management

The current recommendation for management of oral premalignant lesions is that moderate and severely dysplastic oral lesions are removed either by surgery, laser or cryotherapy, while lesions with no or mild dysplasia are followed up every sixth month or third month respectively. Nonetheless, removal of the lesion was not found to significantly reduce the risk of OSCC development[51].

1.4 Raman Spectroscopy

The current methods used in the diagnosis of oral premalignant and malignant lesions have their limitations. The standard method which is a conventional oral exam and histopathology is limited by intra and inter observer errors in addition to sampling errors[48,50]. Moreover dysplasia or OSCC may develop in an area of normal looking mucosa. Adjuncts such as oral brush biopsy and toluidine blue staining also have their limitations as they may produce false negative results and there is no information as to whether they can predict the probability of malignant transformation[52]. This demonstrates the need for new techniques for screening and

diagnosis. Optical diagnostics techniques, such as reflectance imaging, fluorescence imaging, and Raman spectroscopy are fast and non-invasive. They can have potential applications in the diagnosis of dysplasia and cancer which is discussed in more detail in chapter 2.

1.4.1 Theory

When electro-magnetic (EM) radiation interacts with a sample, it may be absorbed, or scattered. Most scattering is elastic, named Rayleigh scatter after the physicist who first described it, whereby the emitted (scattered) photon has the same energy as the incident photon. Mie scattering, named after the German physicist who first described it, is a similar process which dominates when the scatterers are larger than the wavelength of the light[53]. In 1928, the Indian physicist C.V Raman demonstrated experimentally that a small amount of the scattered radiation, about 1 in $1x10^6$, is of a different energy than the incident photon, and the phenomenon came to be known as the Raman effect[54]. The Raman effect is the result of coupling of the molecular vibrational states with the photon, via the induced polarisation. If the sample molecules gain energy from the incident photon, the emitted photon has less energy than the incident one, as a result of the generation of a vibrational quantum. This effect is called Stokes Raman scattering. Conversely, if the molecule is in excited higher vibrational state it may lose energy to the emitted photon and go back to the ground state and the emitted photon would have more energy than the incident one. This effect is called anti- Stokes Raman scattering. Whether or not a molecule is Raman active depends on the polarisability of a sample, which determines the degree of scattering when exposed to EM radiation[54]. The Raman scattered light can be collected by a spectrometer and displayed as a Raman spectrum, in which the peaks (bands) correspond to Raman frequency shifts (measured in wavenumbers cm^{-1}) caused by the characteristic vibrations in the molecules of a sample.

The presence of an electric field E induces in the molecule an electric dipole μ given by;

$$\mu = \alpha E$$

Equation 1-1

where α is the polarisability, If the electric field is oscillating, which is the case for photons, the equation is given by;

$$\mu = \alpha E_0 \cos(2\pi \nu_0 t)$$

Equation 1-2

where E_0 is the electric field strength of the incident field, and ν_0 is the frequency. An oscillating dipole will radiate electromagnetic energy at the frequency of oscillation. Polarisability is related to the degree to which electrons in a molecule can be displaced relative to the nucleus by the electromagnetic field of a photon. This displacement is described below.

$$q = q_0 \cos(2\pi \nu_{vib} t)$$

Equation 1-3

where q_0 is the amplitude of nuclear displacement and ν_{vib} is the frequency of the vibrational mode. If the nuclear displacement is small, then the polarisability can be approximated using the following equations.

$$\alpha = \alpha_0 + \left(\frac{\partial \alpha}{\partial \alpha}\right) q$$

Equation 1-4

where α_0 is the polarisability of a molecule in its equilibrium position and $(\partial\alpha / \partial q)$ is the rate of change of α with respect to the change in q, evaluated at the equilibrium position. Combining Equation 1-3 and Equation 1-4 produces.

$$\alpha = \alpha_0 + \left(\frac{\partial \alpha}{\partial \alpha}\right) q_0 cos(2\pi \nu_{vib} t)$$

Equation 1-5

Combining Equation 1-2 and Equation **1-5** results in.

$$\mu = \alpha_0 E_0 \cos(2\pi \nu_0 t) + \left(\frac{\partial \alpha}{\partial \alpha}\right) q_0 E_0 cos(2\pi \nu_0 t) cos(2\pi \nu_{vib} t)$$

Equation 1-6

This equation can be rearranged to describe three processes.

$$\mu = \alpha_0 E_0 \cos(2\pi\nu_0 t) + \left(\frac{\partial\alpha}{\partial q}\frac{q_0 E_0}{2}\right)\{\cos[(2\pi(\nu_0 - \nu_{vib})t] + \cos[2\pi(\nu_0 + \nu_{vib})t]\}$$

Equation 1-7

The first term describes Rayleigh scattering, as the scattered photon has the same frequency as the incident photon (ν_0). The second term describes Stokes scatter, as the difference between incident and scattered photon frequency is ν_0-$\nu_{vib,}$ while the third term describes anti-Stokes scatter, as the difference between incident and scattered photon is ν_0+ν_{vib}. The Boltzman distribution determines the relative intensities of Stokes and anti-Stokes scattering, which is dependent on the number of molecules in an excited state compared to those in the ground state. At room temperature, most of the molecules are in the ground state, and hence Stokes scattering is much more prevalent than anti-Stokes scattering.

1.4.2 Instrumentation

The different components of a Raman microspectrometer are shown in schematic form in **Error! Reference source not found.**. The source of the monochromatic incident light is a laser a nd different laser wavelengths can be used, from ultra violet through visible to near infra-red, the choice of wavelength depending on the application. The interference filter is a clean-up filter which only allows the laser output through, while the neutral density filter determines the laser intensity, which is adjustable. For biological samples, coupling the Raman spectrometer to a microscope facilitates focusing on different regions of the cell or tissue. The objective lens both delivers the incident laser light and collects the backscattered (emitted) light. The holographic notch filter reflects the same wavelength as the incident light to remove all the Rayleigh scattered light and everything outside this range is considered Raman scatter and is transmitted. The grating is used to disperse the light and the groove density (measured in grooves/mm) determines the spectral resolution, higher groove density corresponding to higher resolution. Typically, gratings between 300 and 1800 grooves/mm are used. Other

determinants of spectral resolution include the wavelength, longer wavelengths having a higher spectral resolution, and the spectrometer length, which is the distance between the grating and the detector, longer distances providing higher resolution. Charge coupled device (CCD) detectors are commonly used with Raman spectroscopy as they are very sensitive to light. They also allow multichannel operation, so the entire Raman spectrum can be detected in a single acquisition.

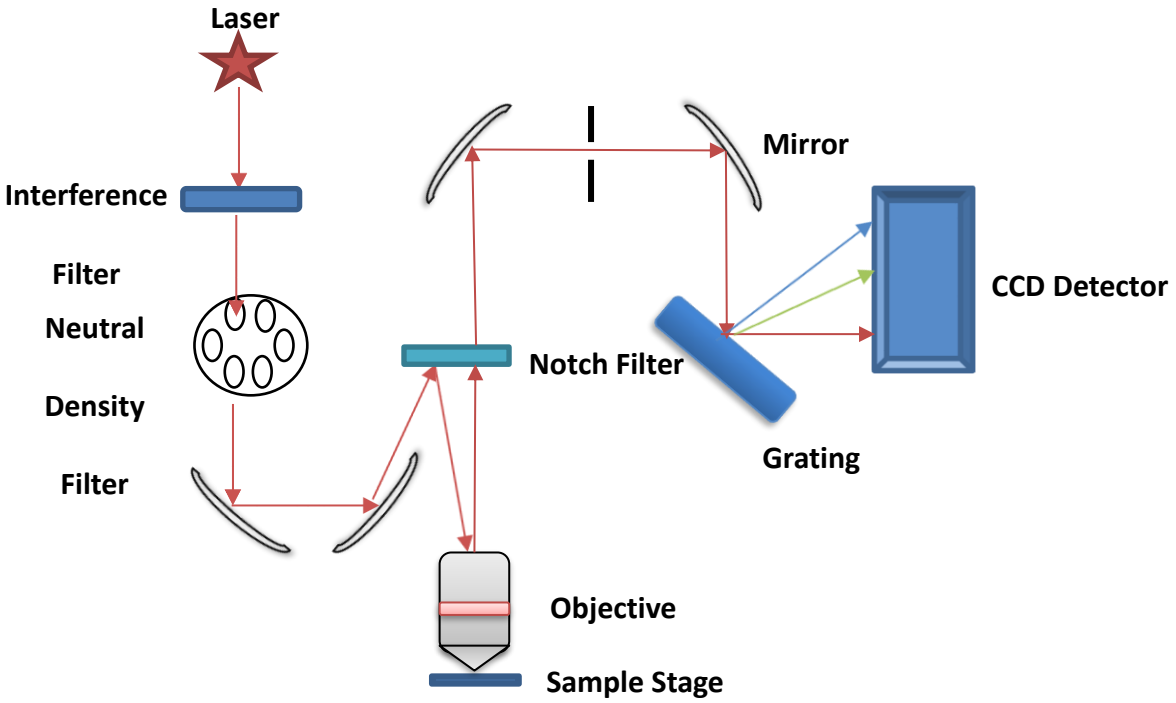

Figure 1.1 A schematic of a Raman microspectrometer based on the Horiba Jobin Yvon LabRAM HR 800*

* Raman spectrometer model used in this study.

1.4.3 Use in Diagnostics

There has been a lot of interest in the use of Raman spectroscopy in medical diagnostics since its introduction to the field of diagnostics nearly 20 years ago[55]. Its qualities, such as minimal sample preparation, speed, non-invasiveness, label free nature, and the fact that it gives both

qualitative and quantitative information on the molecular content of a sample make it particularly suited to such applications. Raman spectroscopy has shown promise in the field of microbiology by not only identifying the bacterial signatures but also response to antibiotics[56]. Furthermore, it has been studied for use in the diagnosis of coronary atherosclerosis and blood components[57,58]. Surface-enhanced Raman scattering (SERS) has been studied for use in detecting various biomolecules such as glucose, hemoglobins and RNAs[59]. It can also detect low levels of viral pathogens[60].

1.4.4 Use in Cancer Diagnosis

The majority of the research on the diagnostic applications of Raman spectroscopy has been aimed at cancer diagnosis, either through *in–vitro*, *ex-vivo* (such as cytology, histology or the use of biofluids) or *in-vivo* techniques. Raman spectroscopy was successfully used to differentiate between normal and neoplastic lymphocytic cell lines mainly based on changes in DNA and protein profiles[61]. *Ex-vivo* studies have been carried out on breast histological samples and one study found that Raman Spectroscopy could discriminate between breast cancer and normal/benign conditions with a sensitivity and specificity of 94% and 96% respectively[62]. Similarly, Raman Spectroscopy has been used in cervical pathology to identify cancerous and precancerous stages[63]. Biofluids have a number of advantages which make them ideal for diagnostic tests as their collection is very simple, can be done repeatedly, and is non-invasive. SERS on serum samples was used to identify prostate specific antigen (PSA) with diagnostic accuracy of up to 98%[64,65]. SERS on saliva samples could discriminate healthy from OSCC with an accuracy of 73%.[66] A number of studies have looked into the *in-vivo* applications of Raman spectroscopy. Theoretically, Raman spectroscopy can be a very powerful diagnostic aid and could be used on mucosal and epithelial surfaces such as oral, cervical and skin by direct contact with the Raman probe and on the visceral surfaces by use with a needle or an endoscopic instrument. A study used Raman spectroscopy in the diagnosis

of skin cancers and discriminating different cancerous and benign lesions which yielded very high sensitivity but lower specificity[67]. Another study used Raman spectroscopy during gastrointestinal endoscopy by coupling the fiberoptic Raman probe with the endoscopic instrument, and compared normal to diseased states[68]. A good application for *in-vivo* Raman spectroscopy could be the examination of surgical margins during cancer surgery and one study has found promising results with margin assessment in breast cancer surgery[69]. However, these studies are hampered by small patient numbers which in turn reduces the ability of the classifiers, which are based on machine learning algorithms. Nevertheless, they demonstrate the possibility of Raman applications for *in-vivo* diagnostics.

1.4.5 Use in Oral Cancer

There has been a lot of interest in the use of Raman spectroscopy for the diagnosis of oral cancers, especially as the oral cavity is very accessible which facilitates *ex-vivo* and *in-vivo* Raman spectroscopic diagnosis. Inadequate resection margins in oral cancer surgery increase the likelihood of local recurrence[70]. The use of Raman spectroscopy as an aid in delineation of OSCC surgical margins has shown that OSCC can be discriminated from surrounding normal structures with a high degree of accuracy though it's more likely to misclassify with surrounding normal and dysplastic epithelium[71]. Water concentration was found to be higher in tumours compared to normal tissue[72]. An *in-vivo* study study by Malik et al found that Raman spectroscopy can predict local recurrence in oral cancers with a sensitivity of 80% and specificity of 30%[73].

1.4.6 Use in Oral dysplasia and premalignant lesions

There have been relatively few studies looking at the use of Raman spectroscopy for dysplastic oral lesions. One study that induced dysplasia in the palate of a rat model was able to distinguish between normal mucosa and low and high grade dysplasia with accuracies of 85 and 100% respectively[74]. Another study looking at surgical margins in sections of OSCC found that the

accuracy of the Raman classification for dysplastic tissue was only 48%[71]. Using OSCC and dysplastic cell lines and comparing them to normal cells, a study has found that Raman spectroscopy could discriminate between malignant, dysplastic and normal cells based on varying nucleic acid, protein and lipid profiles[75]. Interestingly, in all of these studies, the differences between malignant and normal were very noticeable, while the dysplastic changes seem to fall somewhere in between. Similar results have been reported from tissue studies which looked at normal, inflammatory or benign, premalignant and malignant oral lesions[76-78].

Overall these studies suggest that Raman spectroscopy can discriminate between normal mucosa and malignancy but in the case of oral dysplasia there have been no studies to show the effect of the different degrees on the classification of Raman spectroscopy. The use of Raman spectroscopy for oral premalignant and malignant lesion diagnosis is discussed in more detail in chapter 2, which is a review of optical techniques in oral cancer diagnosis.

References

1. Torre LA, Bray F, Siegel RL, Ferlay J, Lortet-Tieulent J, Jemal A. Global Cancer Statistics, 2012. *Ca-a Cancer Journal for Clinicians* 2015;65:87-108.

2. Warnakulasuriya S. Global epidemiology of oral and oropharyngeal cancer. *Oral Oncology* 2009;45:309-316.

3. Chaturvedi AK, Anderson WF, Lortet-Tieulent J, Curado MP, Ferlay J, Franceschi S, Rosenberg PS, Bray F, Gillison ML. Worldwide Trends in Incidence Rates for Oral Cavity and Oropharyngeal Cancers. *Journal of Clinical Oncology* 2013;31:4550-4559.

4. Registry NC. Cancer in Ireland 1994-2015 with estimates for 2015-2017: Annual Report of the National Cancer Registry. Cork, Ireland: National Cancer Registry, 2017.

5. Hanahan D, Weinberg RA. Hallmarks of Cancer: The Next Generation. *Cell* 2011;144:646-674.

6. Weston A, Harris CC. Multistage Carcinogenesis. In: DW KR, Pollock RR, Weichselbaum, ed. Holland-Frei Cancer Medicine. Hamilton: BC Decker, 2003.

7. Pfeifer GP, Denissenko MF, Olivier M, Tretyakova N, Hecht SS, Hainaut P. Tobacco smoke carcinogens, DNA damage and p53 mutations in smoking-associated cancers. *Oncogene* 2002;21:7435-7451.

8. Hecht SS, Hoffmann D. Tobacco-specific nitrosamines, an important group of carcinogens in tobacco and tobacco-smoke. *Carcinogenesis* 1988;9:875-884.

9. Hashibe M, Brennan P, Benhamou S, Castellsague X, Chu C, Paula Curado M, Dal Maso L, Dauct AW, Fabianova E, Wunsch-Filho V, Franceschi S, Hayes RB, Herrero R, Koifman S, La Vecchia C, Lazarus P, Levi F, Mates D, Matos E, Menezes A, Muscat J, Eluf-Neto J, Olshan AF, Rudnai P, Schwartz SM, Smith E, Sturgis EM, Szeszenia-Dabrowska N, Talamini R, Wei Q, Winn DM, Zaridze D, Zatonski W, Zhang Z-F, Berthiller J, Boffetta P. Alcohol drinking in never users of tobacco, cigarette smoking in never drinkers, and the risk of head and neck cancer: Pooled analysis in the international head and neck cancer epidemiology consortium. *Journal of the National Cancer Institute* 2007;99:777-789.

10. Muscat JE, Richie JP, Thompson S, Wynder EL. Gender differences in smoking and risk for oral cancer. *Cancer Research* 1996;56:5192-5197.

11. Boffetta P, Hashibe M. Alcohol and cancer. *Lancet Oncology* 2006;7:149-156.

12. Nelson DE, Jarman DW, Rehm J, Greenfield TK, Rey G, Kerr WC, Miller P, Shield KD, Ye Y, Naimi TS. Alcohol-Attributable Cancer Deaths and Years of Potential Life Lost in the United States. *American Journal of Public Health* 2013;103:641-648.

13. Hashibe M, Brennan P, Chuang S-C, Boccia S, Castellsague X, Chen C, Curado MP, Dal Maso L, Daudt AW, Fabianova E, Fernandez L, Wuensch-Filho V, Franceschi S, Hayes RB, Herrero R, Kelsey K, Koifman S, La Vecchia C, Lazarus P, Levi F, Lence JJ, Mates D, Matos E, Menezes A, McClean MD, Muscat J, Eluf-Neto J, Olshan AF, Purdue M, Rudnai P,

Schwartz SM, Smith E, Sturgis EM, Szeszenia-Dabrowska N, Talamini R, Wei Q, Winn DM, Shangina O, Pilarska A, Zhang Z-F, Ferro G, Berthiller J, Boffetta P. Interaction between Tobacco and Alcohol Use and the Risk of Head and Neck Cancer: Pooled Analysis in the International Head and Neck Cancer Epidemiology Consortium. *Cancer Epidemiology Biomarkers & Prevention* 2009;18:541-550.

14. Critchley JA, Unal B. Health effects associated with smokeless tobacco: a systematic review. *Thorax* 2003;58:435-443.

15. Boffetta P, Hecht S, Gray N, Gupta P, Straif K. Smokeless tobacco and cancer. *Lancet Oncology* 2008;9:667-675.

16. Jeng JH, Chang MC, Hahn LJ. Role of areca nut in betel quid-associated chemical carcinogenesis: current awareness and future perspectives. *Oral Oncology* 2001;37:477-492.

17. Bhide SV, Shivapurkar NM, Gothoskar SV, Ranadive KJ. Carcinogenicity of betel quid ingredients: feeding mice with aqueous extract and the polyphenol fraction of betel nut. *British Journal of Cancer* 1979;40:922-926.

18. Kreimer AR, Clifford GM, Boyle P, Franceschi S. Human papillomavirus types in head and neck squamous cell carcinomas worldwide: A systematic review. *Cancer Epidemiology Biomarkers & Prevention* 2005;14:467-475.

19. Ang KK, Harris J, Wheeler R, Weber R, Rosenthal DI, Nguyen-Tan PF, Westra WH, Chung CH, Jordan RC, Lu C, Kim H, Axelrod R, Silverman CC, Redmond KP, Gillison ML. Human Papillomavirus and Survival of Patients with Oropharyngeal Cancer. *New England Journal of Medicine* 2010;363:24-35.

20. zurHausen H. Papillomavirus infections - A major cause of human cancers. *Biochimica Et Biophysica Acta-Reviews on Cancer* 1996;1288:F55-F78.

21. Jovanovic A, Schulten E, Kostense PJ, Snow GB, Vanderwaal I. Tobacco and alcohol related to the anatomical site of oral squamous cell carcinoma. *Journal of Oral Pathology & Medicine* 1993;22:459-462.

22. Zini A, Czerninski R, Sgan-Cohen HD. Oral cancer over four decades: epidemiology, trends, histology, and survival by anatomical sites. *Journal of Oral Pathology & Medicine* 2010;39:299-305.

23. (AJCC) AJCoC. AJCC Cancer Staging Manual. Chicago, Illinois.: Springer-Verlag, 2002.

24. Roland NJ, Caslin AW, Nash J, Stell PM. Value of grading squamous cell carcinoma of the head and neck. *Head and Neck-Journal for the Sciences and Specialties of the Head and Neck* 1992;14:224-229.

25. Huang SM, Bock JM, Harari PM. Epidermal growth factor receptor blockade with C225 modulates proliferation, apoptosis, and radiosensitivity in squamous cell carcinomas of the head and neck. *Cancer Research* 1999;59:1935-1940.

26. Ciardiello F, Caputo R, Bianco R, Damiano V, Fentanini G, Cuccato S, De Placido S, Bianco AR, Tortora G. Inhibition of growth factor production and angiogenesis in human

cancer cells by ZD1839 (Iressa), a selective epidermal growth factor receptor tyrosine kinase inhibitor. *Clinical Cancer Research* 2001;7:1459-1465.

27. Benchekroun MT, Saintigny P, Thomas SM, El-Naggar AK, Papadimitrakopoulou V, Ren H, Lang W, Fan Y-H, Huang J, Feng L, Lee JJ, Kim ES, Hong WK, Johnson FM, Grandis JR, Mao L. Epidermal Growth Factor Receptor Expression and Gene Copy Number in the Risk of Oral Cancer. *Cancer Prevention Research* 2010;3:800-809.

28. Laimer K, Spizzo G, Gastl G, Obrist P, Brunhuber T, Fong D, Barbieri V, Jank S, Doppler W, Rasse M, Norer B. High EGFR expression predicts poor prognosis in patients with squamous cell carcinoma of the oral cavity and oropharynx: A TMA-based immunohistochemical analysis. *Oral Oncology* 2007;43:193-198.

29. Ulanovski D, Stern Y, Roizman P, Shpitzer T, Popovtzer A, Feinmesser R. Expression of EGFR and Cerb-B2 as prognostic factors in cancer of the tongue. *Oral Oncology* 2004;40:532-537.

30. Langdon JD, Partridge M. Expression of the tumour suppressor gene p53 in oral cancer. *British Journal of Oral & Maxillofacial Surgery* 1992;30:214-220.

31. Sakai E, Tsuchida N. Most human squamous cell carcinomas in the oral cavity contain mutated p53 tumor-suppressor genes. *Oncogene* 1992;7:927-933.

32. Shin DM, Kim J, Ro JY, Hittelman J, Roth JA, Hong WK, Hittelman WN. Activation of p53 gene expression in premalignant lesions during head and neck tumorigenesis. *Cancer Research* 1994;54:321-326.

33. Li L, Fukumoto M, Liu D. Prognostic significance of p53 immunoexpression in the survival of oral squamous cell carcinoma patients treated with surgery and neoadjuvant chemotherapy. *Oncology Letters* 2013;6:1611-1615.

34. Nylander K, Dabelsteen E, Hall PA. The p53 molecule and its prognostic role in squamous cell carcinomas of the head and neck. *Journal of Oral Pathology & Medicine* 2000;29:413-425.

35. Baldin V, Lukas J, Marcote MJ, Pagano M, Draetta G. Cyclin D1 is a nuclear protein required for cell cycle progression in G1. *Genes & Development* 1993;7:812-821.

36. Michalides R, Vanveelen N, Hart A, Loftus B, Wientjens E, Balm A. Overexpression of cyclin D1 correlates with recurrence in a group of forty-seven operable squamous cell carcinomas of the head and neck. *Cancer Research* 1995;55:975-978.

37. Bova RJ, Quinn DI, Nankervis JS, Cole IE, Sheridan BF, Jensen MJ, Morgan GJ, Hughes CJ, Sutherland RL. Cyclin D1 and p16(INK4A) expression predict reduced survival in carcinoma of the anterior tongue. *Clinical Cancer Research* 1999;5:2810-2819.

38. Varela-Centelles P, Lopez-Cedrun JL, Fernandez-Sanroman J, Seoane-Romero JM, de Melo NS, Alvarez-Novoa P, Gomez I, Seoane J. Key points and time intervals for early diagnosis in symptomatic oral cancer: a systematic review. *International Journal of Oral and Maxillofacial Surgery* 2017;46:1-10.

39. Massano J, Regateiro FS, Januario G, Ferreira A. Oral squamous cell carcinoma: Review of prognostic and predictive factors. *Oral Surgery Oral Medicine Oral Pathology Oral Radiology and Endodontics* 2006;102:67-76.

40. Genden EM, Ferlito A, Silver CE, Takes RP, Suarez C, Owen RP, Haigentz M, Jr., Stoeckli SJ, Shaha AR, Rapidis AD, Pablo Rodrigo J, Rinaldo A. Contemporary management of cancer of the oral cavity. *European Archives of Oto-Rhino-Laryngology* 2010;267:1001-1017.

41. Shah JP, Gil Z. Current concepts in management of oral cancer - Surgery. *Oral Oncology* 2009;45:394-401.

42. Luryi AL, Chen MM, Mehra S, Roman SA, Sosa JA, Judson BL. Treatment Factors Associated With Survival in Early-Stage Oral Cavity Cancer Analysis of 6830 Cases From the National Cancer Data Base. *Jama Otolaryngology-Head & Neck Surgery* 2015;141:593-598.

43. Dionne KR, Warnakulasuriya S, Zain RB, Cheong SC. Potentially malignant disorders of the oral cavity: Current practice and future directions in the clinic and laboratory. *International Journal of Cancer* 2015;136:503-515.

44. Bouquot JE, Speight PM, Farthing PM. Epithelial dysplasia of the oral mucosa—Diagnostic problems and prognostic features. *Current Diagnostic Pathology*;12:11-21.

45. van der Waal I. Potentially malignant disorders of the oral and oropharyngeal mucosa; terminology, classification and present concepts of management. *Oral Oncology* 2009;45:317-323.

46. Pindborg J, Reichart P, Smith C, Van der Waal I. World Health Organization International Histological Classification of Tumours. Histological typing of cancer and precancer of the oral mucosa. Berlin: Springer, 1997.

47. Ho MW, Risk JM, Woolgar JA, Field EA, Field JK, Steele JC, Rajlawat BP, Triantafyllou A, Rogers SN, Lowe D, Shaw RJ. The clinical determinants of malignant transformation in oral epithelial dysplasia. *Oral Oncology* 2012;48:969-976.

48. Scully C. Challenges in predicting which oral mucosal potentially malignant disease will progress to neoplasia. *Oral Diseases* 2014;20:1-5.

49. Arduino PG, Bagan J, El-Naggar AK, Carrozzo M. Urban legends series: oral leukoplakia. *Oral Diseases* 2013;19:642-659.

50. Abbey LM, Kaugars GE, Gunsolley JC, Burns JC, Page DG, Svirsky JA, Eisenberg E, Krutchkoff DJ, Cushing M. Intraexaminer and interexaminer reliability in the diagnosis of oral epithelial dysplasia. *Oral surgery, oral medicine, oral pathology, oral radiology, and endodontics* 1995;80:188-191.

51. Holmstrup P, Vedtofte P, Reibel J, Stoltze K. Long-term treatment outcome of oral premalignant lesions. *Oral Oncology* 2006;42:461-474.

52. Potter TJ, Summerlin DJ, Campbell JH. Oral malignancies associated with negative transepithelial brush biopsy. *Journal of Oral and Maxillofacial Surgery* 2003;61:674-677.

53. Kerker M. The scattering of light, and other electromagnetic radiation. Academic Press, 1969.

54. Hollas JM. Modern Spectroscopy. West sussex, England: John Wiley and Sons, 2004:483.

55. Puppels GJ, Demul FFM, Otto C, Greve J, Robertnicoud M, Arndtjovin DJ, Jovin TM. Studying single living cells and chromosomes by confocal Raman microspectroscopy. *Nature* 1990;347:301-303.

56. Kastanos EK, Kyriakides A, Hadjigeorgiou K, Pitris C. A novel method for urinary tract infection diagnosis and antibiogram using Raman spectroscopy. *Journal of Raman Spectroscopy* 2010;41:958-963.

57. Buschman HP, Motz JT, Deinum G, Romer TJ, Fitzmaurice M, Kramer JR, van der Laarse A, Bruschke AV, Feld MS. Diagnosis of human coronary atherosclerosis by morphology-based Raman spectroscopy. *Cardiovascular Pathology* 2001;10:59-68.

58. Pilotto S, Pacheco MTT, Silveira L, Villaverde AB, Zangaro RA. Analysis of near-infrared Raman spectroscopy as a new technique for a transcutaneous non-invasive diagnosis of blood components. *Lasers in Medical Science* 2001;16:2-9.

59. Tu Q, Chang C. Diagnostic applications of Raman spectroscopy. *Nanomedicine-Nanotechnology Biology and Medicine* 2012;8:545-558.

60. Driskell JD, Kwarta KM, Lipert RJ, Porter MD, Neill JD, Ridpath JF. Low-level detection of viral pathogens by a surface-enhanced Raman scattering based immunoassay. *Analytical Chemistry* 2005;77:6147-6154.

61. Chan JW, Taylor DS, Zwerdling T, Lane SM, Ihara K, Huser T. Micro-Raman spectroscopy detects individual neoplastic and normal hematopoietic cells. *Biophysical Journal* 2006;90:648-656.

62. Haka AS, Shafer-Peltier KE, Fitzmaurice M, Crowe J, Dasari RR, Feld MS. Diagnosing breast cancer by using Raman spectroscopy. *Proceedings of the National Academy of Sciences of the United States of America* 2005;102:12371-12376.

63. Lyng FM, Faolain EO, Conroy J, Meade AD, Knief P, Duffy B, Hunter MB, Byrne JM, Kelehan P, Byrne HJ. Vibrational spectroscopy for cervical cancer pathology, from biochemical analysis to diagnostic tool. *Experimental and Molecular Pathology* 2007;82:121-129.

64. Grubisha DS, Lipert RJ, Park HY, Driskell J, Porter MD. Femtomolar detection of prostate-specific antigen: An immunoassay based on surface-enhanced Raman scattering and immunogold labels. *Analytical Chemistry* 2003;75:5936-5943.

65. Li SX, Zhang YJ, Xu JF, Li LF, Zeng QY, Lin L, Guo ZY, Liu ZM, Xiong HL, Liu SH. Noninvasive prostate cancer screening based on serum surface-enhanced Raman spectroscopy and support vector machine. *Applied Physics Letters* 2014;105.

66. Connolly JM, Davies K, Kazakeviciute A, Wheatley AM, Dockery P, Keogh I, Olivo M. Non-invasive and label-free detection of oral squamous cell carcinoma using saliva surface-enhanced Raman spectroscopy and multivariate analysis. *Nanomedicine-Nanotechnology Biology and Medicine* 2016;12:1593-1601.

67. Lui H, Zhao J, McLean D, Zeng H. Real-time Raman Spectroscopy for In Vivo Skin Cancer Diagnosis. *Cancer Research* 2012;72:2491-2500.

68. Shim MG, Song L, Marcon NE, Wilson BC. In vivo near-infrared Raman spectroscopy: Demonstration of feasibility during clinical gastrointestinal endoscopy. *Photochemistry and Photobiology* 2000;72:146-150.

69. Haka AS, Volynskaya Z, Gardecki JA, Nazemi J, Lyons J, Hicks D, Fitzmaurice M, Dasari RR, Crowe JP, Feld MS. In vivo margin assessment during partial mastectomy breast surgery using Raman spectroscopy. *Cancer Research* 2006;66:3317-3322.

70. Smits RWH, Koljenovic S, Hardillo JA, ten Hove I, Meeuwis CA, Sewnaik A, Dronkers EAC, Schut TCB, Langeveld TPM, Molenaar J, Hegt VN, Puppels GJ, de Jong RJB. Resection margins in oral cancer surgery: Room for improvement. *Head and Neck-Journal for the Sciences and Specialties of the Head and Neck* 2016;38:E2197-E2203.

71. Cals FLJ, Schut TCB, Hardillo JA, de Jong RJB, Koljenovic S, Puppels GJ. Investigation of the potential of Raman spectroscopy for oral cancer detection in surgical margins. *Laboratory Investigation* 2015;95:1186-1196.

72. Barroso EM, Smits RWH, van Lanschot CGF, Caspers PJ, ten Hove I, Mast H, Sewnaik A, Hardillo JA, Meeuwis CA, Verdijk R, Hegt VN, de Jong RJB, Wolvius EB, Schut TCB, Koljenovic S, Puppels GJ. Water Concentration Analysis by Raman Spectroscopy to Determine the Location of the Tumor Border in Oral Cancer Surgery. *Cancer Research* 2016;76:5945-5953.

73. Malik A, Sahu A, Singh SP, Deshmukh A, Chaturvedi P, Nair D, Nair S, Krishna CM. In vivo Raman spectroscopy-assisted early identification of potential second primary/recurrences in oral cancers: An exploratory study. *Head and Neck-Journal for the Sciences and Specialties of the Head and Neck* 2017;39:2216-2223.

74. Schut TCB, Witjes MJH, Sterenborg H, Speelman OC, Roodenburg JLN, Marple ET, Bruining HA, Puppels GJ. In vivo detection of dysplastic tissue by Raman spectroscopy. *Analytical Chemistry* 2000;72:6010-6018.

75. Carvalho LFCS, Bonnier F, O'Callaghan K, O'Sullivan J, Flint S, Byrne HJ, Lyng FM. Raman micro-spectroscopy for rapid screening of oral squamous cell carcinoma. *Experimental and Molecular Pathology* 2015;98:502-509.

76. Malini R, Venkatakrishna K, Kurien J, Pai KM, Rao L, Kartha VB, Krishna CM. Discrimination of normal, inflammatory, premalignant, and malignant oral tissue: A Raman spectroscopy study. *Biopolymers* 2006;81:179-193.

77. Li Y, Wen ZN, Li LJ, Li ML, Gao N, Guo YZ. Research on the Raman spectral character and diagnostic value of squamous cell carcinoma of oral mucosa. *Journal of Raman Spectroscopy* 2010;41:142-147.

78. Guze K, Pawluk HC, Short M, Zeng H, Lorch J, Norris C, Sonis S. Pilot study: Raman spectroscopy in differentiating premalignant and malignant oral lesions from normal mucosa and benign lesions in humans. *Head and Neck-Journal for the Sciences and Specialties of the Head and Neck* 2015;37:511-517.

Chapter 2: Recent advances in optical diagnosis of oral cancers: review and future perspectives

Adapted from 'Singh, S.P., Ibrahim, O., Byrne, H. J., Mikkonen, J. W., Koistinen, A. P., Kullaa, A. M., Lyng, F. M. (2015), Recent advances in optical diagnosis of oral cancers: Review and future perspectives. Head Neck. doi: 10.1002/hed.24293'

OI contributed figures and parts of the text.

Keywords: Raman spectroscopy, Infrared spectroscopy, Fluorescence spectroscopy, optical diagnosis, oral cancer, oral dysplasia

2.1 Abstract

Optical diagnosis techniques offer several advantages over traditional approaches, including objectivity, speed and cost, and these label-free, non-invasive methods have the potential to change the future work-flow of cancer management. The oral cavity is particularly accessible and thus such methods may serve as alternate/adjunct tools to traditional methods. Recently, *in vivo* human clinical studies have been initiated with a view to clinical translation of such technologies. A comprehensive review of optical methods in oral cancer diagnosis is presented. Following an introduction to the epidemiology and aetiological factors associated with oral cancers currently employed diagnostic methods and their limitations are presented. A thorough review of fluorescence, infrared absorption and Raman spectroscopic methods in oral cancer diagnosis is presented. The applicability of minimally invasive methods based on serum and saliva is also discussed. The review concludes with a discussion on future demands and scope of developments from a clinical point of view.

2.2 Oral Cancers: An Overview

Oral squamous cell carcinoma (OSCC) ranks as the 15th most common cancer in the world and 10th most frequent in males. It accounts for ~2.1% of total cancer cases worldwide. Incidence rates are high among males in south central Asia and among females in eastern and central Europe[1]. Although mortality from oral cancer has decreased in the past few decades, it is still high and has a five year survival rate of 50%[77]. Several oral lesions and conditions are associated with an increased potential for malignant transformation. Of these, the most commonly occurring is leukoplakia, defined as 'a predominantly white lesion of the oral mucosa that cannot be characterized as any other definable lesion' Figure 2.1 (B). A wide range of malignant transformation rates have been reported, from 0.13-36.4[78]%, depending on the presence and degree of dysplasia, location in the oral cavity and maturity of the lesion[3,4]. Conversely, erythroplakia, defined as 'a fiery red patch which cannot be characterized clinically or pathologically as any other definable lesion'[3], is less prevalent and has a higher potential for malignant transformation (14.3[79]-66.7[80] %)[5]. Oral submucous fibrosis is a premalignant oral condition arising mostly due to areca nut or betel quid chewing[6]. It has a reported transformation rate of 7.6%[6]. Oral lichen planus is an inflammatory disease of the oral mucosa. Like leukoplakia, it presents as a white plaque or patch. However, its malignant transformation rate is much lower than leukoplakia, ~1%[7] Figure 2.1 (C).

A number of risk factors are associated with oral cancer, including cigarette smoking and alcohol consumption, which are responsible for 42% and 16% of oral cancer deaths respectively[8]. The carcinogenicity of cigarette smoke has long been established, resulting in DNA damage and increase in P53 mutations[9]. The association between alcohol and oral cancer was reported to be dose dependent and a number of factors may contribute to its carcinogenicity, including acetaldehyde, an alcohol metabolite thought to be carcinogenic[10]. Moreover, alcohol is thought to act as a solvent for other carcinogens[10]. Oral habits such as

smokeless tobacco and betel quid chewing are also implicated in oral cancer development[11]. They are more common in the Asian population; in India, 50% of oral cancers arise due to smokeless tobacco chewing[11]. The carcinogenicity of smokeless tobacco arises from the production of nitrosamines[11]. Oral squamous cell carcinoma has also been associated with the Epstein Bar (EBV) and Human Papilloma (HPV) Viruses, although their putative role is controversial. Around 23% of OSCC were found to be positive for high risk HPV 16 and 18 [12].

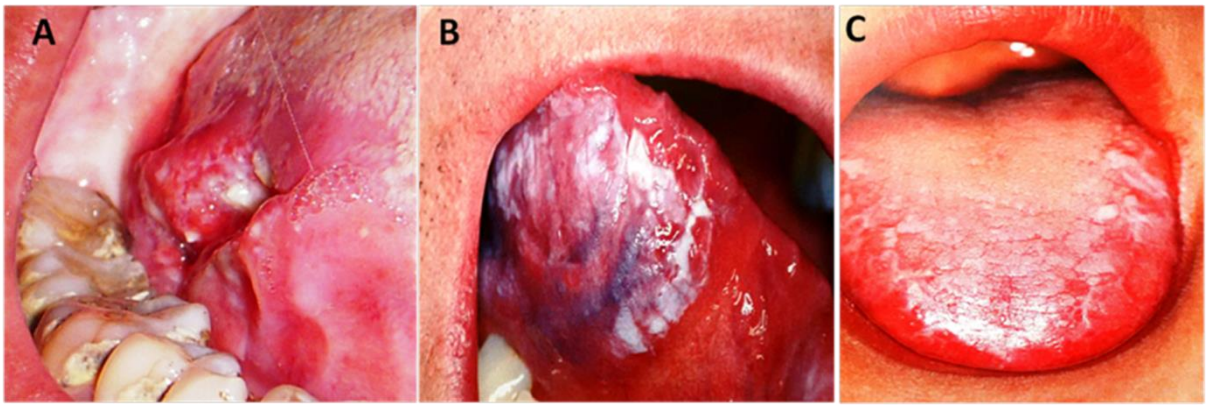

Figure 2.1 Clinical presentation of (A), tongue cancer (B) leukoplakia and (C) lichen planus

2.2.1 Current Screening/Diagnostic methods and limitations:

Screening tests or diagnostic aids presently available for oral cancer include conventional oral examination (COE), staining with toluidine blue, oral brush biopsy and scalpel biopsy coupled with histology.

2.2.2 Conventional Oral Examination (COE):

Conventional oral examination (COE), using normal (incandescent) light, has long been the standard screening method for oral abnormalities. As it is a visual method, it cannot identify early mucosal abnormalities that may or may not lead to oral cancer. Approximately 5-15% of the general population has oral mucosal abnormalities and the vast majority of these lesions are benign in nature [13,] Furthermore, only a small percentage of leukoplakias are progressive or become malignant and COE cannot discriminate between these and their non-progressive

counterparts. Therefore, while COE may be useful in discovering some oral lesions, its potential in identifying all potentially premalignant or biologically relevant lesions that are likely to progress to cancer is questionable.

2.2.3 Toluidine blue staining

Toluidine blue (TB), has been used for more than 40 years as an aid to detection of mucosal abnormalities of the cervix and the oral cavity. TB is a metachromatic, acidophilic dye that binds preferentially to tissues undergoing rapid cell division (inflammatory, regenerative and neoplastic tissue), resulting in preferential staining of abnormal tissue. Overall, TB appears to be useful in detecting carcinomas, but is positive in only ~50% of lesions with dysplasia. In addition, it frequently stains common, benign conditions such as non-specific ulcers. The high rate of false positive stains and the low specificity in staining dysplasia are some of the accepted limitations of the technique [14].

2.2.4 Oral brush biopsy

Oral brush biopsy extracts a complete trans-epithelial biopsy specimen, with cellular representation from each of the three layers (basal, intermediate and superficial). Because the brush biopsy detects only cellular atypia, positive results must be confirmed with a scalpel biopsy for definitive diagnosis. This technique has therefore been criticized for adding time and cost to the diagnosis of oral lesions without additional benefit to the patient[15]. Overall, it is a method of identifying unsuspected oral cancers found during a visual examination, at early and curable stages[16].

2.2.5 Histology

Histological risk stratification, currently the gold standard for oral cancer diagnosis, requires biopsy, staining and microscopic examination by a pathologist[17]. However, removal of tissue or biopsy is an inherently invasive procedure and carries risk of complications in the proximity of vital anatomy. Sampling errors in collecting or interpreting biopsies due to inter-observer

discrepancy can be significant. Once removed, the tissue can undergo biochemical changes which can lead to artifacts. In many diseases, tissue involvement is not uniform, potentially leading to sampling errors. Especially in oral cancers, some early lesions are clinically indistinguishable from benign conditions. Furthermore, histologically, identification of subtle changes in precancerous lesions or in normal mucosa that are indicative of early neoplastic transformation is subjective and can lead to inter-observer variations [18].

It is therefore conceivable that the primary prevention of the disease would involve activities to reduce or eliminate the use of tobacco and alcohol. Secondary prevention includes activities that are aimed to detect the disease at an early stage which would lead to better prognosis and lower morbidity. Current methods of detection of oral cancers are based largely on visual observations of abnormalities in tissue or cellular morphology and are therefore limited in terms of sensitivity and specificity, particularly at early stages. In the following section, a general discussion on the application of optical spectroscopic methods as an alternate/adjunct diagnostic tool for oral cancer is presented.

2.3 Optical spectroscopy in oral cancer diagnosis

Spectroscopy is the study of the frequency dependence of the interaction of electromagnetic radiation (light) with matter. Generally, light interacts with matter through absorption, emission and scattering/reflection. In each case, the spectrum of the interaction gives information about, and is characteristic of, the structure and chemical content of the sample. Optical measurements provide quantitative information based on the spectroscopic signature of the biochemical constituents of the sample that can be rapidly analyzed to yield an objective diagnosis, even in the hands of a non-expert operator. Diagnosis is based on biochemical changes underlying the pathology rather than visual or microscopic changes in cellular or tissue morphology. Devices to make these measurements have become inexpensive, robust, and portable, because of advances in computing, optical, fiber-optical, and semiconductor technology. Approaches

based on fluorescence, Fourier-transform infrared absorption and Raman scattering spectroscopy have shown potential for improved detection of oral cancers. A brief introduction of these techniques and their potential applications in oral cancer diagnosis is presented in the following sub-sections. Figure 2.2 provides a schematic illustration of their typical method of application.

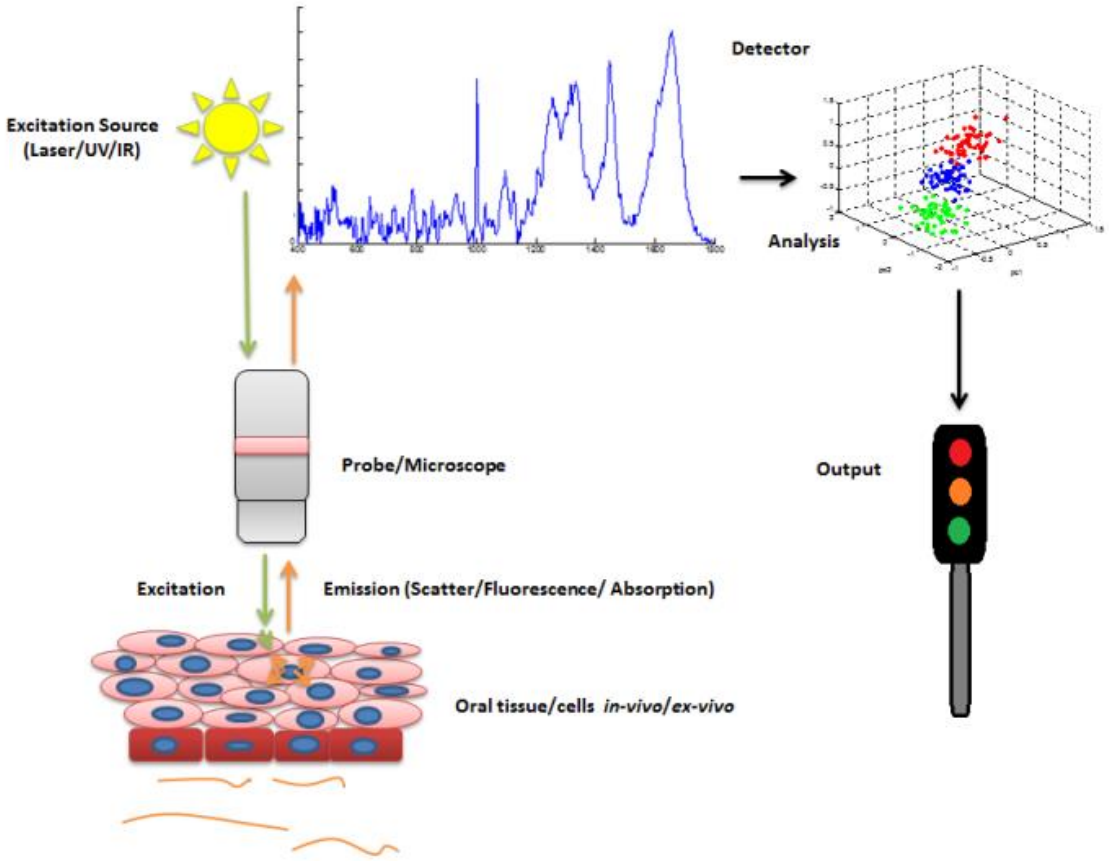

Figure 2.2 A schematic of the typical application of optical spectroscopic techniques for diagnostic applications.

The light source is delivered via a probe or microscope (for *in-vivo* or *ex vivo*/*in-vitro* applications respectively) to the sample (cells, tissue or biofluid). Upon excitation by an appropriate source, molecules can either; go to an excited state and reemit light in the form of

fluorescence (UV/visible lamp), absorb the light to generate vibrations within the molecules (Infrared lamp), or, by interaction with the vibrational modes of the molecules in the cells; the light is Raman scattered (visible or near infrared laser). The emitted/transmitted/scattered light is then collected by the probe or microscope and passed to a detector. The operator can then perform analysis on the resulting spectra and, using a prepared classifier, the output can for example be a yes, no, or maybe for the presence of cancer. The technique can be modified according to the application; *in-vivo*, *ex-vivo* (histological or cytological) or *in vitro*.

2.3.1 Fluorescence spectroscopy

When a molecule is illuminated at an excitation wavelength lying within the absorption spectrum of that molecule, it absorbs the energy and undergoes a transition from the ground state to an excited state. The molecule can then relax back from the excited state to the ground state by emission of light at specific emission wavelengths. In the UV/visible/Near infrared region of the spectrum (~200-1000nm), light emission takes the form of fluorescence (or occasionally phosphorescence). A fluorescence emission spectrum represents the fluorescence intensity measured over a range of emission wavelengths at a fixed excitation wavelength and can provide information relating to the molecular characteristics of the fluorophore, Figure 2.3.

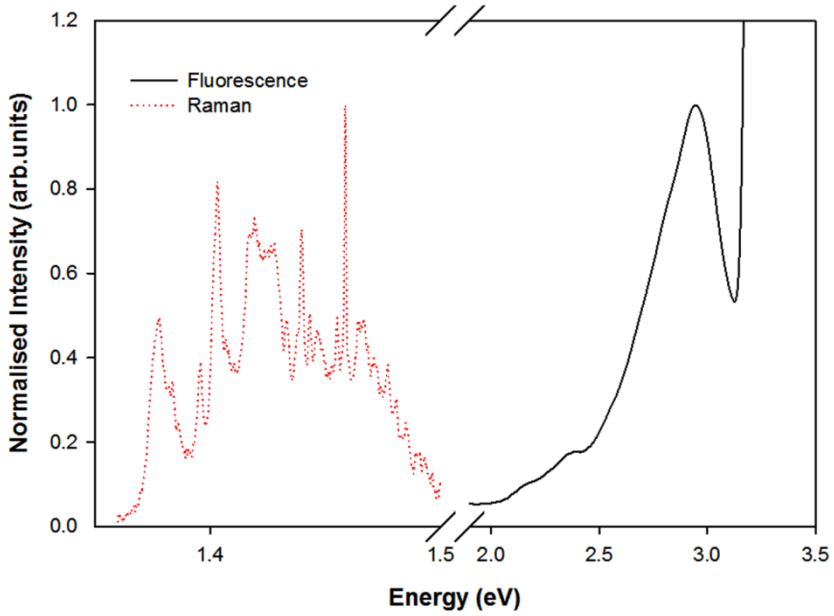

Figure 2.3 Comparison of typical fluorescence spectrum (riboflavin) and typical Raman spectrum of tissue (both normalised) plotted on an energy scale.

The intrinsic bandwidth of the fluorescence feature is very broad, compared to the Raman spectrum, which has a multitude of narrow bands which are shifted from the source wavelength of 785nm (~1.6eV). The energy shift of the Raman band is a measure of the vibrational energy and for comparison with infra-red spectroscopy is usually expressed in wavenumbers (1/cm). Note the energy scales for the two spectra are different.

In the late 1970s, cancer diagnosis based on auto-fluorescence (also called natural, intrinsic or endogenous fluorescence) of naturally occurring fluorophores such as collagen, elastin, keratin and NADH was initiated [19]. The presence of disease can lead to changes in blood concentration, nuclear size, collagen content or epithelial thickness, which can alter the concentration and characteristics of the fluorophores. In oral cancers, it was demonstrated that the epithelial layer shields the strongly fluorescing collagen layer leading to a low intensity of fluorescence in cancers[20]. An *ex vivo* study used hamster buccal pouch as an experimental model to identify

spectral markers associated with different stages of oral carcinogenesis [21]. Onizawa *et al.*, compared fluorescence spectra from human and hamster biopsies and oral cancer cell lines, suggesting that variation in the riboflavin and porphyrin fluorescence can be used as a spectroscopic marker for normal and cancerous conditions[22]. Ingrams *et al.* further showed that normal and cancerous human biopsies can be discriminated based on their autofluorescence spectral profile[23]. Another *ex vivo* study by Muller *et al.*, explored the feasibility of quantifying the spectroscopic response of different grades of malignancy[24].

The first *in vivo* study using autofluorescence spectroscopy by Harris *et al.* reported differences between healthy and tumor mucosa based on the porphyrin emission band[25]. These differences were attributed to microorganisms living on ulcerating or necrotic surfaces. *In vivo* methods have also been explored to understand oral cancer progression in animal models[26]. Gillenwater *et al.* recorded *in vivo* autofluorescence from oral mucosa of 8 healthy volunteers and 15 patients with premalignant or malignant lesions[27]. Decreased intensity in the blue spectral regions, and increased porphyrin fluorescence in the red were observed. Based on the ratio between these, a sensitivity of 82% and specificity of 100% were reported [27]. Various other studies have provided further evidence in support of *in vivo* fluorescence spectroscopy for non-invasive oral cancer diagnosis[28-30]. A recent study by Shaizu *et al.* showed that autofluorescence spectroscopy can be used to identify oral cavity disorders caused by long-term tobacco habits. Their findings suggest that lower collagen levels and increased ratios of flavin adenine dinucleotide (FAD) to nicotinamide adenine dinucleotide (NADH) can serve as prognostic markers for oral cancer risk [31].

However, tissue contains few natural fluorophores and their spectroscopic features are broad and overlapping, making them poorly distinguishable, reducing the specificity of fluorescence spectroscopy for diagnostic applications.

2.3.2 Fourier-transform infrared spectroscopy

Vibrational Spectroscopy is a subset of spectroscopy which analyses vibrations within a molecule (or material). The vibrations are characteristic of the molecular structure and, in polyatomic molecules, give rise to a spectroscopic "fingerprint". The spectrum of vibrational energies or frequencies (expressed as wavenumbers, cm^{-1}) can thus be employed to characterise a molecular structure, or changes to it due to the local environment or external factors (radiation, chemical agents). Vibrational energies fall within the mid Infrared (IR) region of the electromagnetic spectrum and are commonly probed through IR absorption spectroscopy. High energy or frequency vibrations are characteristic of light, tightly bound groups such as C-H, N-H and O-H, whereas low frequencies are associated with heavier groups, or collective vibrations such as ring breathing or skeletal stretches in macromolecules (Figure 2.4).

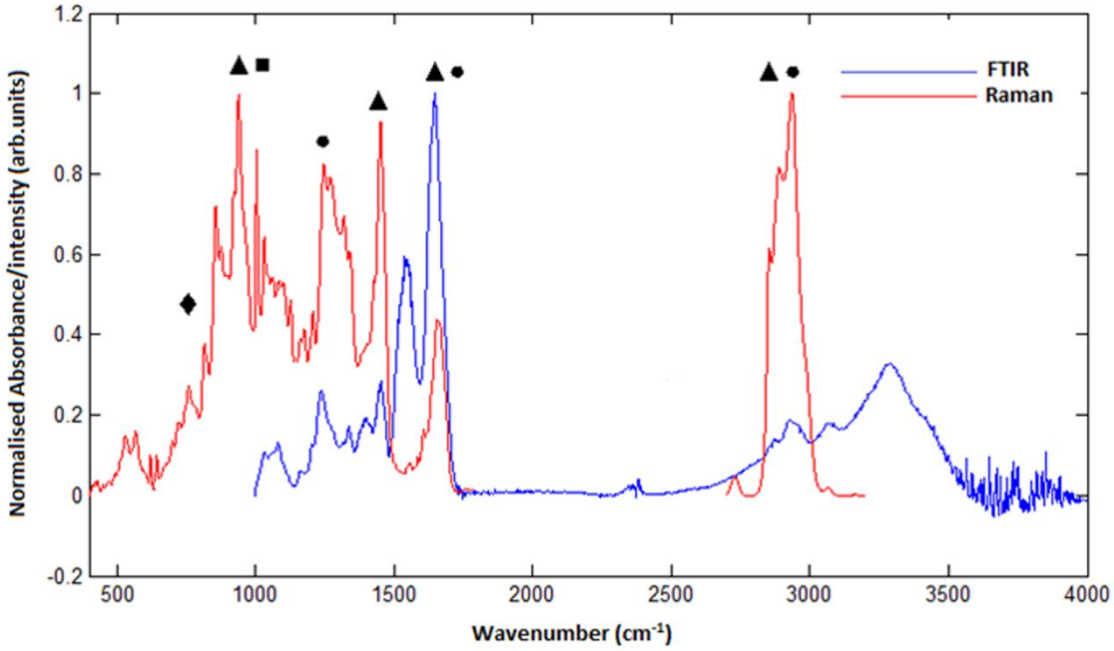

Figure 2.4 Comparison of typical IR absorption and Raman spectra of human tissue samples. The IR spectrum is in the mid infrared region of the spectrum, and the spectrum is less rich in information than the Raman spectrum. The Raman spectrum is expressed as wavenumber shift from the source laser line, although as shown in Figure 2.3, the scattered light is in the visible region of the spectrum. Both show typical features of lipids (●), proteins (▲), carbohydrates (■) and nucleic acids (♦). Note the strong absorption due to trace water in the FTIR spectrum in the region of ~3300cm-1.

IR spectroscopy is now a routine technique for materials characterisation and has found numerous applications in forensics, environmental science and pharmacology[32]. Applications to tissue samples for (cancer) diagnostic applications were first reported in the early 90s, and since this time a range of pathologies has been investigated[33].

Wu *et al.* demonstrated that, on the basis of lipid and protein content, normal and tumor oral tissues can be discriminated[34]. In another study, of 10 normal sub-gingival tissues (NST) and 15 oral squamous cell carcinoma (SCC) tissues, Fukuyama *et al.* demonstrated that the normal

spectra are strongly influenced by the presence of collagen. They also suggested that spectra are influenced by keratin, which exists in the ectodermal cells[35]. A study using FTIR spectroscopy to understand oral carcinogenesis in animal models have also been reported [36]. FTIR imaging methods have also been explored to analyze different aspects of oral cancers. A study by Schultz *et al.*, to assess changes in biochemistry of well and poorly differentiated oral/oropharyngeal SCC by infrared microspectroscopy, demonstrated that DNA and keratin can provide spectral markers to differentiate between normal and SCC biopsies[37]. Bruni *et al.*, by generating three-dimensional IR chemical maps, demonstrated that proliferating and regressive states of head and neck tumours can be identified[38]. Towards high throughput, automated analysis, Pallua *et al*. demonstrated that good quality FTIR images can be obtained from formalin fixed paraffin embedded tissue microarray sections providing molecular level information as the basis for diagnosis[39].

Compared to fluorescence, FTIR provides a detailed fingerprint of the biochemical content of the sample. However, although FTIR has been used for the analysis of human tissues *ex vivo*, the application of this method for *in vivo* diagnosis is limited, due to the short penetration depth and the fact that water is highly absorptive in the mid-IR range. Conventional optical fibres have limited transparency in the IR region, and therefore, *in vivo* studies are less frequent than fluorescence or Raman fibre optical applications. New developments based on attenuated total reflection (ATR) elements might help in implementing *in vivo* applications.

2.3.3 Raman spectroscopy

Raman spectroscopy is a complementary technique to FTIR and has its origin in the discovery of the Raman effect in 1928, for which C.V. Raman was awarded the Nobel prize in 1930[40]. Similar to IR spectroscopy, Raman entails the coupling of incident radiation with molecular vibrations and the resultant spectrum is similarly characteristic of the material. However,

whereas IR spectroscopy involves the absorption of radiation, Raman spectroscopy is a scattering technique, whereby the incident radiation couples with the vibrating polarisation of the molecule and thus generates or annihilates a vibration. The differing underlying mechanisms results in a complementarity of the techniques. Vibrations of asymmetric, polar bonds thus tend to be strong in IR spectra, whereas Raman is particularly suitable as a probe of symmetric, nonpolar groups. Notably, O-H vibrations of water are very strong in IR spectra, but are extremely weak in Raman spectra, rendering Raman a potentially more suitable technique for *in vivo* applications Figure 2.3. A further implication of the differing physical origins of the techniques is that, whereas IR monitors the absorption of IR radiation, Raman scattering can be employed in the UV, visible or near IR regions of the spectrum Figure 2.2. Raman scattering thus offers intrinsically higher spatial resolution for mapping or profiling in a confocal microscopy mode, the limit of spatial resolution being determined by the wavelength (<1μm for Raman, ~5-10 μm for IR). The application of Raman spectroscopy to biomolecules was first demonstrated as early as the 1960s and by the 1970s biomedical applications were explored[41]. Whole cell, tissue and *in vivo* studies carried out on a range of pathologies have demonstrated the potential for diagnostic applications[42].

Raman spectroscopic applications in oral cancer diagnostics started with the analysis of normal and dysplastic tissue in a rat model by Schut *et al.* (2000). Dysplasia in the palate was induced by topical application of the carcinogen 4-nitroquinoline 1-oxide and sensitivity and specificity of 100% were observed[43]. This was followed by a study of human oral cancer biopsies by Venkatakrishna *et al*, they recorded spectra of 49 biopsies and obtained an average classification efficiency of 88%[44]. In 2004, a study carried out by Krishna *et al.* demonstrated the applicability of formalin fixed oral tissues for optical pathology, revealing significant differences in the epithelial region of normal and malignant samples, arising from the protein composition, conformational/structural changes, and possible increase in protein content in

malignant epithelia[45]. In 2006, Malini *et al.* demonstrated the efficacy of Raman spectroscopic methods in discriminating normal, cancerous, precancerous and inflammatory conditions[46]. Lipid rich features in normal conditions and prominent protein features in tumors and other pathological conditions were observed. Classification between different groups using multivariate statistical methods produced 100% sensitivity and specificity[46]. Raman mapping of tissue sections further elucidated biochemical changes within different epithelial layers which are associated with disease onset[47]. A study by Sunder *et al.* demonstrated that oral carcinomas of different pathological grades can also be differentiated on the basis of the relative intensities of bands associated with lipids and proteins[48].

In vivo Raman spectroscopy using fibreoptic probes for identifying site specific variations in the oral cavity was reported by Guze *et al.* in 2009, indicating that different oral sites can be discriminated on the basis of level of keratinization[49]. Bergholt *et al.*, (2011), characterized the Raman spectroscopic profiles of different oral cavity regions (inner lip, attached gingiva, floor, dorsal tongue, ventral tongue, hard palate, soft palate, and buccal mucosa)[50]. Fitting of reference biochemicals (hydroxyapatite, keratin, collagen, DNA, and oleic acid) and partial least squares-discriminant analysis (PLS-DA) were employed to assess the inter-anatomical variability. The findings suggest that histological and morphological characteristics of different sites have a significant influence on the *in vivo* Raman spectra, and different sites can be classified with an overall sensitivity and specificity of 85%[50] . Singh *et al.* demonstrated that *in vivo* spectra can be acquired in clinically implementable timescales and demonstrated the feasibility of classification of normal and pathological conditions[51]. This was followed by another study exploring tobacco induced cancer field effects in the oral mucosa[52]. Sahu *et al.* demonstrated that *in vivo* Raman spectroscopy methods can also be utilized to understand age-related changes in the oral mucosa[53]. These findings were further

verified by a recent study showing anatomical variability and feasibility of identifying pathological conditions with *in vivo* Raman spectroscopy [54].

2.4 Minimally invasive methods in oral cancer diagnosis

Bio fluids such as blood, urine, lymph, and saliva can provide substantial information about human health and are being widely investigated for clinical diagnosis of various diseases including oral cancers. The attraction of these specimens lies in the fact that they can be used for mass screening, due to ease in collection, transport and low cost[55]. Studies have been carried out on physiochemical properties of saliva using surface enhanced laser desorption and ionization time of flight (SELDI-TOF) coupled with mass spectrometry (MS) and high performance liquid chromatography (HPLC) to identify proteomic and enzymatic markers associated with oral cancer[56]. Other techniques such as laser-induced fluorescence coupled with HPLC, and capillary electrophoresis coupled mass spectroscopy have been employed to characterise salivary metabolites in oral cancer patients[57,58].

Recently, optical methods based on Raman, infrared absorption, and fluorescence spectroscopies have also been exploited for such investigations. For example, enhanced levels of porphyrin in blood have been used as a diagnostic marker for various cancers including oral cancers[59,60]. Yuvaraj *et al.* characterized different salivary metabolites associated with oral cancers by fluorescence spectroscopy[61]. FTIR spectroscopy has been applied to study sputum in order to diagnose oral cancers and discrimination between normal and cancerous samples was achieved on the basis of changes in the protein and glycoprotein structure within cells[62]. Surface-Enhanced Raman spectroscopy methods (SERS) have been used to differentiate between normal and oral cancer patients using spectra acquired from saliva[63]. A recent study by Elumalai *et al.* demonstrated that Raman spectroscopy of urine samples of healthy subjects and oral cancer patients can offer potential diagnostic information with a discrimination accuracy of 94%[64]. The analysis of exfoliated oral cells by optical methods also holds enormous

promise for early disease detection and diagnosis. Diem and co-workers have carried out multiple studies on spectral cytopathology of oral exfoliated cells[65,66]. Their findings are suggestive of the tremendous potential of spectroscopic methods in identifying minor changes associated with disease onset. Nevertheless, diagnosis based on biofluids suffers from limitations such as low analyte concentration, longer acquisition time, prone to experimental errors etc. Considerable efforts have been undertaken to develop standard protocols and sensitive instrumentation. Signal enhancements with the help of nano-particles or surface coating is an active area of research [67]. Concentration of samples using centrifugal filtration devices has been shown to offer an alternative which allows measurement of the analytes in the native aqueous environment[68]. This also allows fractionation according to molecular weight of the constituent analytes, potentially allowing the targeting of molecular biomarkers of a disease. Appropriate modification of the instrumentation, especially automation for collection and analysis of body fluids is also an area which requires constant development. Efforts should also be undertaken for large scale trials and database development to overcome inter-laboratory and instrument variabilities [69].

2.5 Summary and Outlook

Although the oral cavity is easily accessible to inspection, oral cancer patients often present at an advanced stage when treatment is less successful, thereby leading to high morbidity and mortality. Early detection is the best way to ensure patient survival and quality of life. The current gold standard for clinical diagnosis of oral lesions is biopsy and subsequent histopathological confirmation. The process is invasive, time-consuming and prone to inter-observer variability. An alternate method of diagnosis that can enable non-invasive diagnosis of the oral cavity in individuals with suspicious oral lesions is warranted.

It is now well recognized that techniques based on optical spectroscopy can play a very important role towards this end. Spectroscopic measurements of tissue biochemistry, with sensitivity and specificity to localize changes enhanced by imaging, represent a measure of health (or disease) unattainable in current practice, and can provide sensitivities for early stage detection of biochemical, rather than simply morphological, abnormalities. Table 1 lists the advantages and disadvantages of the current screening/diagnostic methods and optical spectroscopy methods. Among the spectroscopic techniques described, fluorescence is perhaps the most technologically accessible, as it is simply based on the analysis of light which is emitted after illumination with a UV lamp. The emitted light is in the visible range and therefore probes can use free space or low grade, inexpensive fibre optics. The technique detects only the small fraction of endogenous biomolecules which are fluorescent, however, and relies on identifying pathology specific biomarkers amongst them. FTIR spectroscopy, on the other hand, produces a label free fingerprint of the complete biochemical content of the tissue, cell or biofluid, and this can explore more global and specific pathological changes. However, water is an extremely strong FTIR absorber, and so *in vivo* diagnostic applications may be limited. Raman spectroscopy provides a similar complete, label free fingerprint of the sample, and also couples to benefits of working in the visible region of the spectrum. Water is a weak Raman scatterer, and so the technique is more adaptable to routine *in vivo* patient screening or *ex vivo* spectral histology or cytology. The prospect is therefore of a high sensitivity and specificity, automatable, objective quantitative label free probe of early stage disease development and progression, based on the biomolecular content of the patient sample.

Table 2-1 Advantages and disadvantages of current screening / diagnostic methods and optical spectroscopy methods

Technique	Advantages	Disadvantages
Conventional oral examination	Well accepted screening method No instrumentation or reagents required Rapid	Subjective Requires clinical expertise and experience Unable to identify potentially pre-malignant lesions
Toluidine Blue staining	No instrumentation required Rapid	Subjective Requires clinical expertise and experience Reagents required Low specificity for dysplasia
Oral brush biopsy	Less invasive method for trans-epithelial biopsy Rapid	Subjective Requires clinical expertise and experience Reagents and instrumentation required Must be confirmed with scalpel biopsy and histology
Histology	Well accepted gold standard method Definitive diagnosis of tumour stage Stromal invasion can be determined Tumour margins can be determined	Subjective Requires clinical expertise and experience Pre-malignant lesions difficult to distinguish from benign conditions Reagents and instrumentation required Invasive Inter-observer variations Sampling errors Slow
Fluorescence spectroscopy	Objective Can be used by non-specialists with suitable diagnostic algorithms No reagents required as based on intrinsic fluorescence of fluorophores such as collagen, elastin, keratin and NADH Can be used *ex vivo* or *in vivo* Can be used for cells, tissues and biofluids	Instrumentation required Low specificity due to relatively few natural fluorophores with broad, overlapping features
Infra Red spectroscopy	Objective Can be used by non-specialists with suitable diagnostic algorithms No reagents required as based on a fingerprint of the biochemical composition	Instrumentation required Limited use *in vivo* due to short penetration depth and interference from water

	Mainly used *ex vivo* but *in vivo* may be possible using ATR-FTIR spectroscopy Can be used for cells, tissues and biofluids Short spectral acquisition times	Low spatial resolution but can be improved with ATR-FTIR spectroscopy Multivariate data analysis needed to extract information from the spectral data
Raman spectroscopy	Objective Can be used by non-specialists with suitable diagnostic algorithms No reagents required as based on a fingerprint of the biochemical composition Can be used *ex vivo* or *in vivo* Can be used for cells, tissues and biofluids High spatial resolution allowing subcelluar imaging Increased penetration depth using SORS	Instrumentation required Long spectral acquisition times Multivariate data analysis needed to extract information from the spectral data

Variable thickness and degree of keratinisation at different sites in the oral cavity can influence the diagnostic efficacy of optical methods, especially for early lesions. This issue has been addressed extensively by the biomedical spectroscopic community. Various studies have successfully demonstrated the potential of spectroscopic methods in identifying anatomical variability due to different levels of keratinization. For example, a study by Rupananda et al. showed a higher fluorescence due to porphyrins in the tongue compared to other oral sites [29], while Guze et al found that Raman spectra can be clustered according to sites in the oral cavity [49]. Similar findings were reported by Bergholt et al., who found that the sites clustered into three groups; (1) buccal, inner lip, and soft palate; (2) dorsal, ventral tongue, and floor; (3) gingiva and hard palate [50]. These studies have provided evidence in support of inherent differences between different locations and suggested that each site be treated independently. For example, spectral models developed using spectra from buccal mucosa cancers cannot be used for identifying abnormalities at tongue or palate. Most of the recent studies have been performed under these guidelines, where tumours of specific sites are treated separately[51-54]. As with all optical techniques, the depth sensitivity is limited by the absorption and scattering of the tissue.

Operation in the near infrared can optimise the depth sensitivity of Raman probes, and novel methodologies such as spatially offset Raman spectroscopy (SORS) promise increased penetration depths of several millimetres for deeper set lesions [70]. Such technological advances potentially place Raman ahead of the field as candidate for *in vivo* optical diagnostic applications.

In the coming years, large scale clinical trials must be conducted to gain the amount of site-specific data necessary for developing adequate size training and test sets for robust algorithm development and analysis. The standard models for each of the individual sites in the oral cavity should be tested rigorously, preferably double-blinded, as multi-centric studies, before they are considered for routine use. Several technological advances in terms of fiberoptic probes and miniaturization of instruments are also required for real time and routine diagnosis. Efficient suppression of background signal, optimization of collection optics, and incorporation of miniaturized interference filters in the fiber probes are some of the issues that are to be addressed effectively. Further improvements in data analysis algorithms are also required for developing less cumbersome, rapid, unambiguous, objective and user friendly interfaces from the point of view of routine clinical use where a clinician or a technician can analyze a given spectrum against all available models to diagnose a case. The prospective adaptation of optical spectroscopy methods for routine clinical diagnosis would decrease the number of follow-up clinic visits and patient anxiety by minimizing waiting times for histopathological diagnosis. The technology poses no known risks to the patients, and therefore could be a safe alternative/adjunct to the current diagnostic methods.

References

1. Ferlay J, Soerjomataram I, Dikshit R, Eser S, Mathers C, Rebelo M et al. Cancer incidence and mortality worldwide: Sources, methods and major patterns in GLOBOCAN 2012. Int J Cancer 2014;136:359-386.

2. Warnakulasuriya S. Global epidemiology of oral and oropharyngeal cancer. Oral Oncol 2009;45:309-316.

3. Pindborg J, Reichart P, Smith C, Van der Waal I. World Health Organization International Histological Classification of Tumours. Histological typing of cancer and precancer of the oral mucosa. Berlin: Springer; 1997.

4. Silverman S, Jr., Gorsky M, Lozada F. Oral leukoplakia and malignant transformation. A follow-up study of 257 patients. Cancer 1984;53: 563-8.

5. Lumerman H, Freedman P, Kerpel S. Oral epithelial dysplasia and the development of invasive squamous cell carcinoma. Oral Surg Oral Med Oral Pathol Oral Radiol Endod 1995;79: 321-9.

6. Murti PR, Bhonsle RB, Pindborg JJ, Daftary DK, Gupta PC, Mehta FS. Malignant transformation rate in oral submucous fibrosis over a 17-year period. Community Dent Oral Epidemiol 1985;13: 340-1.

7. Silverman S, Jr., Gorsky M, Lozada-Nur F. A prospective follow-up study of 570 patients with oral lichen planus: persistence, remission, and malignant association. Oral Surg Oral Med Oral Pathol 1985;60: 30-4.

8. Blot WJ, McLaughlin JK, Winn DM, Austin DF, Greenberg RS, Preston-Martin S et al. Smoking and drinking in relation to oral and pharyngeal cancer. Cancer Res 1988;48: 3282-7.

9. Pfeifer GP, Denissenko MF, Olivier M, Tretyakova N, Hecht SS, Hainaut P. Tobacco smoke carcinogens, DNA damage and p53 mutations in smoking-associated cancers. Oncogene 2002;21: 7435-51.

10. Boffetta P, Hashibe M. Alcohol and cancer. Lancet Oncol. 2006;7:149-156

11. Boffetta P, Hecht S, Gray N, Gupta P, Straif K. Smokeless tobacco and cancer. Lancet Oncol 2008;9: 667-75.

12. Kreimer AR, Clifford GM, Boyle P, Franceschi S. Human papillomavirus types in head and neck squamous cell carcinomas worldwide: a systematic review. Cancer Epidemiol Biomarkers Prev 2005;14: 467-75.

13. Sankaranarayanan R, Ramadas K, Thomas G, Muwonge R, Thara S, Mathew B, Rajan B, Trivandrum Oral Cancer Screening Study G. Effect of screening on oral cancer mortality in Kerala, India: a cluster-randomised controlled trial. Lancet 2005;365: 1927-33.

14. Gandolfo S, Pentenero M, Broccoletti R, Pagano M, Carrozzo M, Scully C. Toluidine blue uptake in potentially malignant oral lesions in vivo: clinical and histological assessment. Oral oncol 2006;42: 89-95.

15. Fist S. The oral brush biopsy: separating fact from fiction. Oral Surg Oral Med Oral Pathol Oral Radiol Endod 2003;96: 654-5.

16. Eisen D, Frist S. The relevance of the high positive predictive value of the oral brush biopsy. Oral oncol 2005;41: 753-5.

17. Suvarna K, Layton C, Bancroft JD. Bancroft's Theory and Practice of Histological Techniques. Oxford: Churchill Livingstone, 2012:654.

18. Abbey LM, Kaugars GE, Gunsolley JC, Burns JC, Page DG, Svirsky JA et al. Intraexaminer and interexaminer reliability in the diagnosis of oral epithelial dysplasia. Oral Surg Oral Med Oral Pathol Oral Radiol Endod 1995;80: 188-91.

19. Profio AE, Doiron DR. A feasibility study of the use of fluorescence bronchoscopy for localization of small lung tumours. Phys Med Biol 1977;22: 949-57.

20. Kolli VR, Savage HE, Yao TJ, Schantz SP. Native cellular fluorescence of neoplastic upper aerodigestive mucosa. Arch Otolaryngol Head Neck Surg 1995;121: 1287-92.

21. Farwell DG, Meier JD, Park J, Sun Y, Coffman H, Poirier B et al. Time-resolved fluorescence spectroscopy as a diagnostic technique of oral carcinoma: Validation in the hamster buccal pouch model. Arch Otolaryngol Head Neck Surg 2010;136: 126-33.

22. Onizawa K, Okamura N, Saginoya H, Yusa H, Yanagawa T, Yoshida H. Analysis of fluorescence in oral squamous cell carcinoma. Oral oncol 2002;38: 343-48.

23. Ingrams DR, Dhingra JK, Roy K, Perrault DF, Jr., Bottrill ID, Kabani S et al. Autofluorescence characteristics of oral mucosa. Head Neck 1997;19: 27-32.

24. Muller MG, Valdez TA, Georgakoudi I, Backman V, Fuentes C, Kabani S et al. Spectroscopic detection and evaluation of morphologic and biochemical changes in early human oral carcinoma. Cancer 2003;97: 1681-92.

25. Harris DM, Werkhaven J. Endogenous porphyrin fluorescence in tumors. Lasers Surg Med 1987;7: 467-72.

26. Wang CY, Tsai T, Chen HC, Chang SC, Chen CT, Chiang CP. Autofluorescence spectroscopy for in vivo diagnosis of DMBA-induced hamster buccal pouch pre-cancers and cancers. J Oral Pathol Med 2003;32: 18-24.

27. Gillenwater A, Jacob R, Ganeshappa R, Kemp B, El-Naggar AK, Palmer JL et al. Noninvasive diagnosis of oral neoplasia based on fluorescence spectroscopy and native tissue autofluorescence. Arch Otolaryngol Head Neck Surg 1998;124: 1251-8.

28. Chaturvedi P, Majumder SK, Krishna H, Muttagi S, Gupta PK. Fluorescence spectroscopy for noninvasive early diagnosis of oral mucosal malignant and potentially malignant lesions. J Cancer Res Ther 2010;6: 497-502.

29. Mallia RJ, Subhash N, Sebastian P, Kumar R, Thomas SS, Mathews A, Madhavan J. In vivo temporal evolution of ALA-induced normalized fluorescence at different anatomical locations of oral cavity: application to improve cancer diagnostic contrast and potential. Photodiagnosis Photodyn Ther 2010;7: 162-75.

30. Schwarz RA, Gao W, Daye D, Williams MD, Richards-Kortum R, Gillenwater AM. Autofluorescence and diffuse reflectance spectroscopy of oral epithelial tissue using a depth-sensitive fiber-optic probe. Appl opt 2008;47: 825-34.

31. Nazeer Shaiju S, Ariya S, Asish R, Salim Haris P, Anita B, Arun Kumar G et al. Habits with killer instincts: in vivo analysis on the severity of oral mucosal alterations using autofluorescence spectroscopy. J biomed opt 2011;16: 087006.

32. Messerchmidt R., Harthcock M. (1988). Infrared Microscopy, Theory and Applications, New York, Marcel Dekker

33. Dukor RK. Vibrational Spectroscopy in the Detection of Cancer Handbook of Vibrational Spectroscopyed.: John Wiley & Sons, Ltd, 2006.

34. Wu JG, Xu YZ, Sun CW, Soloway RD, Xu DF, Wu QG et al. Distinguishing malignant from normal oral tissues using FTIR fiber-optic techniques. Biopolymers 2001;62: 185-92.

35. Fukuyama Y, Yoshida S, Yanagisawa S, Shimizu M. A study on the differences between oral squamous cell carcinomas and normal oral mucosas measured by Fourier transform infrared spectroscopy. Biospectroscopy 1999;5: 117-26.

36. Krishnakumar N, Sulfikkarali NK, Manoharan S, Nirmal RM. Screening of chemopreventive effect of naringenin-loaded nanoparticles in DMBA-induced hamster buccal pouch carcinogenesis by FT-IR spectroscopy. Mol Cell Biochem 2013;382: 27-36.

37. Schultz CP, Liu KZ, Kerr PD, Mantsch HH. In situ infrared histopathology of keratinization in human oral/oropharyngeal squamous cell carcinoma. Oncol Res 1998;10: 277-86.

38. Bruni P, Conti C, Giorgini E, Pisani M, Rubini C, Tosi G. Histological and microscopy FT-IR imaging study on the proliferative activity and angiogenesis in head and neck tumours. Faraday discuss 2004;126: 19-26; discussion 77-92.

39. Pallua JD, Pezzei C, Zelger B, Schaefer G, Bittner LK, Huck-Pezzei VA et al. Fourier transform infrared imaging analysis in discrimination studies of squamous cell carcinoma. Analyst 2012;137: 3965-74.

40. Raman C.V. and Krishnan K.S. A change of wavelength in light scattering. Nature 1928: 121,501.

41. Walton AG, Deveney MJ, Koenig JL. Raman spectroscopy of calcified tissue. Calcif Tissue Res 1970;6: 162-7.

42. Hanlon EB, Manoharan R, Koo TW, Shafer KE, Motz JT, Fitzmaurice M et al. Prospects for in vivo Raman spectroscopy. Phys Med Biol 2000;45: R1-59.

43. Bakker Schut TC, Witjes MJ, Sterenborg HJ, Speelman OC, Roodenburg JL, Marple ET et al. In vivo detection of dysplastic tissue by Raman spectroscopy. Anal chem 2000;72: 6010-8.

44. Venkatakrishna K, Kurien J, Keerthilata MP, Valiathan M, Kumar NN, Krishna CM et al. Optical pathology of oral tissue: A Raman Spectroscopy diagnostic method. Current Science 2001;80:101-105.

45. Krishna CM, Sockalingum GD, Kurien J, Rao L, Venteo L, Pluot M et al. Micro-Raman spectroscopy for optical pathology of oral squamous cell carcinoma. Appl Spectrosc 2004;58: 1128-35.

46. Malini R, Venkatakrishna K, Kurien J, Pai KM, Rao L, Kartha VB et al. Discrimination of normal, inflammatory, premalignant, and malignant oral tissue: a Raman spectroscopy study. Biopolymers 2006;81: 179-93.

47. Cals FLJ, Bakker Schut TC, Koljenović S, Puppels GJ, de Jong RJB. Method development: Raman spectroscopy-based histopathology of oral mucosa. J Raman Spectrosc 2013;44: 963-72.

48. Sunder NS, Rao Nirmala N, Kartha VB, Ullas G, Kurien J. Laser Raman spectroscopy: A novel diagnostic tool for oral cancer. J Orofac Sci.2011;3:15-19.

49. Guze K, Short M, Sonis S, Karimbux N, Chan J, Zeng H. Parameters defining the potential applicability of Raman spectroscopy as a diagnostic tool for oral disease. J Biomed Opt 2009;14: 014016.

50. Bergholt MS, Zheng W, Huang Z, Characterizing variability in in vivo Raman spectroscopic properties of different anatomical sites of normal tissue in the oral cavity. J Raman Spectrosc 2012;43:255-262.

51. Singh SP, Deshmukh A, Chaturvedi P, Krishna CM. In vivo Raman spectroscopic identification of premalignant lesions in oral buccal mucosa. J Biomed Opt 2012;17: 105002.

52. Singh SP, Sahu A, Deshmukh A, Chaturvedi P, Krishna CM. In vivo Raman spectroscopy of oral buccal mucosa: a study on malignancy associated changes (MAC)/cancer field effects (CFE). Analyst 2013;138: 4175-82.

53. Sahu A, Deshmukh A, Ghanate AD, Singh SP, Chaturvedi P, Krishna CM. Raman spectroscopy of oral buccal mucosa: a study on age-related physiological changes and tobacco-related pathological changes. Technol Cancer Res Treat 2012;11: 529-41.

54. Krishna H, Majumder SK, Chaturvedi P, Gupta PK. Anatomical variability of in vivo Raman spectra of normal oral cavity and its effect on oral tissue classification. Biomed Spectrosc Imaging 2013;2: 199-217.

55. Rajasekaran R, Aruna PR, Koteeswaran D, Padmanabhan L, Muthuvelu K, Rai RR et al. Characterization and diagnosis of cancer by native fluorescence spectroscopy of human urine. Photochem Photobiol 2013;89: 483-91.

56. Bigler LR, Streckfus CF, Dubinsky WP. Salivary biomarkers for the detection of malignant tumors that are remote from the oral cavity. Clin. Lab. Med. 2009;29: 71-85.

57. Sugimoto M, Wong DT, Hirayama A, Soga T, Tomita M. Capillary electrophoresis mass spectrometry-based saliva metabolomics identified oral, breast and pancreatic cancer-specific profiles. Metabolomics 2010;6: 78-95.

58. Venkatakrishna K, Kartha VB, Pai KM, Krishna CM, Ravikiran O, Kurian J et al. HPLC-LIF for early detection of oral cancer. Current Science 2003;84: 551-57.

59. Meng JW, Wang XJ, Ma HP, Ren XG, Xu XR, Ren WM. Protoporphyrin IX fluorescence from the plasma of tumor-implanted mouse. J Lumin 1999;83–84: 251-4.

60. Madhuri S, Vengadesan N, Aruna P, Koteeswaran D, Venkatesan P, Ganesan S. Native fluorescence spectroscopy of blood plasma in the characterization of oral malignancy. Photochem Photobiol 2003;78: 197-204.

61. Yuvaraj M, Udayakumar K, Jayanth V, Prakasa Rao A, Bharanidharan G, Koteeswaran D et al. Fluorescence spectroscopic characterization of salivary metabolites of oral cancer patients. J Photochem Photobiol B 2014;130: 153-60.

62. Menzies GE, Fox HR, Marnane C, Pope L, Prabhu V, Winter S et al. Fourier transform infrared for noninvasive optical diagnosis of oral, oropharyngeal, and laryngeal cancer. Transl Res 2014;163: 19-26.

63. Olivo M, Bhuvaneswari R, Keogh I. Advances in Bio-Optical Imaging for the Diagnosis of Early Oral Cancer. Pharmaceutics 2011;3: 354-78.

64. Elumalai B, Prakasarao A, Ganesan B, Dornadula K, Ganesan S. Raman spectroscopic characterization of urine of normal and oral cancer subjects. J Raman Spectrosc 2015;46:84-93.

65. Papamarkakis K, Bird B, Schubert JM, Miljkovic M, Wein R, Bedrossian K et al. Cytopathology by optical methods: spectral cytopathology of the oral mucosa. Lab Invest 2010;90: 589-98.

66. Diem M, Mazur A, Lenau K, Schubert J, Bird B, Miljkovic M et al. Molecular pathology via IR and Raman spectral imaging. J Biophotonics 2013;6: 855-86.

67. Kah JCY, Kho KW, Lee CGL, Richard CJ, Sheppard, Shen ZX et al. Early diagnosis of oral cancer based on the surface plasmon resonance of gold nanoparticles. Int J Nanomedicine 2007;2: 785-98.

68. Bonnier F, Baker MJ, Byrne HJ. Vibrational spectroscopic analysis of body fluids: avoiding molecular contamination using centrifugal filtration. Anal Methods 2014;6:5155

69. Byrne HJ, Baranska M, Puppels GJ, Stone N, Wood B, Gough KM et al. Spectropathology for the Next Generation: Quo Vadis?. Analyst 2015;140:2066-73.

70. Matousek P, Stone N. Recent advances in the development of Raman spectroscopy for deep non-invasive medical diagnosis. J Biophotonics 2013; 6: 7–19.

Chapter 3: Use of Raman Spectroscopy for the Study of Cell Cycle Phase and Biomarker Expression Levels in Oral Squamous Cell Carcinoma Cells

3.1 Introduction

The cell cycle is a highly regulated process with defined phases. G1 is the phase after the previous cell division during which the cell grows. The S phase is the DNA synthesis phase, in which the cell replicates its genetic material. In the G2 phase, transcription and translation are co ordinated to prepare for Mitosis (M phase). The cell cycle is associated with checkpoints in which the cell assesses its environment to ensure the conditions are appropriate for cell cycle progression. There are two checkpoints, one at the G1/S boundary and another at the G2/M boundary. Deregulation of the cell cycle can result in tumourogenesis[1] and is often signalled by the overexpression of certain biomarkers, as, for example cyclin D1. Cyclin D1is one of a family of D type cyclins which also include D2 and D3. It is important for the G1 to S phase transition as it binds with the cyclin dependent kinases 4 and 6 to form an active complex that phosphorylates and inactivates retinoblastoma protein (RB) promoting cell cycle progression[2]. The overexpression of cyclin D1 leads to faster progression from G1 to S phase, which in turn results in increased proliferation and an increased propensity for the development of mutations. Cyclin D1 is overexpressed in a number of carcinomas such as breast, oesophageal, ovarian, hepatocellular, colorectal, and head and neck carcinoma[3-8]. Another biomarker, Proliferating cell nuclear antigen (PCNA), required for DNA replication, is synthesised in the late G1 and S phases of the cell cycle[9]. It acts as a polymerase clamp as well as a sliding platform for the recruitment of other replication proteins such as DNA helicase, ligase, nuclease, and histone chaperones[10]. Levels of PCNA have been found to correlate with increased dysplasia in oral

epithelial cells[11,12]. A thorough understanding of cell cycle dynamics is important for cancer research and tumour targeting. The ability to monitor the altered expression of biomarkers could prove valuable in cancer screening.

Flow cytometry has been widely used in the study of cell cycle dynamics, as Propidium iodide (PI) is commonly used to quantify the DNA content which is characteristic of the cell cycle phase. Quantitative image analysis which utilizes fluorescent dyes has also been used to identify certain biomarkers that vary throughout the cell cycle[13]. Both these techniques rely on prior knowledge of the biomarkers to be studied and can only give information on a few biomarkers at a time.

Using inhibitors to arrest the cell cycle at the various phases, previous studies have examined the use of Raman spectroscopy in the discrimination of the cell cycle phases. Using a prostate cancer cell line, and fixing the cells at the different cell cycle phases, one study found the greatest differences between the G2M and G1 phases and slight differences between the G1 and S phases[14]. Similar findings were made by another study looking at live human osteosarcoma cells, although, unlike the former, where the differences were dominated by nucleic acids, proteins and lipids, here the differences were mainly in lipids[15]. Using one synchronous cell cycle and analysing fibroblast cells with FTIR spectroscopy in two hour intervals, one study found that there were differences in the lipid, and nucleic acid profiles at the different time intervals[16]. The aforementioned studies combine G2 and M phases of the cell cycle in the analysis, which was also the approach in this study. This is due to the fact that, in flow cytometry analysis, which uses DNA fluorescent markers, the phases that can be distinguished are G0/G1 which make up a Gaussian peak with 1x the DNA content, G2M with a Gaussian peak of 2x the DNA content and S phase which the population in between G0/G1 and G2M.

The aim of the present study was to investigate the Raman profiles of oral squamous cell carcinoma cells at defined phases of the cell cycle and to correlate these with cyclin D1 and PCNA expression in the cells at the different cell cycle phases as assessed by flow cytometry. In order to assess whether label free Raman signatures can be correlated with established biomarkers.

3.2 Materials and Methods

3.2.1 Cell culture

SCC-4 cells (ATCC, Manassas, VA), a human tongue squamous cell carcinoma cell line, were cultured in DMEM F-12 media (Sigma-Aldrich) supplemented with 10% (v/v) foetal bovine serum (FBS) (Sigma-Aldrich), 1% (v/v) Penicillin/streptomycin and 400 ng/ml hydrocortisone (Sigma-Aldrich). They were incubated at 37°C with 5% CO_2 and regularly passaged at 80% confluency to maintain exponential growth. The passage number for the experiments did not exceed 17. Studies have shown that cells transform at high passage numbers (~40) and show altered expression of mRNAs involved in regulated secretion adhesion and proliferation.

3.2.2 Cell Synchronisation

A double thymidine block, described previously[17], which arrests cells in the S phase of the cell cycle, was used to synchronise the cells. Excess thymidine inhibits DNA synthesis, thereby arresting cells in G1, prior to DNA replication, or in S phase. A double thymidine block ensures that any cells that were in mid or late S phase during the first block will be captured in late G1 or early S phase in the second block. SCC-4 cells were cultured in T-125 flasks, they were trypsinised at 30% confluency, harvested and counted. The confluency/density of cells affects their proliferation rate which can slow down at confluency above 50%[18]. Cells were counted

using a coulter counter, 500,000 cells were seeded into a T-25 flask with 5 ml medium. Thymidine was added to the flasks to a concentration of 2 mM and incubated with the cells for 18 hours. The cells were then washed with PBS and fresh media was added to release them from the Thymidne block, they were then incubated for 9 hours. 2mM Thymidine was then added to the flasks for a second thymidine block and the cells were incubated for 17 hours. The selected time points were; at time of release from thymidine (0 hours), 6 hours after release, and 12 hours after thymidine release. The controls were unsynchronised cells (not treated with thymidine), unstained cells (no primary or secondary antibody), negative control cells (no primary antibody) and cells with no PI. All time points and controls were completed in triplicate. Experiments were performed for detecting both cyclin D1 and PCNA.

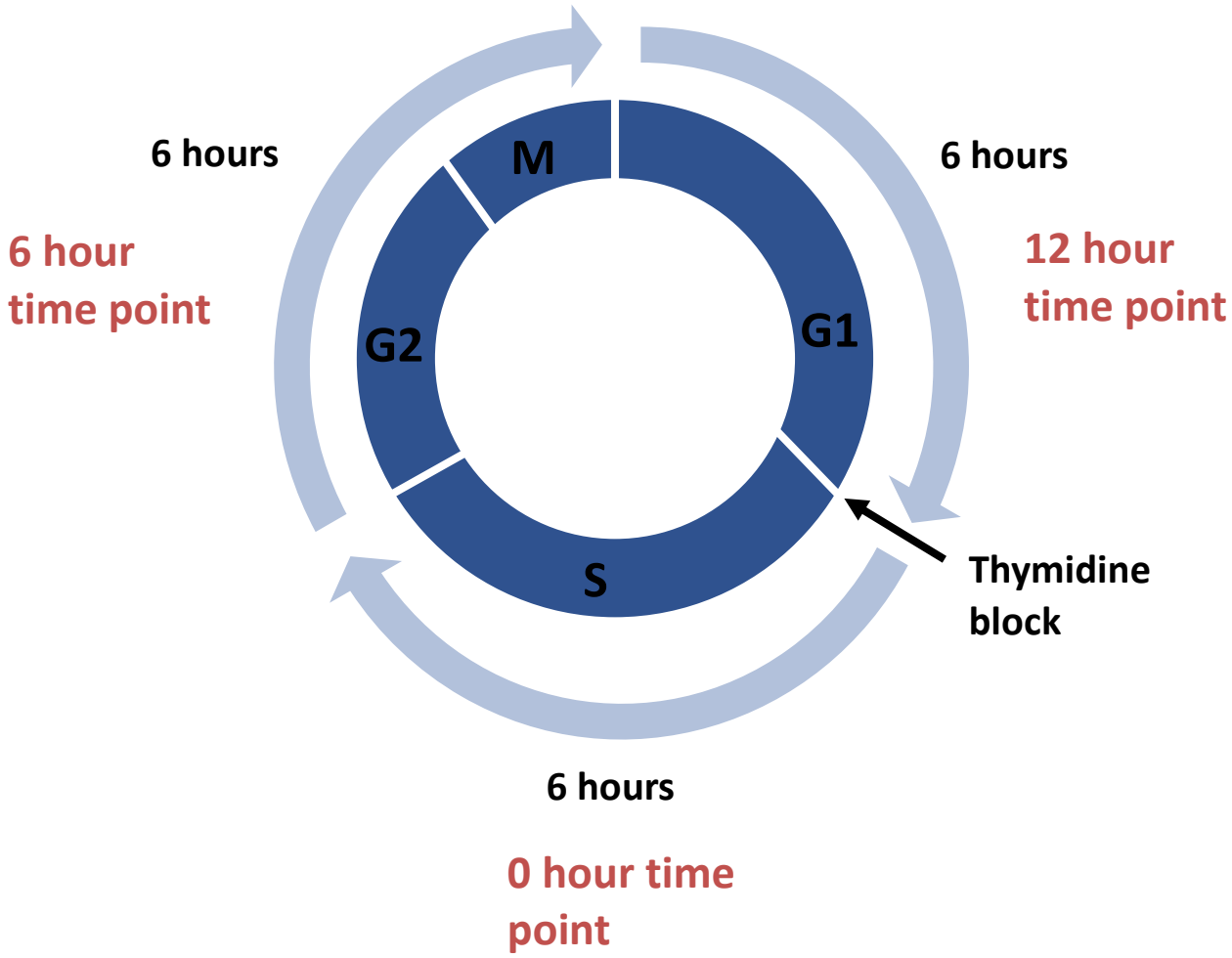

Figure 3.1 A schematic of the SCC4 cell cycle. SCC4 cells have an 18 hour cycle (doubling time) and spend 6 hours in each of the phases (G1, S, and G2M). The thymidine block arrests the cells at the G1/S boundary so when cells are released they enter S phase.

3.2.3 Flow Cytometry

Cells were harvested by trypsinisation, washed with PBS, then resuspended in ice cold methanol and stored at 4°C overnight. The fixed cells were pelleted and the pellet was dried to remove the methanol. The cells were then permeabilised with 0.2% Triton X-100 (BDH) in PBS (v/v), washed with PBS, then treated with a primary antibody; for cyclin D1, monoclonal rabbit antihuman cyclin D1 antibody (Dako) (1:50 dilution in PBS) and for PCNA, a mouse monoclonal [PC10] to PCNA (abcam) (1:50 dilution in PBS). After another PBS wash, for cyclin D1 detection, an anti-rabbit IgG Fluorescein isothiocyanate (FITC) conjugated antibody (Sigma-Aldrich) (1:100 dilution in PBS) was incubated with the cells and for PCNA detection a goat Anti-mouse IgG Alexa Fluor conjugated antibody (abcam) (1:100 dilution in PBS) was used. Subsequently, the cells were re-suspended in 0.5 ml of PI-RNase (BD Biosciences) and analysed with a BD Accuri C6 flow cyctometer. The threshold was set at 10,000 events and, using forward and side scatter characteristics, gates were set to exclude cell debris. The controls were used to determine the quadrants by determining positive signal from background fluoresence so the threshold for positivity could be set accordingly. PI and FITC/Alexa Flour were plotted in the y and x axis respectively so that cells in the lower left quadrant were negative for both and those in the upper right quadrant were positive for both. Cell cycle phase was determined by DNA content; PI intercalates with DNA and facilitates DNA quantity measurement in the 560-590 nm range of the spectrum using a 585/15 nm optical filter. An excitation wavelength of 488 nm was used and Cyclin D1 and PCNA expression was detected with a 533/30 nm optical filter.

3.2.4 Raman Spectroscopy

125,000 cells were seeded onto calcium fluoride (CaF_2) discs (Crystan, UK) for Raman spectroscopy, treated with thymidine and fixed at the previously described time points. The cells were fixed with 4% formalin, washed with PBS, then stored in 0.9% physiological saline at 4°C. A Horiba Jobin Yvon LabRAM HR 800 Dual Microscope Raman Spectroscope with a 785nm laser was used to capture the cell spectra. The LabRAM system is a confocal Raman spectrometer with a motorised XY sample stage and interchangeable gratings of which the 300 grooves/mm grating was used, giving a dispersion of ~1.5cm^{-1} per pixel. The confocal pin hole of the system was set to 100μm and a 16 bit dynamic range charge coupled device (CCD) detector was used which is Peltier cooled to reduce thermal noise. A 60X /0.9W immersion objective (LumplanF1 Olympus, Japan) was used to focus on the samples and collect the backscattered light. Point spectra were taken from the nuclei of the cells. The spectral acquisition time was 40 seconds per point over two accumulations, and the range over which the Raman scattered light was detected was 400-1800 cm^{-1}. 74 spectra, one per cell, were collected overall for each time point from two independent experiments.

Data Analysis

All data analysis was carried out using Matlab (Mathworks, US), with the PLS-Toolbox (Eigenvector Research Inc.) and in-house algorithms.

Spectral Pre-Processing

The raw Raman spectra were first smoothed using a Savitzky-Golay filter (13 points, 5th order). Savitzky-Golay filter increases the signal to noise ratio without distorting the signal. The baseline was then corrected using the rubberband method[19], and finally the spectra were vector normalised (to reduce any variability caused by the fluctuation of excitation power)[19].

Principal component analysis (PCA)

PCA is a form of unsupervised multivariate analysis, which has become a standard processing technique for Raman Spectral data[20]. PCA explains the variance in the data by finding combinations of the original dimensions that describe the largest variance between the data sets. The output is in the form of a complementary set of score and loading plots termed principal components (PCs) [20,21].

Linear discriminant analysis (LDA) and Classification Model

LDA is a supervised form of multivariate analysis based on discriminant functions (LDs) which maximize the variance between groups and minimize the variance within groups. PCA is first used to reduce the data into PCs which are then used to build an LDA classification model with leave one out cross validation (LOOCV). In LOOCV all the spectra except for one are used as a training set and a prediction is made for the left out spectrum. This is repeated so that each spectrum is left out and predicted once[22].

3.3 Results

3.3.1 Cell Cycle Analysis

DNA content was determined by flow cytometry and related to cell cycle phase as shown in Figure 3.2 (representative measurement), and tabulated in Table 3-1 (average of 6 measurements). At the time of thymidine release, most of the cells were arrested in S phase, 6 h after release, the majority of the cells were in the G2M phase, while 12 h after release most of the cells were in the G1 phase of the cell cycle.

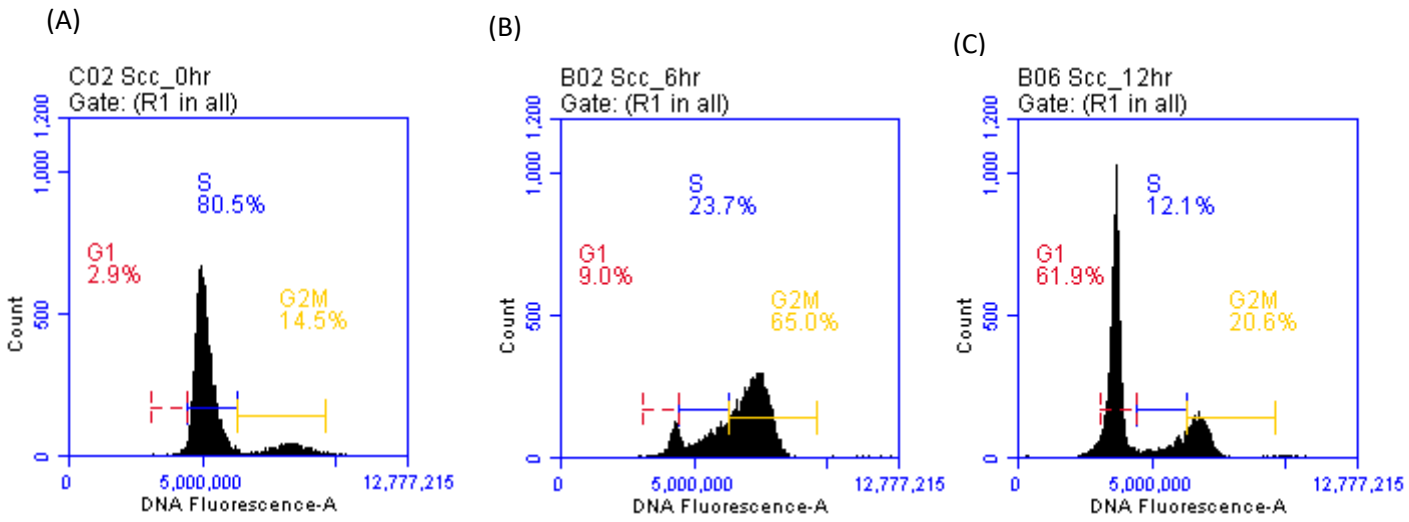

Figure 3.2 A representative plot showing cell cycle profile SCC-4 cells; (A) at time of thymidine release, (B) 6 hours after thymidine release, and (C) 12 hours after release respectively.

Table 3-1 Mean and standard deviation of cell cycle phases at each time point

	Flow cytometry classification (%)		
Time point (h) after thymidine release	**S**	**G2M**	**G1**
0	75±5	12±8	9±3
6	24±12	67±7	9±4
12	9±3	22±1	62±4

3.3.2 Biomarker expression

Cyclin D1 expression was assessed by FITC staining, and 3 measurements were made for each time point. As can be seen in Figure 3.3, Cyclin D1 expression varied according to the time point after release, and therefore cell cycle phase, the highest expression being observed in G2M, followed by G1 and the lowest expression being in the S phase. The expression of PCNA was assessed by an Alexa Fluor conjugated secondary antibody with 3 measurements made for each time point. From Figure 3.4 it appears that PCNA expression is very high in S phase

(~90%) which is reduced to (~60%) in G2M phase and is at its lowest (~10%) in G1 phase of the cell cycle. Using one way ANOVA, which determines if three independent groups have significantly different means, PCNA expression was found to be significantly variable across the different groups (time points). That was not the case with cyclin D1 which was not found to have variance across the groups. However a two tailed t test revealed that S phase expression is significantly lower than G2M.

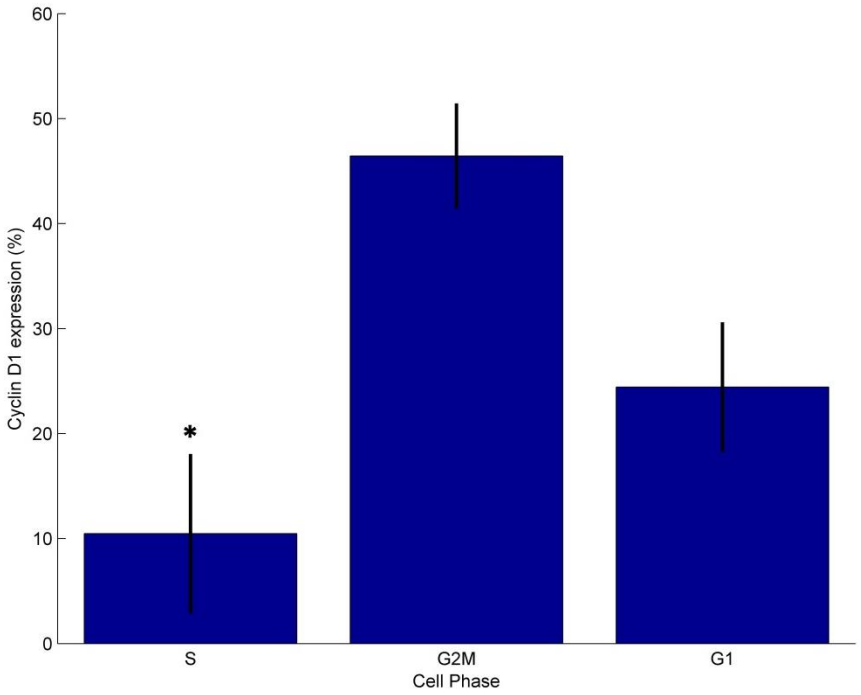

Figure 3.3 Cyclin D1 expression at the different time points, related to cell cycle phases. Expression is highest at G2M, followed by G1 phase and lowest at the S phase. A two tailed t test showed that S phase expression is significantly ($P<0.002$) lower than G2M but not G1.

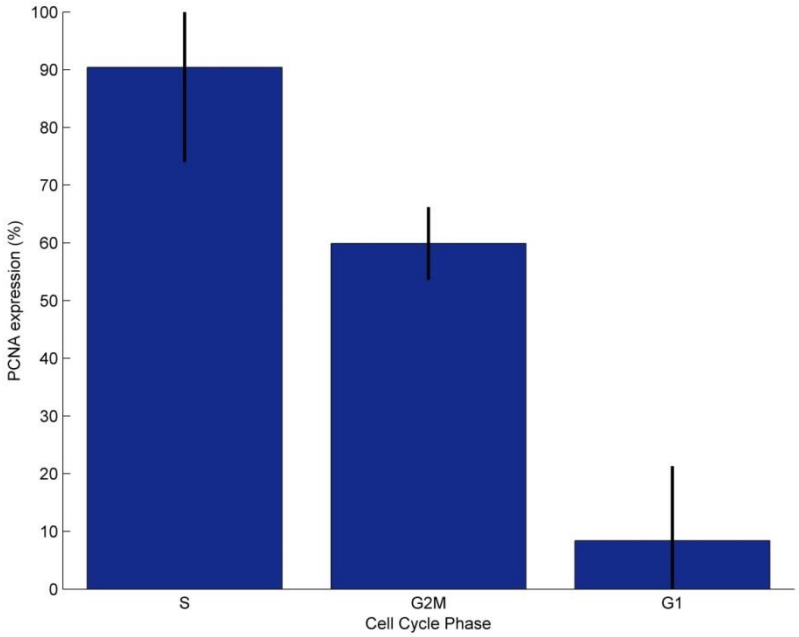

Figure 3.4 PCNA expression at different time points, related to cell cycle phases. PCNA expression is highest in S phase, followed by G2M and lowest in G1. One way ANOVA test showed that PCNA expression is significantly different (P=0.0006) between the different time points.

3.3.3 Raman Spectroscopy

From their mean Raman spectra (Figure 3.5); differences between the release time points, representing the cell cycle phases, were observed. Spectral peak assignments[23,24] are tabulated in Table 3-2. The nucleic acid (600-800 cm^{-1}) and amide 1 regions (1600-1800 cm^{-1}) are more prominent in the G2M phase, the S phase has more prominent protein and lipid features (around 1400 cm^{-1}), while the G1 phase falls between the S and the G2M phases.

Table 3-2 Peak assignments of the main Raman vibrational modes found in the spectra and PC loadings[23,24]

Wavenumbers (cm^{-1})	Assignments
621	C-C twist in phenylalanine
783	DNA/RNA ring breathing
1004	Phenylalanine ring breathing
1092	DNA/RNA O-P-O stretching
1336	DNA bases
1440	Fatty acids
1451	Protein (C-H) bending
1575	DNA/RNA ring mode
1673	Amide 1 β pleated sheet

PCA was performed, pairwise, on the processed Raman spectra, which revealed a distinct separation between the S phase and G1 and G2M phases according to PC1, which explains 47% and 45% of the variance respectively (Figure 3.6). Figure 3.7(A) shows the loading of PC1 for both S vs G1 and S vs G2M. Scores that are on the positive side of a PC in the scatter plot reflect the positive side of the loading plot. Similarly, the negative side of the scatter plot is represented by the negative side of the loading plot[25]. For both cases, the loading is remarkably similar, although there are some differences. The loadings indicate that the S phase is higher in protein content (1451 cm^{-1}, protein C-H bending and 1673 cm^{-1}, Amide 1 vibration) than G1 and G2M and there is variability in all 3 at 783 cm^{-1}. PC2 does not discriminate between the S and G phases, but does, at least partially, discriminate the G1 and G2M phases, for which it explains 8% of the variance. The PC2 loading (Figure 3.7 (B)) shows distinct

nucleic acid bands on the positive side (783cm^{-1}, 1092 cm^{-1}, 1336 cm^{-1} and 1576 cm^{-1}), indicative of higher nucleic acid content in the G2M compared to the G1 phase. The band at 1440 cm^{-1}, on the negative side of PC2, suggests an accumulation of lipids in the G1 phase of the cell cycle.

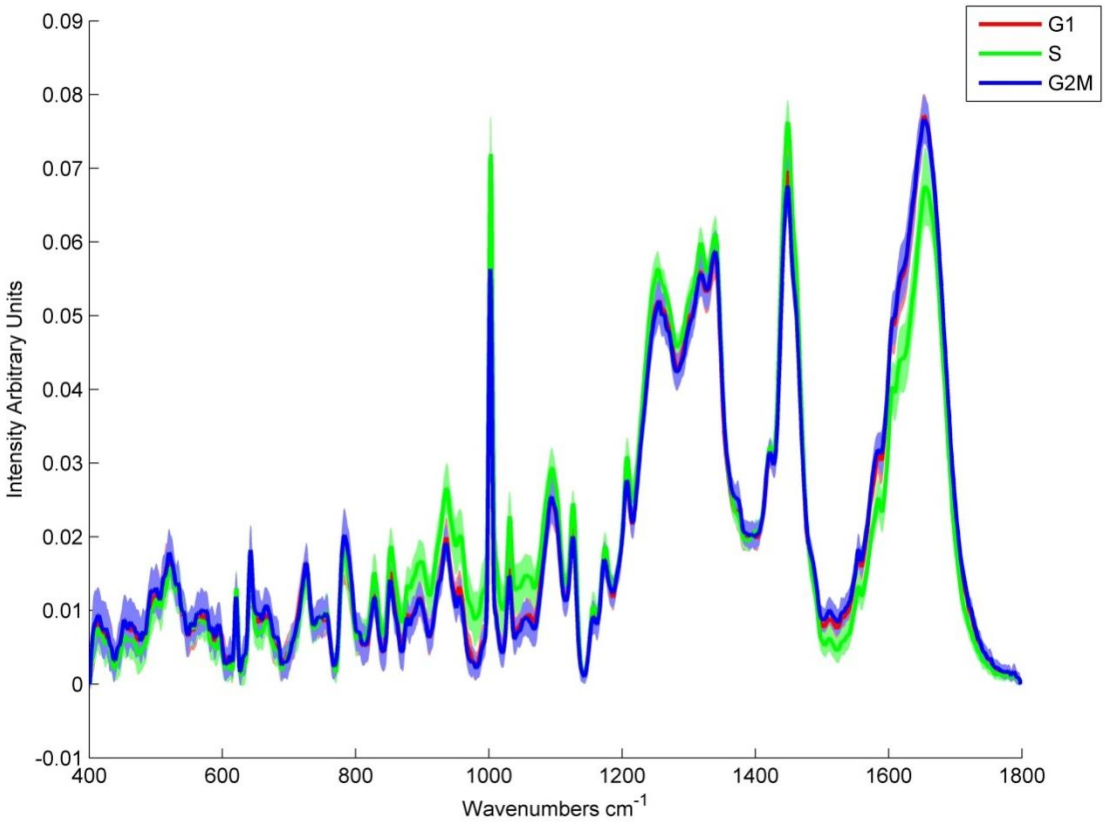

Figure 3.5 Mean Raman spectra from SCC-4 cells in each cell cycle phase G1, S, and G2M. The shading represents the standard deviation.

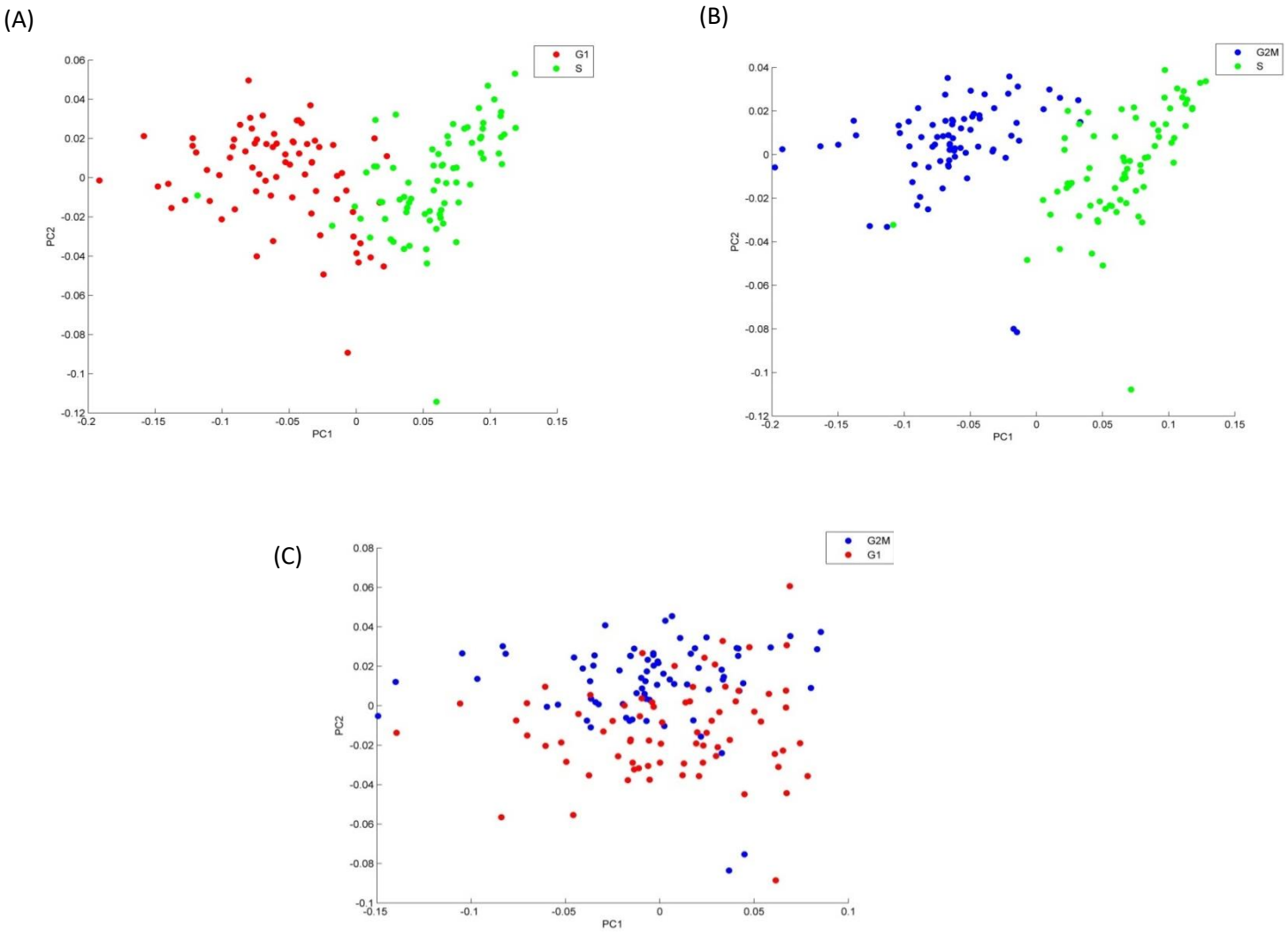

Figure 3.6 Two dimensional scatter plots of the first two principal components after PCA was performed on the spectra from fixed cell nuclei, showing (A) G1 vs S phase (B) S vs G2M and (C) G1 vs G2M. S phase separated from the other two phases according to PC1, while G1 and G2M phase separate according to PC2.

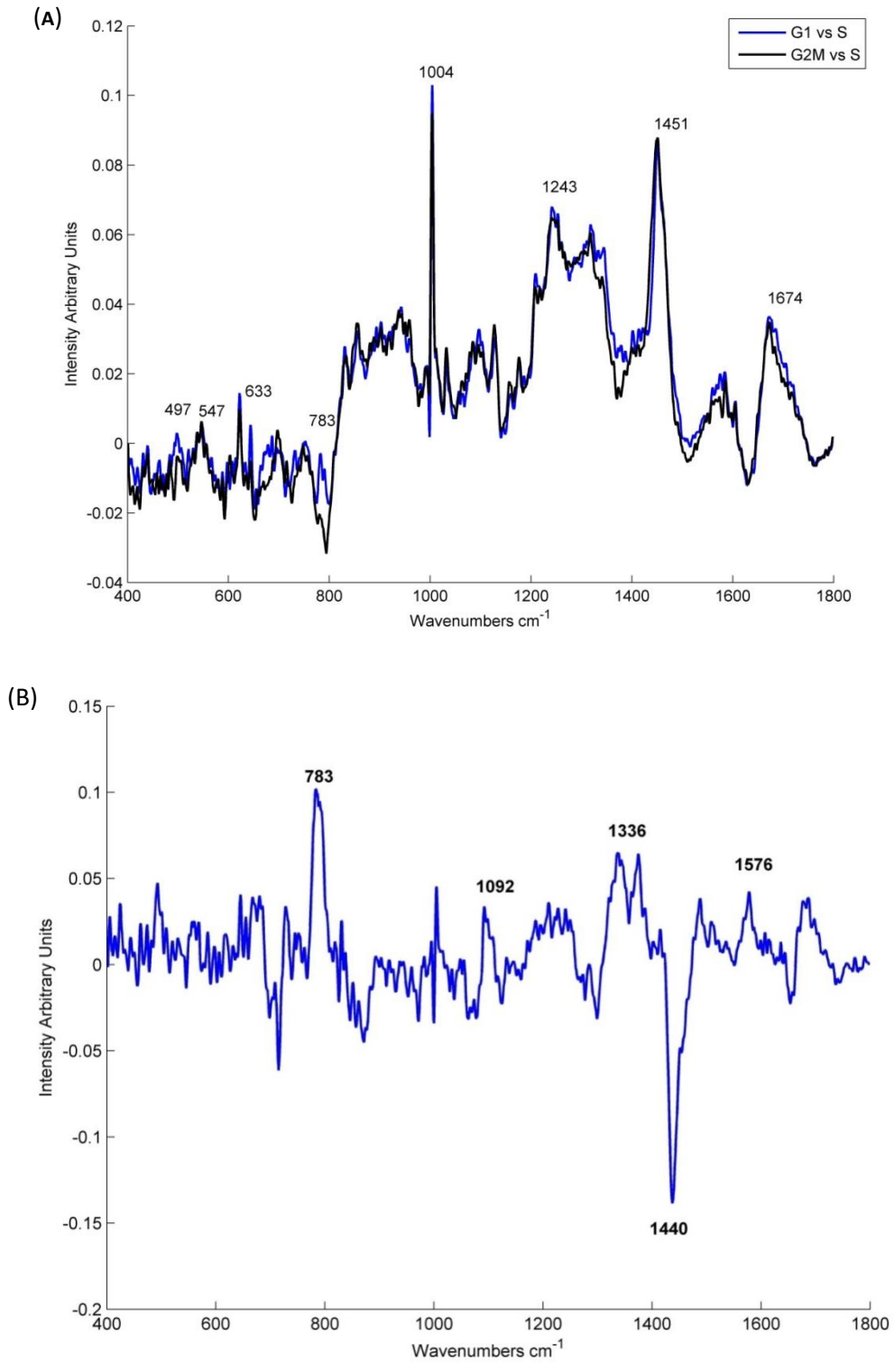

Figure 3.7 (A) Loading of PC1 in G2M vs S phase PCA (black) and G1 vs S phase PCA (blue). S phase is positive in both (B) Loading of PC2 in G2M vs G1 phase PCA. G2M is positive

3.3.4 Classification Model

To enhance the classification, PCA-LDA with leave one out cross validation was performed on the spectra. The resulting confusion matrix, shown in Table 3-3, correctly classified 71 out of 74 spectra (96%) at the 0 hour time point, which is consistent with the predominance of the S phase, 58 of 74 (78%) at the 6 hour time point, consistent with the predominance of the G2M phase and 46 out of 74 (62%) spectra at the 12 hour time point, which corresponds to the G1 phase. Corroborating the flow cytometry data (**Error! Reference source not found.**), the p ercentage of cells correctly classified in each phase from S through G2M then G1 decreases corresponding to decreasing synchronicity. Plotting the linear discriminants (**Error! R eference source not found.**), a monotonic progression of LD1<LD3<LD2 is apparent in the negative peaks at 780 cm^{-1}, 1092 cm^{-1} and 1339 cm^{-1}, all nucleic acid related. The spectral profile is remarkably similar to PC2 which discriminates the G1 and G2M phases in **Error! R eference source not found.** (B). LD1 discriminates between G2M and S phase, LD2 discriminates between G1 and G2M phase and LD3 discriminates G1 and S phase, and the similarity of the discriminants indicates that nucleic acid content is the primary biochemical difference between the cell cycle phases.

Table 3-3 A confusion matrix utilising LDA with leave one out cross validation of the principal component scores showing the Raman predicted percentage of cells at each phase of the cell cycle.

	Raman Classification (%)		
Cell Cycle Stage	***S***	***G2M***	**G1**
S	*96*	*0*	*4*
G2M	*0*	*78*	*22*

G1	*7*	*31*	*62*

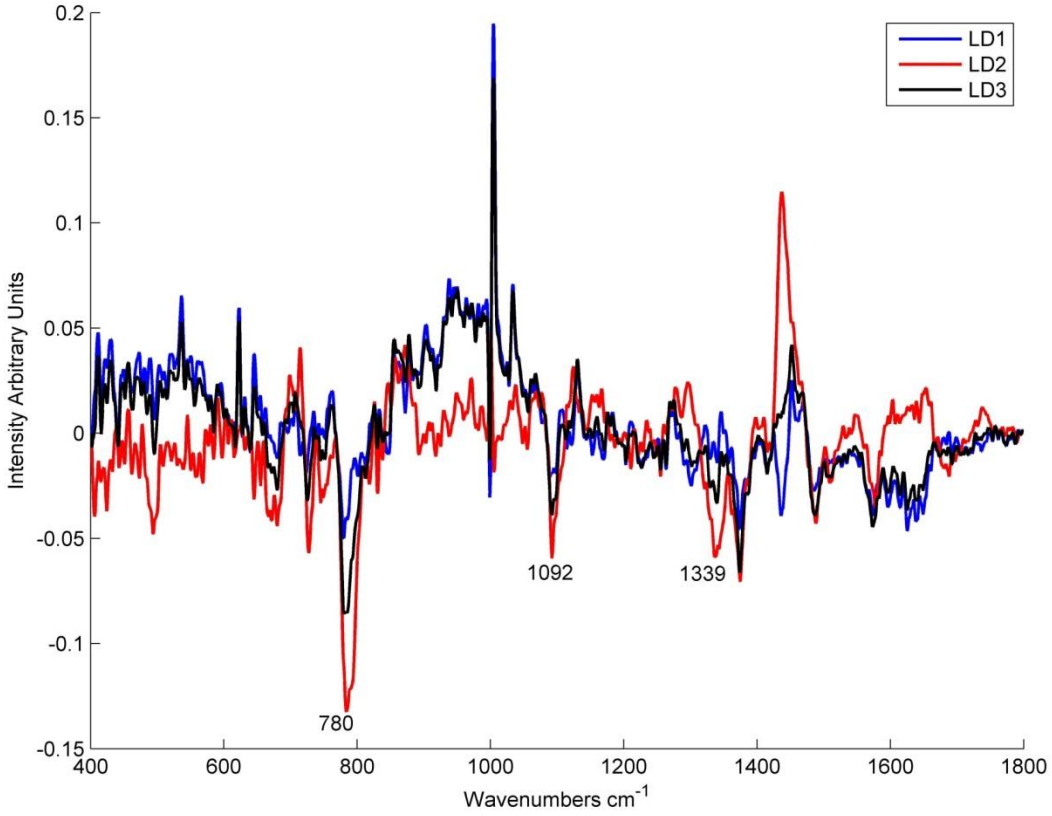

Figure 3.8 Linear Discriminants, LD1 discriminates between G2M and S phase, LD2 discriminates between G1 and G2M phase and LD3 discriminates G1 and S phase.

Spectra of cyclin D1 and PCNA proteins on CaF_2 slides were recorded by Raman spectroscopy (**Error! Reference source not found.**) to determine whether their varying levels at the d ifferent stages of the cell cycle could be reflected in the PC and LD loadings. The characteristic peaks at 812 and 1557 cm^{-1} of cyclin D1 and at 851 and 1446 cm^{-1} of PCNA were not, however, distinct/apparent in either the PC or LD loadings.

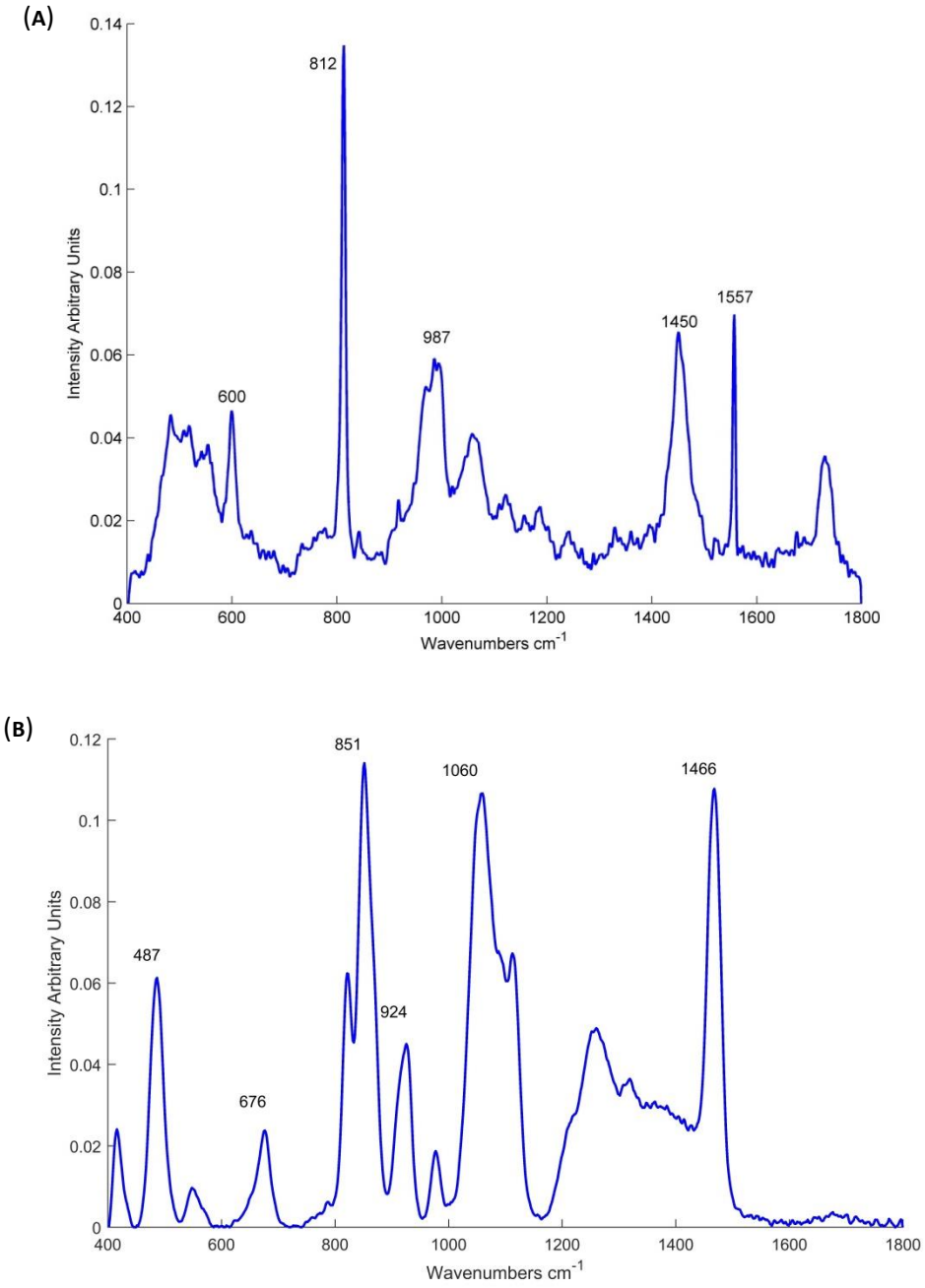

Figure 3.9 (A) Spectrum of cyclin D1 (B) Spectrum of PCNA

3.4 Discussion

The Raman data showed a good separation between S phase and G1 and G2M phases using PCA. Furthermore, the LDA model showed that the classification was highest at S phase followed by G2M and G1 phase. This is consistent with the flow cytometry results which indicated that the cells were well synchronised at the time of arrest (75% S phase), while the synchronicity was reduced in the G2M (67%) and G1 (61%) phases. An important finding was that the Raman classification at each phase was higher than its flow cytometry counterpart. This may be due to the fact that flow cytometry classification is dependent on just the nucleic acid content, while Raman classification takes into account all the biological molecules within the nucleus.

Previous cell cycle studies using Raman spectroscopy have used several methods to synchronise the cells at various phases. Matthews et al. used thymidine to synchronise the cells at the start of the S phase and nocodazole for synchronisation at the G2/M boundary[14], while Swain et al. used serum starvation to arrest the cells in the G0/G1 boundary, aphidicolin to synchronise the cells in S phase and nocodazole to synchronise them at the G2/M boundary[15]. In this study it was decided to use one cell cycle synchronisation method as opposed to several. Although this results in less synchronisation in the latter stages, it eliminates any possible differences due to synchronisation method that can influence the analysis, notably the chemical signature profiles in the Raman spectra. The differences between G1 and G2M phase were mainly due to higher lipid (1440cm^{-1}) content in the former and higher nucleic acids (783cm^{-1}, 1092 cm^{-1}, 1336 cm^{-1} 1576 cm^{-1}) in the latter, which is consistent with previous findings that showed more lipid (700 cm^{-1}, 1438 cm^{-1}) in G1 phase and nucleic acids (669cm^{-1}, 784cm^{-1}, 1100cm^{-1}, 1340cm^{-1}, 1577 cm^{-1}) in G2M phase[14]. It is important to note that flow cytometry preparations involve a cell permeabilisation step which could lead to alterations in

phospholipids. The linear discriminants show a similar progression whereby the nucleic acid related peaks (780 cm^{-1}, 1092 cm^{-1} and 1339 cm^{-1}) are highest in G2M followed by G1 phase and lowest in S phase. This is expected, as the DNA condenses in the G2M phase in preparation for cell division. The main differences between the S phase and the other two phases, G1 and G2M, were in the protein content (1451cm^{-1}, 1672cm^{-1}). This may be due to the fact that the expression of many proteins changes throughout the cell cycle so that the differences could relate to the changes in specific proteins as opposed to global protein change.

The Raman spectral profiles in the different cell cycle phases show little evidence of contributions of the biomarkers Cyclin D1 and PCNA. Cyclin D1 levels are moderately higher in G2M and G1, compared to S phase of the cell cycle. This pattern of cyclin D1 expression has been reported previously, yet its cause is not well understood[26-28]. An explanation could be that cyclin D1 levels are lowest in S phase as the result of proteasomal degradation following phosphorylation of Thr-286, which occurs specifically in S phase[28]. On the other hand, PCNA is synthesised in late G1 and reaches its maximum in S phase[9,29]. The localization of PCNA within the nucleus reportedly changes throughout the cell cycle. While its equally distributed in the nucleus in the G1 and G2 phases, in S phase it aggregates into foci at sites of replication[30].

A previous study has shown a Raman signature of PCNA with similar peaks at 483, 675, 849, 922 and 1466 cm^{-1} [31]. While no previous studies have examined the Raman spectrum of cyclin D1, a study by Kumar et al., showing oral tissue with different degrees of cyclin D1 and relating it back to Raman spectroscopy using a range of 1200-1800 cm^{-1} found that the tissues with higher cyclin D1 expression had prominent peaks at 1454 cm^{-1} and 1560-1583 cm^{-1} consistent with the cyclin D1 Raman spectrum measured in his study[32]. Cyclin D1 and PCNA are proteins with no specific distinguishing moieties which might give them a distinctive Raman signature, compared to other proteins. Thus, it is concluded that, in the absence of more refined data-

mining algorithms, they cannot be used as specific spectroscopic markers for deregulation of the cell cycle.

In summary this study found that Raman spectroscopy can be used to identify the different phases of the cell cycle and is perhaps only limited by the efficacy of the cell cycle block. Furthermore, data on lipid, protein and nucleic acid profiles of the cells can be generated as opposed to other methods which are limited in the information they provide. However, changes in particular biomarkers could not be demonstrated with Raman spectroscopy, perhaps due to the fact that hundreds of proteins are up or down regulated at different points in the cell cycle which makes it difficult to assess particular ones with an unlabelled method.

The major differences between the phases in the cell cycle are due to variations in nucleic acid and protein content of the cells, which are similar to the differences between the degrees of dysplasia. Hence, its ability to discriminate the different phases of the cell cycle gives an indication of the precision of Raman Spectroscopy in identifying biomolecular changes in the SCC4 cells which can later be translated to oral tissue samples to identify differences between pathologies. In the next chapter the protocols for pre-processing Raman spectra of oral FFPP tissue sections are discussed.

References

1. Otto T, Sicinski P. Cell cycle proteins as promising targets in cancer therapy. *Nature Reviews Cancer* 2017;17:93-115.

2. Alao JP. The regulation of cyclin D1 degradation: roles in cancer development and the potential for therapeutic invention. *Molecular Cancer* 2007;6.

3. Gillett C, Fantl V, Smith R, Fisher C, Bartek J, Dickson C, Barnes D, Peters G. Amplification and overexpression of cyclin D1 in breast cancer detected by immunohistochemical staining. *Cancer Research* 1994;54:1812-1817.

4. Morgan RJ, Newcomb PV, Hardwick RH, Alderson D. Amplification of cyclin D1 and MDM-2 in oesophageal carcinoma. *European Journal of Surgical Oncology* 1999;25:364-367.

5. Worsley SD, Ponder BAJ, Davies BR. Overexpression of cyclin D1 in epithelial ovarian cancers. *Gynecologic Oncology* 1997;64:189-195.

6. Nishida N, Fukuda Y, Komeda T, Kita R, Sando T, Furukawa M, Amenomori M, Shibagaki I, Nakao K, Ikenaga M, Ishizaki K. Amplification and overexpression of the cyclin D1 gene in aggressive human hepatocellular carcinoma. *Cancer Research* 1994;54:3107-3110.

7. McKay JA, Douglas JJ, Ross VG, Curran S, Murray GI, Cassidy J, McLeod HL, Aberdeen Colorectal I. Cyclin D1 protein expression and gene polymorphism in colorectal cancer. *International Journal of Cancer* 2000;88:77-81.

8. Matthias C, Branigan K, Jahnke V, Leder K, Haas J, Heighway J, Jones PW, Strange RC, Fryer AA, Hoban PR. Polymorphism within the cyclin D1 gene is associated with prognosis in patients with squamous cell carcinoma of the head and neck. *Clinical Cancer Research* 1998;4:2411-2418.

9. Kurki P, Vanderlaan M, Dolbeare F, Gray J, Tan EM. Expression of proliferating cell nuclear antigen (PCNA)/cyclin during the cell cycle. *Experimental Cell Research* 1986;166:209-219.

10. Kubota T, Nishimura K, Kanemaki MT, Donaldson AD. The Elg1 Replication Factor C-like Complex Functions in PCNA Unloading during DNA Replication. *Molecular Cell* 2013;50:273-280.

11. Liu SC, Klein-Szanto AJP. Markers of proliferation in normal and leukoplakic oral epithelia. *Oral Oncology* 2000;36:145-151.

12. Tsuji T, Shrestha P, Yamada K, Takagi H, Shinozaki F, Sasaki K, Maeda K, Mori M Proliferating cell nuclear antigen in malignant and pre-malignant lesions of epithelial origin in the oral cavity and the skin: an immunohistochemical study. *Virchows Archiv a-Pathological Anatomy and Histopathology* 1992;420:377-383.

13. Stacey DW, Hitomi M. Cell cycle studies based upon quantitative image analysis. *Cytometry Part A* 2008;73A:270-278.

14. Matthews Q, Jirasek A, Lum J, Duan X, Brolo AG. Variability in Raman Spectra of Single Human Tumor Cells Cultured in Vitro: Correlation with Cell Cycle and Culture Confluency. *Applied Spectroscopy* 2010;64:871-887.

15. Swain RJ, Jell G, Stevens MA. Non-invasive analysis of cell cycle dynamics in single living cells with Raman micro-spectroscopy. *Journal of Cellular Biochemistry* 2008;104:1427-1438.

16. Whelan DR, Bambery KR, Puskar L, McNaughton D, Wood BR. Synchrotron Fourier transform infrared (FTIR) analysis of single living cells progressing through the cell cycle. *Analyst* 2013;138:3891-3899.

17. Boehme SA, Lenardo MJ. Propriocidal apoptosis of mature T lymphocytes occurs at S phase of the cell cycle. *European Journal of Immunology* 1993;23:1552-1560.

18. Schorl C, Sedivy JM. Analysis of cell cycle phases and progression in cultured mammalian cells. *Methods* 2007;41:143-150.

19. Baker MJ, Trevisan J, Bassan P, Bhargava R, Butler HJ, Dorling KM, Fielden PR, Fogarty SW, Fullwood NJ, Heys KA, Hughes C, Lasch P, Martin-Hirsch PL, Obinaju B, Sockalingum GD, Sule-Suso J, Strong RJ, Walsh MJ, Wood BR, Gardner P, Martin FL. Using Fourier transform IR spectroscopy to analyze biological materials. *Nature Protocols* 2014;9:1771-1791.

20. Chan JW, Taylor DS, Zwerdling T, Lane SM, Ihara K, Huser T. Micro-Raman spectroscopy detects individual neoplastic and normal hematopoietic cells. *Biophysical Journal* 2006;90:648-656.

21. Wold S, Esbensen K, Geladi P. Principal component analysis. *Chemometrics and Intelligent Laboratory Systems* 1987;2:37-52.

22. Stone M. Cross-Validatory Choice and Assessment of Statistical Predictions.*Journal of the Royal Statistical Society Series B-Statistical Methodology* 1974;36:111-147.

23. Jess PRT, Smith DDW, Mazilu M, Dholakia K, Riches AC, Herrington CS. Early detection of cervical neoplasia by Raman spectroscopy. *International Journal of Cancer* 2007;121:2723-2728.

24. Byrne HJ, Sockalingum GD, Stone N. Biomedical Applications of Synchrotron Infrared Microspectroscopy. Cambridge, U.K.: Royal Society of Chemistry, 2011:376.

25. Bonnier F, Byrne HJ. Understanding the molecular information contained in principal component analysis of vibrational spectra of biological systems. *Analyst* 2012;137:322-332.

26. Stacey DW. Cyclin D1 serves as a cell cycle regulatory switch in actively proliferating cells. *Current Opinion in Cell Biology* 2003;15:158-163.

27. Yang K, Hitomi M, Stacey DW. Variations in cyclin D1 levels through the cell cycle determine the proliferative fate of a cell. *Cell Division* 2006;1.

28. Gookin S, Min MW, Phadke H, Chung MY, Moser J, Miller I, Carter D, Spencer SL. A map of protein dynamics during cell-cycle progression and cell-cycle exit. *Plos Biology* 2017;15.

29. Jurikova M, Danihel L, Polak S, Varga I. Ki67, PCNA, and MCM proteins: Markers of proliferation in the diagnosis of breast cancer. *Acta Histochemica* 2016;118:544-552.

30. Schonenberger F, Deutzmann A, Ferrando-May E, Merhof D. Discrimination of cell cycle phases in PCNA-immunolabeled cells. *Bmc Bioinformatics* 2015;16.

31. Martínez-Espinosa J, Reyes-Pablo A, Amtanus-Chequer N, Otero-Aguayo I, Vargas-Mancilla J, Gonzáles-Solis J, Basurto-Islas G, Córdova-Fraga T. Study of Proliferating Cell Nuclear Antigen in Breast Tumors by Enzyme-Linked ImmunoSorbent Assay and Raman Spectroscopy. *International Journal of Optics and Applications* 2013;3:67-71.

32. Kumar P, Bhattacharjee T, Pandey M, Hole A, Ingle A, Krishna CM. Raman spectroscopy in experimental oral carcinogenesis: investigation of abnormal changes in control tissues. *Journal of Raman Spectroscopy* 2016;47:1318-1326.

Chapter 4: Improved protocols for pre-processing Raman spectra of formalin fixed paraffin preserved tissue sections

Adapted from 'Ibrahim O, Maguire A, Meade AD, Flint S, Toner M, Byrne HJ, Lyng FM. Improved protocols for pre-processing Raman spectra of formalin fixed paraffin preserved tissue sections. Analytical Methods 2017;9:4709-4717'

OI contribution; experimentation, data analysis and write up.

4.1 Abstract

Although formalin fixed paraffin preserved (FFPP) tissues are a major resource for retrospective studies of disease progression, their use in vibrational spectroscopy studies has been undermined by issues of contributions of substrate and paraffin wax which persist in the spectra and can compromise spectral analysis. Recognising the microcrystalline nature of the wax in the tissue, which are inhomogeneously oriented with respect to the polarisation of the Raman source laser, in this study, we have developed a novel method for removing the paraffin wax contributions to the spectra using matrices of multiple wax spectra. FFPP tissue sections from the oral mucosca were obtained and, with no further chemical processing, the Raman spectral analysis of two regions, epithelium and connective tissue were compared. Matrices of multiple wax spectra were collected from different regions and subtracted from the epithelial and connective tissue spectra using a least squares analysis with non-negative constraints. Spectra of multiple cell components such as DNA and RNA were used in fitting the least squares model to reduce the residual error. The use of a data matrix of multiple wax spectra, as opposed to a single spectrum, results in a more accurate removal of the wax, hence reducing its contribution to spectral analysis. In unprocessed FFPP tissue sections, the contribution of

the glass substrate is seen to be minimised in comparison to chemically dewaxed FFPP tissue sections. Contributions of the glass substrate were also successfully removed digitally using the same methodology. The combined results indicate that direct analysis of FFPP tissue sections is feasible using Raman spectroscopy, avoiding the need for chemical dewaxing. Additionally, the ability to use glass slides is very important in translation to the clinic.

4.2 Introduction

The standard method used in histopathological tissue processing is formalin fixation followed by paraffin wax embedding. The tissue is first dehydrated through different grades of ethanol, then infiltrated with paraffin wax. In this way, the samples are stabilized and can be stored for years. These formalin fixed paraffin preserved (FFPP) archival tissue libraries can potentially be a vast resource for retrospective studies of patient history and disease progression. Vibrational spectroscopy, including Raman scattering and infra-red absorption, has emerged as a promising candidate for rapid, label free automated screening of tissue pathologies, and the term spectral histopathology has been coined[1]. However, paraffin wax poses a difficulty in vibrational spectroscopic studies of biological tissues, as the wax peaks are prominent and tend to interfere with either FTIR or Raman spectroscopic analysis[2,3]. A number of different approaches to remove the paraffin wax have been tested. Chemical dewaxing agents such as xylene, hexane, and histoclear were found to reduce but not completely eliminate the presence of wax and the reduction was seen to be proportional to the time the tissue remained in the dewaxing agent, resulting in long (up to 18 hours) processing times for optimised protocols[3]. The amount of residual wax was also found to be influenced by the choice of substrate and tissue type. Abnormal tissue, such as metastatic tissue, was found to retain more wax after dewaxing than normal tissue, while calcium fluoride substrates were seen to retain more wax than low E slides[4]. Another disadvantage of chemical dewaxing is that chemical dewaxing

agents have been shown to modify the tissue composition and therefore spectra[5,6]. The process of formalin fixation gives rise to formalin peaks appearing in the spectra at 1041 cm^{-1} and 1492 cm^{-1} which can be removed by washing in PBS[7]. As the molecular structure of paraffin wax is very similar to that of tissue lipids, the Raman spectral profile of the wax overlaps significantly with that of the tissue lipids, especially in the region 1000 cm^{-1} to 1700 cm^{-1}. Because of the structural similarities, the process of dewaxing can result in modification of the tissue lipidic content[6]. Digital wax removal methods such as independent component analysis and non-negatively constrained least squares analysis (NNLS) have been shown to be a promising alternative approach. However, these methods tend to introduce artefacts in the spectra due to over or underestimation of the wax contribution[8,9].

Another consideration in the spectral analysis of biological tissue is substrate choice. As the Raman spectrum of biological samples can be influenced by the optical properties of the substrate[10]. For research purposes, spectroscopists prefer to use spectrally neutral substrates such as calcium fluoride or magnesium fluoride, as they contribute a much lower background signal compared to glass[11]. However, they are significantly more expensive and therefore not a feasible option for routine diagnostic use[11,12]. Glass is commonly used in histopathological diagnosis as it is the clinical standard, is inexpensive and allows the processing of hundreds of samples a day. Its use in Raman spectroscopy, however, is hampered by the fact that glass exhibits a strong fluorescence emission under 785nm excitation[11] , overlaps with the biological spectra in the fingerprint region[12] and its contribution was found to vary with cellular morphology[13]. Notably, the glass contribution is significantly lower at 532nm than at the commonly employed 785nm, making it the wavelength of choice for such clinically oriented studies. Additionally, a shorter wavelength means greater confocality, higher intensity and a higher scattering efficacy[11]. A number of different methodologies have been proposed for removal of the glass contribution, including iterative subtraction of a polynomial[14] or glass

reference spectrum[12] and Kerr et al. have recently performed a comparison of EMCS based techniques[15] to such iterative techniques, suggesting that the former are more effective[13].

The aim of this study was to explore improved methodologies of digitally removing the wax contributions to Raman spectra, for the example of oral tissue sections, thereby retaining the clinically established tissue processing protocols. The improved methodology is based on a recognition that the wax in the tissue has a microcrystalline structure. While this is not a significant factor for macro- or unpolarised micro-spectroscopy, as commonly the case for FTIR, in the case of Raman microspectroscopy, the microcrystalline domains are randomly oriented with respect to the polarisation of the source laser and so contribute inhomogeneously to the response, depending on the sampled spot. This inhomogeneity is accounted for by a matrix of multiple wax spectra used to digitally process the spectra. The same methodology was applied to removal of the glass substrate contributions, illustrating that spectroscopic differentiation of tissue regions can be achieved using Raman spectroscopy, free from confounding factors of wax and substrate contributions.

4.3 Materials and Methods

4.3.1 Sample preparation

Following ethical approval from the Research Ethics Committee, St James' Hospital, Dublin, Ireland, informed consent was obtained from 3 patients who had undergone an oral biopsy which was diagnosed as benign oral hyperplasia. Tissue blocks from these patients were obtained, for use in the study. 10μm parallel sections were cut from the FFPP tissue blocks and mounted on glass slides for Raman spectroscopy.

For the chemical dewaxing of tissue sections, routine xylene dewaxing was performed, which involves sequentially immersing the FFPP tissue sections in two baths of xylene, two of ethanol and one bath of industrial methylated spirits for 5,4,3,2 and 1 minute respectively[3]. Routine Hematoxylin and Eosin (H&E) was performed on parallel tissue sections to aid in the delineation of the different regions in the tissues[16]. 82 component spectra were available from an-in house library of spectra of pure biological macromolecules. Matrigel which is a solubilised basement membrane preparation, was also trialled as a multicomponent reference biological spectrum, at it has previously been employed as such in background correction procedures for FTIR [17]. Cell components were purchased from Sigma Aldrich. The components were placed on calcium fluoride disks prior to Raman spectroscopy measurement. All the components were measured in powder form except for DNA, RNA, cytochrome C, stearic acid, and collagen which were measured in an aqueous solution. The spectra of the 20 components (listed in table 1) selected by the Data Analysis procedure are presented in Supplementary Fig 1. For the Matrigel measurements; matrigel (Sigma Aldrich) was placed on a calcium fluoride disk prior to Raman recording of a matrix of 300 spectral points.

4.3.2 Instrumentation

A confocal Horiba Jobin Yvon LabRam HR 800 Raman (upright) spectroscopic microscope was used to record the spectra of the tissue and biochemical components. The microscope has an automated xyz stage and is coupled to a Peltier cooled CCD detector. A 50mW diode laser with 532 nm wavelength was used and the grating was set at 600 grooves/mm, while the confocal hole was set at 100µm. For mapping acquisition, the regions to map were selected using a 100X objective (MPLAN N Olympus, Japan), which also collected the backscattered light. The spectra were acquired over two accumulations, totalling 20 seconds per spectrum. The step size was set at 5µm and the spectral range was 400-1800cm^{-1}. The spectra of the cell

components were acquired between 10-30 seconds and over 2-3 accumulations depending on the quality of the signal from the specific sample.

4.3.3 Data Analysis

All the data analysis was carried out using Matlab (Mathworks, US) with the PLS-Toolbox (Eigenvector Research Inc.) and in-house algorithms. The spectra were preprocessed by first smoothing using a Savitsky Golay filter (5th order, 13 points). They were then rubberbanded to correct the baseline and vector normalised[18]. Principal component analysis (PCA), an unsupervised multivariate technique, was used to reduce the dimensionality of the data by calculating principal components which describe the greatest variance in the dataset[19]. PCA was employed to demonstrate the spectral differentiation of regions of epithelium and connective tissue, and the PC loadings were examined to elucidate the biochemical origin of the differentiation, as well as contributions of wax or substrate spectral features.

Classical least squares (CLS) fitting is a supervised technique used to estimate the weighted contributions of a set of input spectra to a sample spectrum. It assumes that any complex spectrum is the weighted sum of all the base components that contribute to the spectrum as described in Equation 1[20].

$$A = a_1 C_1 + a_2 C_2 + a_3 C_3 \ldots$$ Equation 4-1

where A represents a sample spectrum, a1, a2 and a3 are component spectra and C1, C2 and C3 are the weighting coefficients, or concentrations, applied to each component spectrum in the summation. If one then considers the case of Raman spectroscopy in which a large number of variables are recorded and not all contributing spectral components are known, then there is

an error (residual) associated with the estimation which will equate to the difference between the sample spectrum and the sum of the weighted spectra:

$$E_j = A_j - (a_{1j}C_1 + a_{2j}C_2 + a_{3j}C_3)$$ Equation 4-2

Where Ej is the error associated with the intensity of the jth term (or jth wavenumber). The least squares method aims to minimise the error in fitting the sample spectrum, A. The minimum error occurs when the differentiation of the sum of squared errors is equal to zero[21]. Differentiation of Equation 4-2 with respect to each of the coefficients results in a set of equations which can be solved using simultaneous equations or matrix mathematics. Non negatively constrained least squares analysis (NNLS) is a technique similar to that of CLS. NNLS is used to estimate the weighted contributions of a set of input spectra in a sample spectrum. However, unlike CLS, NNLS introduces non-negative constraints on the weighting co-efficients of the input spectra[22].

For this study, in lieu of using an average spectrum of wax or glass, matrices acquired from maps of the wax and glass were used. The wax maps were taken from regions in the samples with no tissue, while the glass maps were taken from a clean glass slide. The matrices included about 300 spectral points and were processed in a similar fashion to the sample spectra. To account for spectral drift from day to day, the wax spectra were interpolated to every quarter wavenumber. Interpolated spectra were then shifted in both directions in increments of 0.25cm^{-1} to a maximum of +/-1$cm^{-1,}$ and then added to the original matrix of wax. Using an in-house Matlab algorithm, whereby the Raman spectra of 82 cell components (details in supplementary table 1) were iteratively tested to represent the tissue for NNLS and the combination of components associated with the least residual error was selected for use in the wax and glass subtraction, as listed in Table 4-1 Cell components (Sigma Aldrich) used as inputs for NNLSTable

4-1. The wax and glass matrices were then subtracted from the original processed spectra. The steps are summarised in Figure 4.1 The NNLS procedure weighted the contributions of each in an unsupervised fashion. However, the intention was to optimise the wax removal protocol, rather than to model the tissue analytically, based on the relative contributions of the specific components. Least Squares analysis, either supervised or unsupervised, has previously been used in a number of studies as a spectral analysis protocol[23,24]. CLS was used to determine the wax contribution to the first principal component of the unprocessed, chemically processed and digitally processed tissue.

Table 4-1 Cell components (Sigma Aldrich) used as inputs for NNLS

Cell Components					
Proteins	Lipids	Nucleic acids	Nucleic bases	Glycosaminoglycans	Other
Actin Collagen Cytochrome C L-Histidine L-Serine L-Theronine Peroxidase Ubiquitin Apo E2	Stearic acid P-Choline P-Ethanolamine	RNA DNA	Thymidine Uracil Guanine	Heparin Hyauloronic acid	Taurin

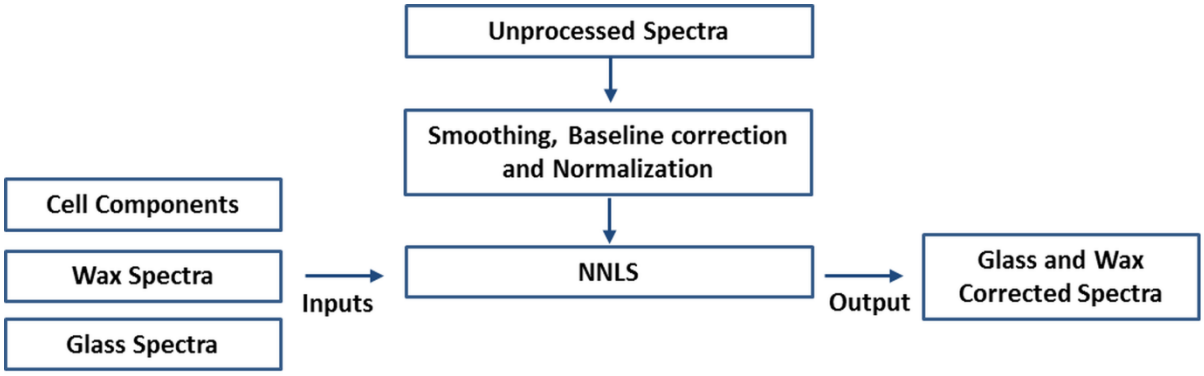

Figure 4.1 Summary of the processing steps for the Raman spectra.

4.4 Results

Figure 4.2 shows a H&E stained FFPP tissue section, highlighting the epithelium and connective tissue regions. Raman maps were taken of the epithelium and connective tissue regions in the unprocessed FFPP tissues, the mean and standard deviation of which can be seen in Fig 3. Initially, PCA was performed on the tissue spectra without removing the glass and wax contributions (Figure 4.4 (A)). The first principal component (PC1), which explained 59% of the variance, does not differentiate the two tissue types, and is dominated by wax peaks at 1063, 1134, 1172, 1296, 1419, 1441 and 1464 cm^{-1} (Figure 4.4 (B)), which account for 38% of the loading. The broad streaking of the datasets indicates a significant variability of these contributions across both datasets. The second principal component (PC2), according to which the epithelium and connective tissue spectra are differentiated, explained 5% of the variance (Fig 4 (C)). The datasets are more tightly clustered with respect to PC2 and the loading has strong peaks at 815, 857, 875, 920 and 1245 cm^{-1}. These relate to collagen type 1 which, together with fibroblast cells, is the main component of the connective tissue25,26. The loading of PC2 also contains contributions from wax, but notably, some of them contribute negatively

to the loading (1419, 1438 cm^{-1}), while some contribute positively (1136, 1296 cm^{-1}) indicating that the spectrum of the wax itself is not uniform across the tissue section. Glass peaks do not appear in the first or second principal component (Figure 4.4 (C)) indicating that the glass contribution to the spectra is not significant. Thus, the differentiation, using Raman microspectroscopy, of the two clearly biochemically distinct regions of tissue is based on their wax content, rather than their biochemical composition, which does not bode well for the potential to distinguish differing pathologies in the same tissue regions.

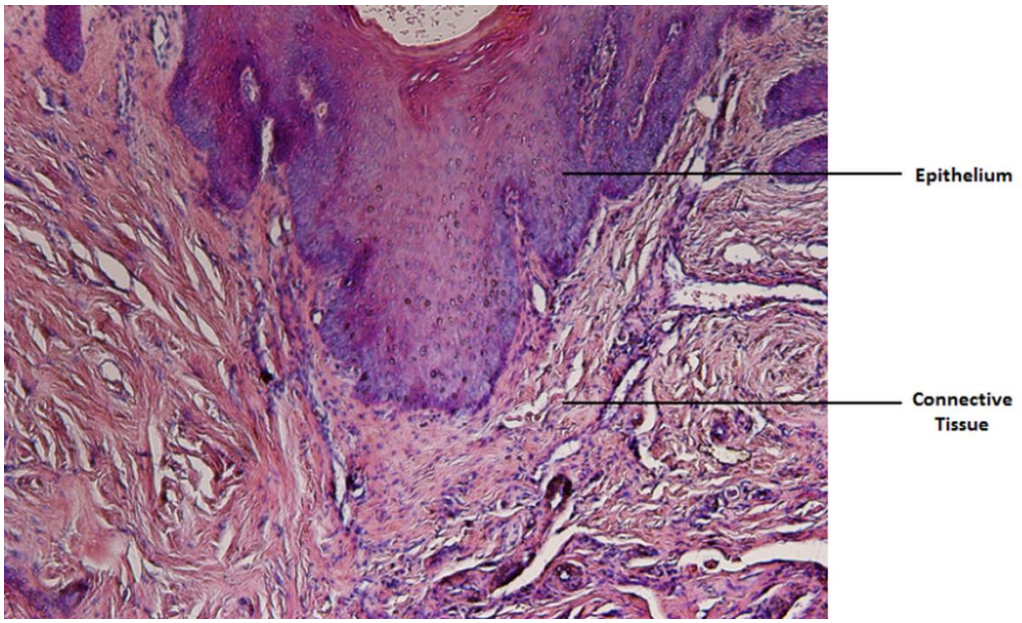

Figure 4.2 Bright field image of H&E stained FFPP tissue showing the epithelium and connective tissue regions.

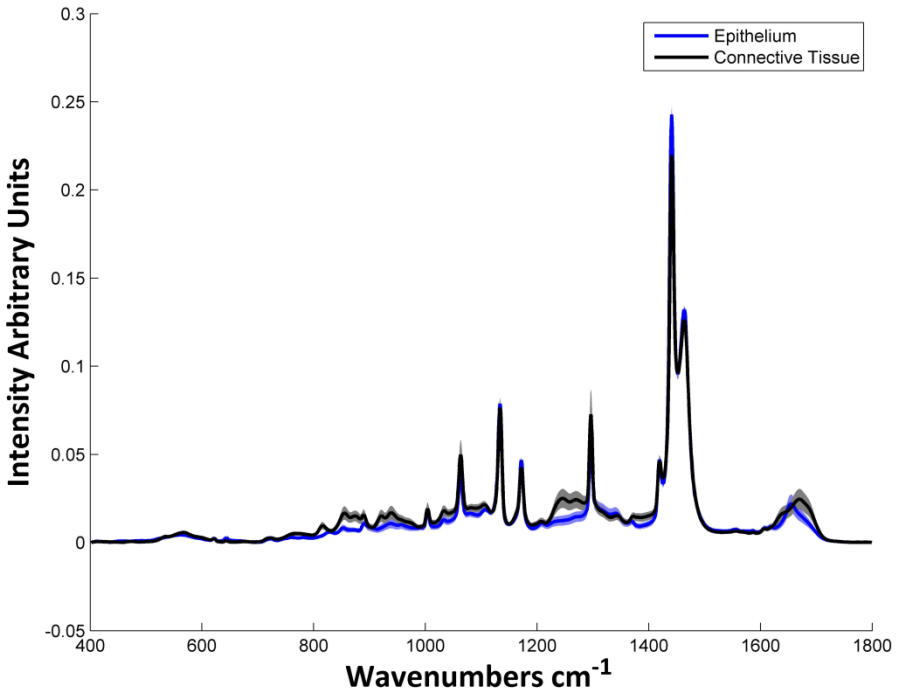

Figure 4.3 Mean Raman spectra of epithelium and connective tissue in the unprocessed tissue sample. Shading denotes the standard deviation.

The chemically dewaxed tissue sections were visually different from the unprocessed tissue sections, as they appeared whiter, indicating increased scatter which may be due to increased porosity as the wax and some of the lipidic content is removed in the dehydration process. Raman analysis of the chemically dewaxed tissue sections showed that, although the wax peaks at 1063cm^{-1} 1134cm^{-1}, 1172cm^{-1}, 1296cm^{-1}, 1419cm^{-1}, 1441cm^{-1} and 1464cm^{-1} were reduced in comparison to the unprocessed tissue, they were not eliminated. Furthermore, the glass contribution in the chemically processed FFPP tissues was higher compared to the unprocessed tissues (Figure 4.5 (A)). Acquiring the spectra for connective tissue was problematic, as many of the spectra were saturated. This may be due to the increased scattering of the tissue after dewaxing, a phenomenon which can be reduced in a water immersion measurement protocol[27]. The epithelium appears to retain more wax and has a higher glass contribution in comparison to the connective tissue (Figure 4.5 (B)).

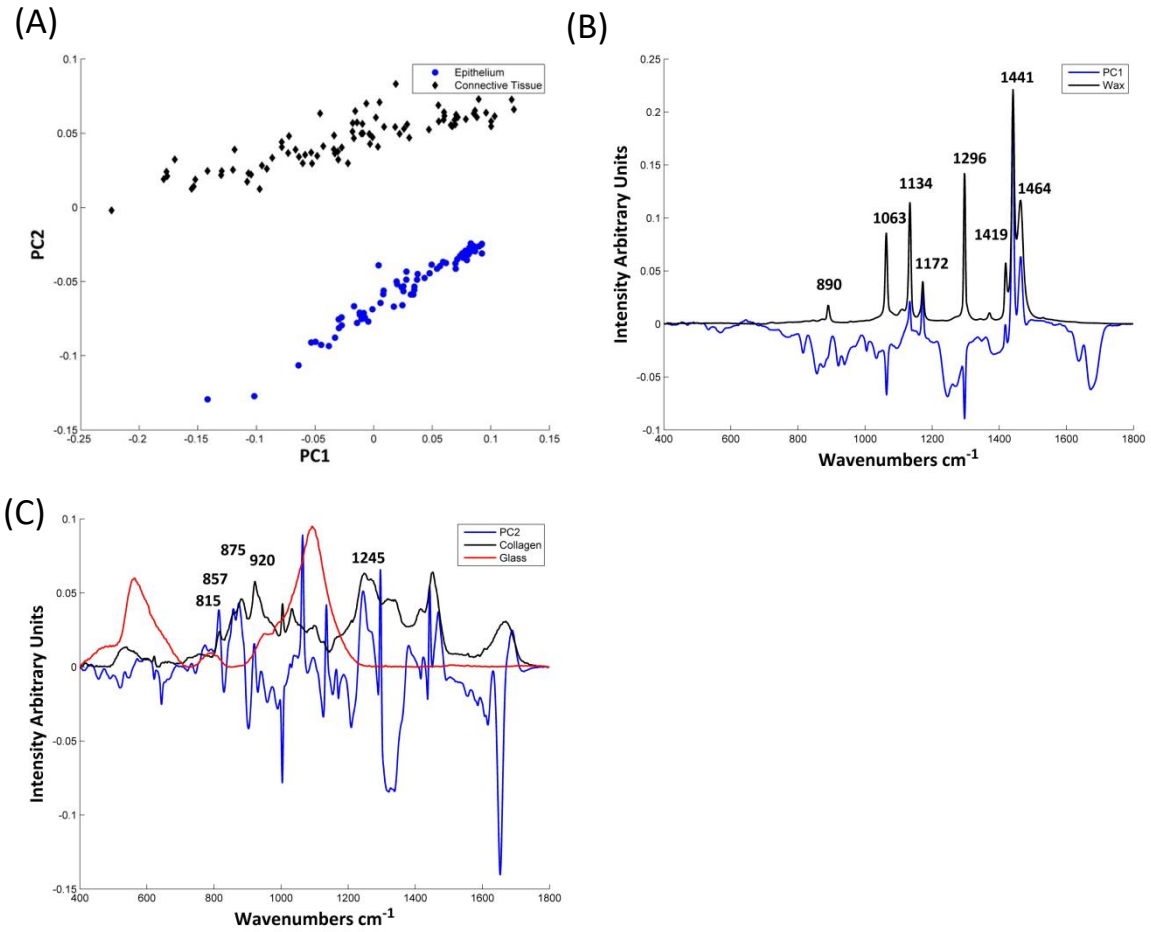

Figure 4.4 (A) PCA scatter plot of unprocessed epithelium and connective tissue shows a clear separation on the second principal component with even distribution along the first principal component. (B) The first principal component is dominated by wax spectral peaks. (C) The second principal component is mainly collagen type 1 associated peaks on the positive side, relating to connective tissue, and protein associated peaks on the negative side, relating to epithelium.

(A) (B)

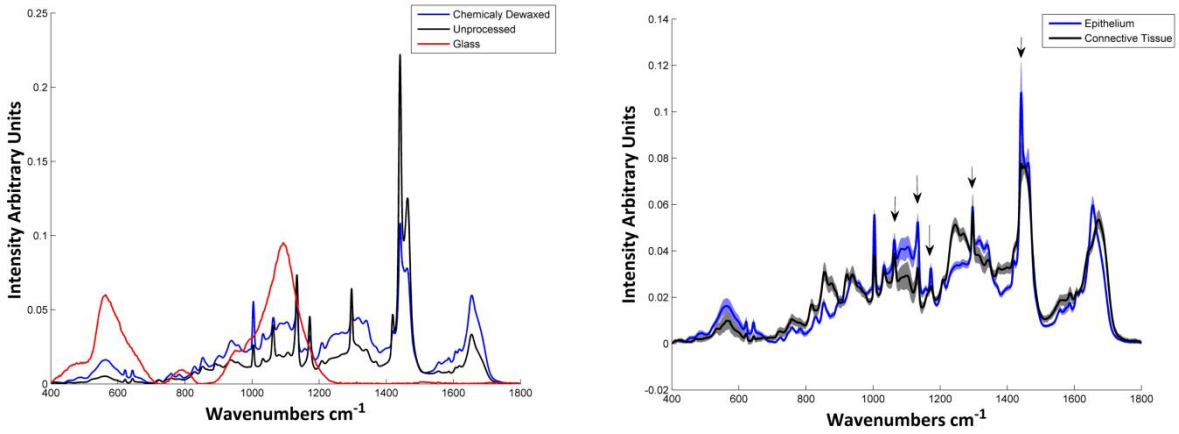

Figure 4.5 (A) Mean Raman spectra of epithelium in the unprocessed (black) and chemically dewaxed (blue) tissue sample and mean Raman spectrum of glass (red). Compared to the unprocessed epithelial tissue, the chemically dewaxed tissue has less wax contribution and more glass. (B) Mean Raman spectra of epithelium and connective tissue in chemically dewaxed FFPP tissue section. Shading denotes the standard deviation. The black arrows highlight peaks from wax. The epithelium has more wax and glass contribution than the connective tissue.

PCA of the epithelium and connective tissue showed that the collagen and protein related peaks 815, 857, 875, 920 and 1245 cm^{-1} had been promoted to the first principal component which explains 75% of the variance (Figure 4.6). However, although the contribution has been significantly reduced, there was still 32% wax contribution in the loading of the first PC, which positively discriminates the epithelium. Additionally, the two broad peaks of glass can be discerned in the loading of the first PC. This is to be expected, as there was a higher contribution of wax and glass in the epithelium.

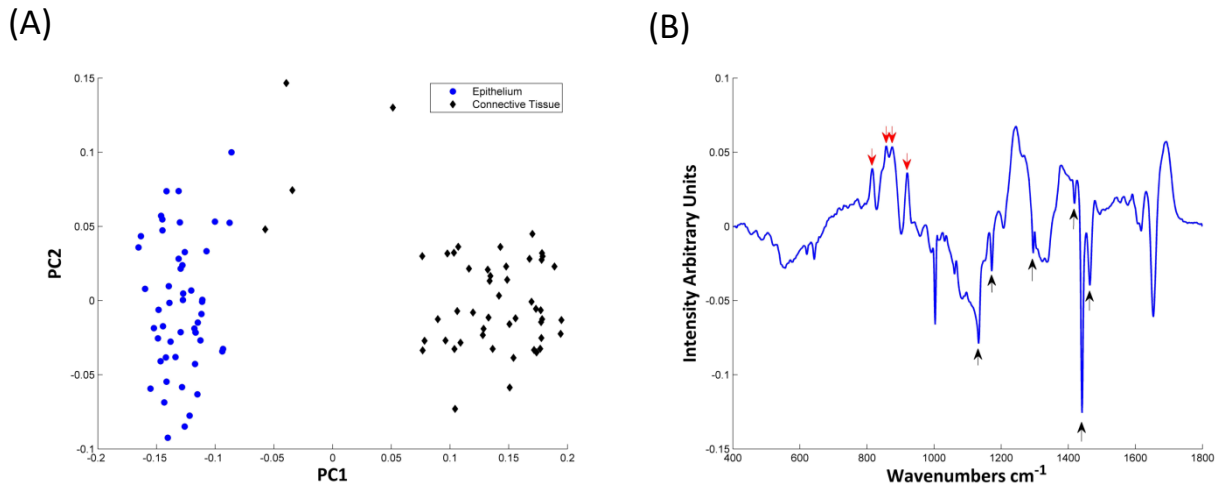

Figure 4.6 (A) PCA scatter plot of chemically dewaxed epithelium and connective tissue shows a separation on the first principal component. (B) On the positive side of the first principal component, collagen type 1 related peaks (red arrows) can be distinguished. While some wax (black arrows) and protein peaks can be distinguished on the negative side.

The spectral dataset for the FFPP sections, in which the wax contribution was removed digitally (using NNLS), were analysed. Wax removal with a single wax spectrum was found to be insufficient, as most of the wax peaks were either over or underestimated. PCA of the matrix of wax spectra clearly illustrates the variability of the spectral signature of the nominally single chemical constituent, as shown in the scatterplot in Figure 4.7 (A). Notably, rather than exhibiting a widely scattered cluster centred about zero, the curved distribution is suggestive of an interdependence of PC1 (Figure 4.7 (B)) and PC2 (Figure 4.7 (C)), each indicating the degree of variability of the wax spectrum on a microscopic level. Although, macroscopically, paraffin is an amorphous wax, on the microscopic scale of the Raman laser spot, it presents a microcrystalline structure[28], and, as the laser is polarised, the registered spectrum is significantly variable, depending on the relative orientation of the laser polarisation and the microcrystalline structures. A single or averaged spectrum does not represent the specific

spectral contributions at any point on the tissue, and therefore a subtraction protocol based on such results in incomplete removal of the spectral contributions of the paraffin.

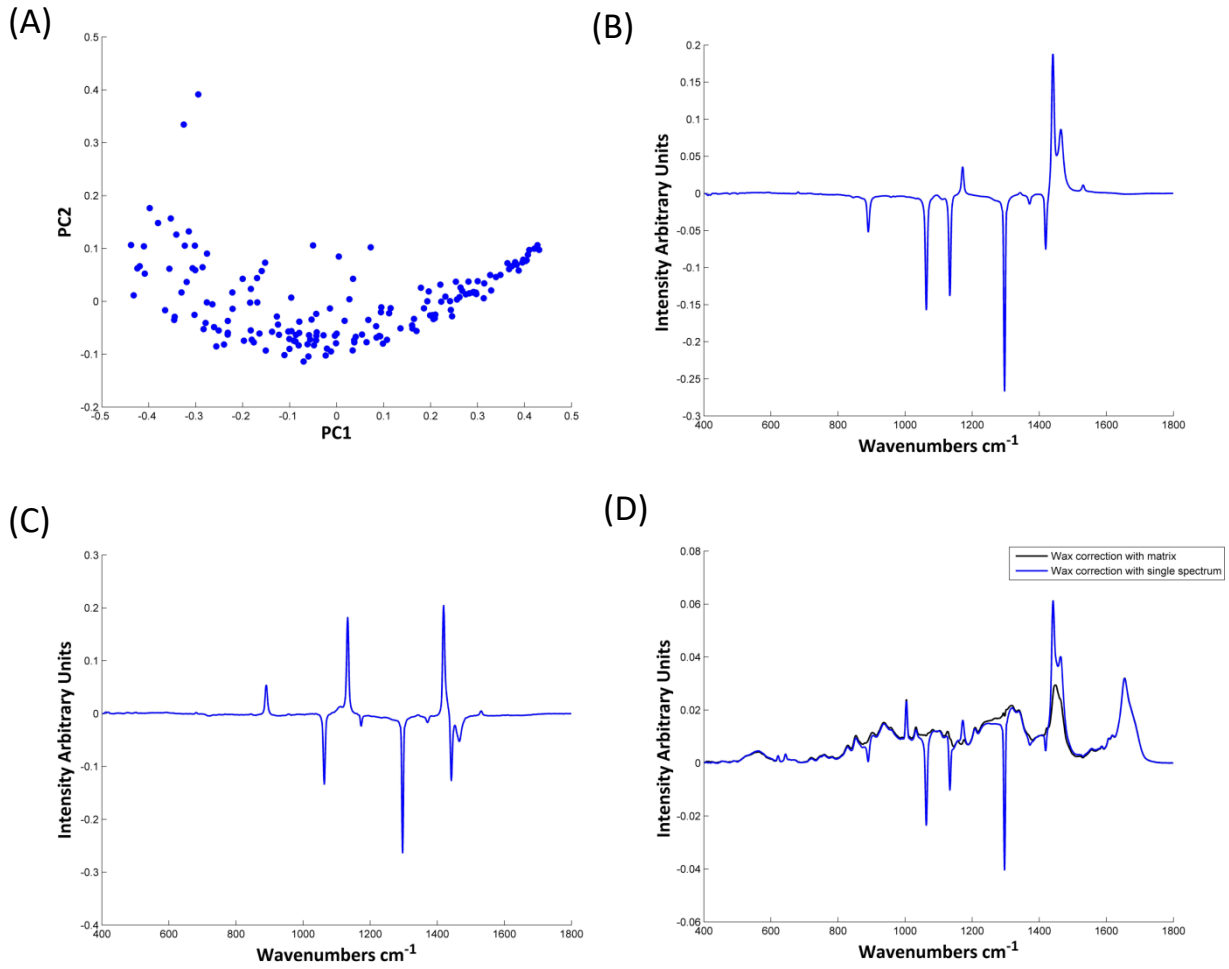

Figure 4.7 (A) PCA scatter plot of Wax matrix. (B) The first Principal component which explains 85% of the variance (C) The second principal component (D) Comparison of digital wax removal in epithelial tissue using a matrix of wax vs a single wax spectrum. Note, although the NNLS protocol constrains the weightings co-efficients to be non-negative, the component spectra can have negative contributions.

Rather than averaging; a matrix of 300 individual spectra retains the intrinsic variability of the wax contributions, each of which is individually weighted in NNLS subtraction. The protocol resulted in much more efficient wax removal, as shown in Figure 4.7 (D). The resultant spectra of epithelium and connective tissue appear more uniform and have reduced wax contribution (Figure 4.8). This was also reflected in the PCA of epithelium and connective tissue, as the wax contribution to the loading of the first PC, which accounted for 90% of the variance, was reduced to 10%. The collagen and protein related peaks at 815 cm^{-1}, 857, 875, 920 and 1245 cm^{-1} can be clearly distinguished in the first PC. Additionally, the spectra were tightly grouped according to PC1 in the PCA scatter plot, suggesting reduced variability within the groups and greater uniformity (Figure 4.9), although considerable point to point sample variability is evident by the spread according to PC2, particularly for the case of the connective tissue.

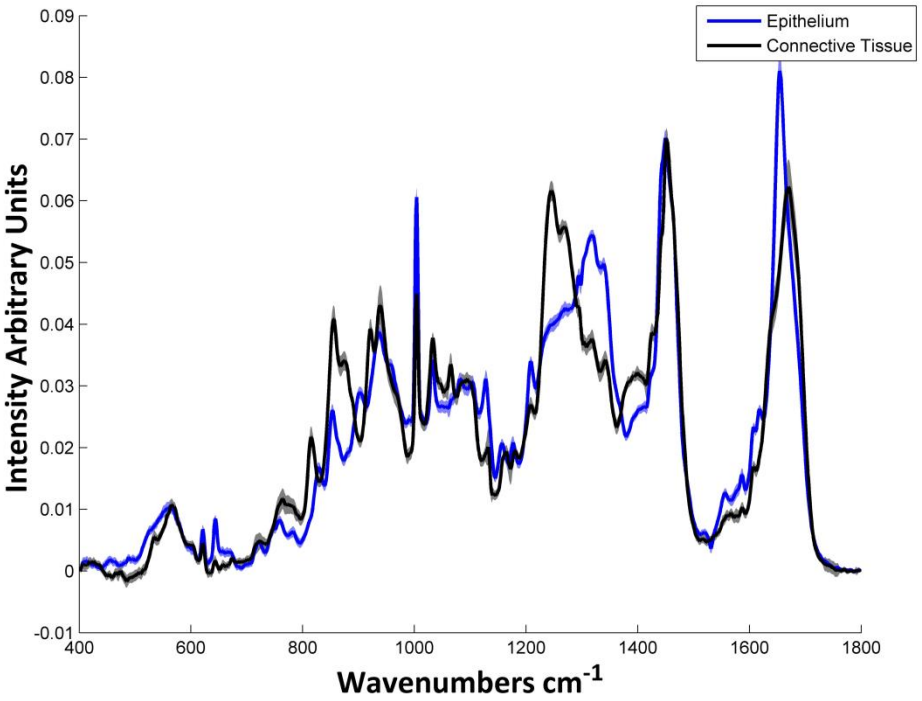

Figure 4.8 Mean Raman spectra of epithelial and connective tissue after digital wax removal. Shading denotes the standard deviation.

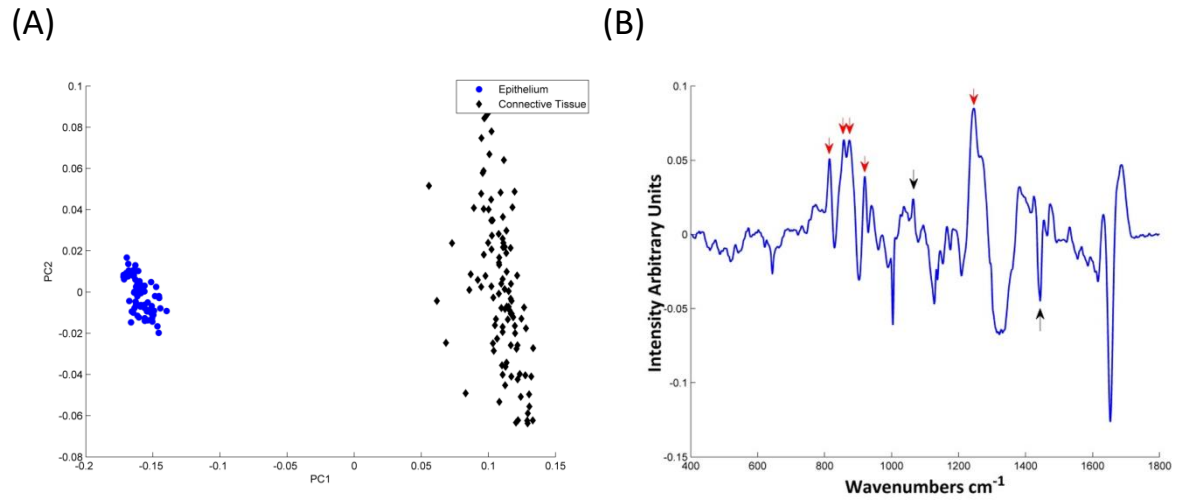

Figure 4.9 (A) PCA scatter plot of epithelium and connective tissue after digital wax removal using the cell components as a model. Epithelium is made up of tightly packed cells whereas connective tissue contains collagen fibrils, fibroblasts, blood vessels and oil ducts leading to a greater variability in the latter according to PC2 (B) First PC after digital wax removal. Wax contribution, black arrows, is reduced. The red arrows refer to 815, 857, 875, 920 and 1245 cm^{-1} which are collagen related peaks.

For the glass removal, NNLS was also used. In a similar fashion to the wax removal, the glass contribution was reduced without affecting the integrity of the spectra (Figure 4.10). However, in contrast to the case of wax, where the use of a matrix conferred a marked improvement, there was no real difference between the use of a glass matrix or single spectrum in glass removal, indicating that the glass spectrum is more spatially homogenous (Figure 4.10 (B)). This is confirmed by the spectra being equally dispersed around the PC1 and PC2 axes, and showing no systematic variability (Figure 4.10 (C)).

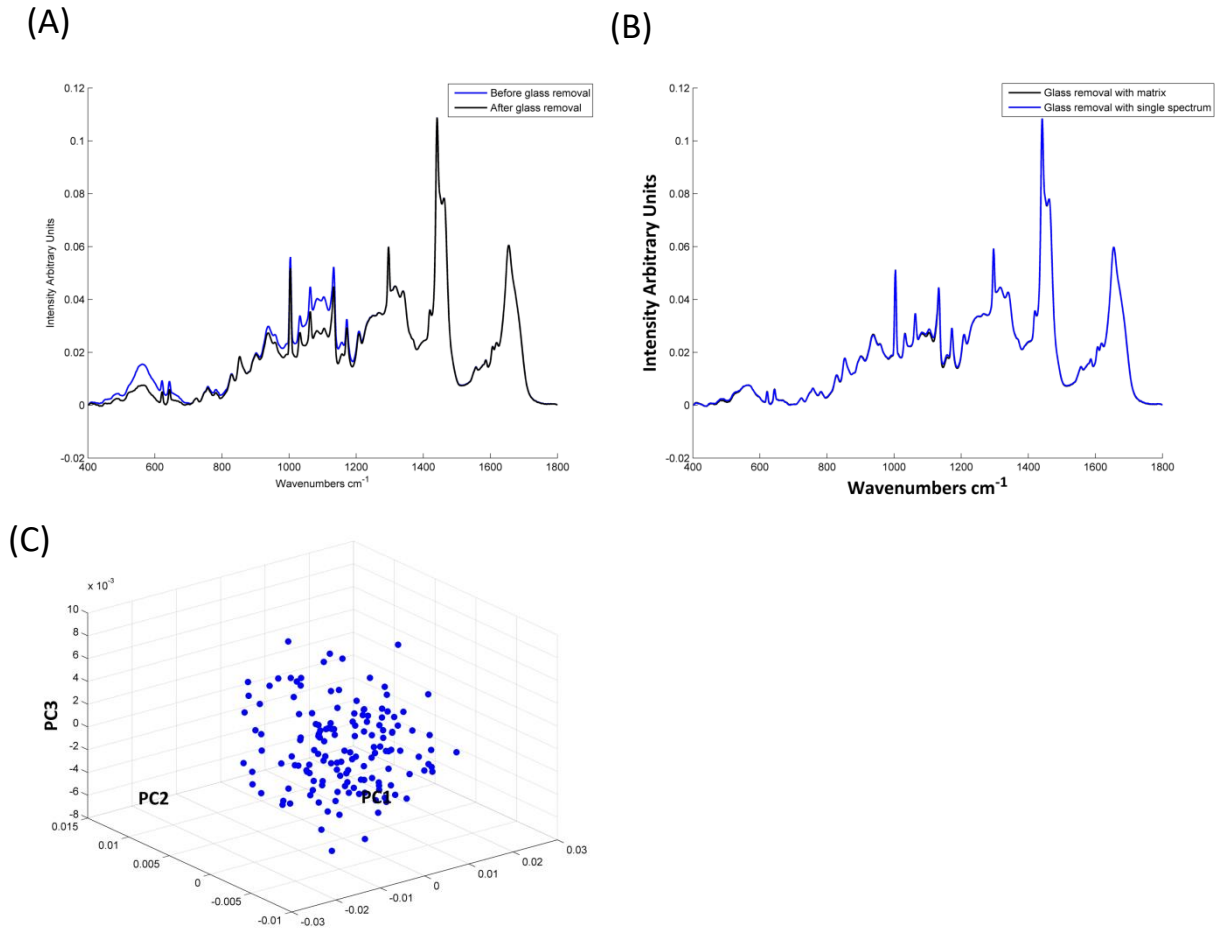

Figure 4.10 (A) Mean Raman spectra of chemically dewaxed epithelial tissue before and after digital glass removal. (B) Mean Raman spectra of chemically dewaxed epithelial tissue with glass removal using a matrix and a single spectrum. (C) PCA scatter plot of the glass matrix.

4.5 Conclusions

One of the advantages of using vibrational spectroscopy techniques, such as Raman spectroscopy, to analyse biological tissues is that they require minimal sample preparation. In this study, chemical dewaxing, which increases the processing time and alters the composition of the tissue, has been substituted by an improved protocol for digital dewaxing. The demand

for an improved protocol for spectroscopic analysis of the FFPP tissue sections had been previously highlighted[29]. As demonstrated in Figure 4.4 the contributions from the wax significantly influence spectral analysis, which establishes the importance of subtracting it. From the results, it is clear that this method of digital removal greatly reduces the spectral contribution of wax, as the variance from the wax contribution to the first principal component is reduced from 38% and 32% in unprocessed and chemically processed samples respectively to 10% in the digitally dewaxed samples. Furthermore, the chemically dewaxed FFPP tissue samples had more glass background in the epithelium and more scattering background in the connective tissue compared to their unprocessed counterparts. This is most likely due to refractive index matching between the wax and glass resulting in reduced scattering of the incident light and Raman bands themselves in the unprocessed samples. The superiority of digital versus chemical wax removal has also previously been reported in FTIR spectroscopy, whereby modified extended multiplicative signal correction (EMSC) was used for the wax removal[30]. Because of the variability between, and within, different types of tissue, while using a single mean cellular spectrum as a model or reference, such as has been previously reported for EMSC, is effective for cytology samples, it underestimates the complexity of histopathological tissue samples which can include epithelium and connective tissue, as well as different types of pathology[13]. Similarly, both EMSC and Independent component analysis rely on a definitive model of wax (such as a three source model[8]) which does not take into account the variability of the paraffin wax spectrum, accentuated in Raman spectroscopy due the polarisation dependence of commonly employed instruments. The use of multiple spectral components for the reference and wax contributions provides flexibility to account for the observed point to point variations of both.

This study is the first to utilize cell components and a wax matrix in the digital removal of wax from FFPP tissue sections. As the wax spectrum is composed of a number of peaks, and the ratio between these peaks is variable from one wax spectrum to another; using a matrix of wax captures this variability which therefore reduces the residual error in the NNLS model and results in improved estimated spectra. Paraffin wax is made up of linear hydrocarbon molecules which can form crystallites on a microscopic scale[21]. As these can be randomly oriented with respect to the laser polarisation, their contribution to the Raman spectrum of the tissue can be highly spatially variable. Polarisation dependent studies are frequently employed to study the orientation of, for example, molecules in liquid crystals[31] and have been employed to study the constituents of bone[32]. A study conducted, exploiting the polarisation dependence in biological tissues, has shown that in probing the deeper layers of the tissues the backscattered light has a greater chance of being depolarised by diffusion compared to the more superficial layers[33].

In contrast, glass has two broad peaks in the fingerprint region. Almost no difference was observed in the subtraction of glass using a single glass spectrum and using a glass matrix. However, this may be due to the fact that the glass contribution was not high in these samples and more or less uniform across the sample, so the matrix subtraction may be more effective in samples which show greater variability.

The cell components were selected from a pool of 82 components based on their fit of the NNLS model and, similar to the wax matrix, they confer a significant improvement on the wax subtraction. Choosing whether to use a single, commercially available component such as Matrigel or collections of biomolecules as representation of tissue constituents can depend on the application and the expected variability of the samples under investigation. For the application demonstrated here, the cell components gave

superior performance in the removal of wax contributions to the spectra as the residual error was reduced from 18% when Matrigel was used in the NNLS correction to 8% when the cell components were used. A further improvement in the efficacy of removal could potentially be achieved by a more representative choice of cellular constituent spectra, targeted at specific tissue types.

By interpolating the wax spectra to every quarter wavenumber and shifting in both directions, the small spectral drifts from day to day calibration were accounted for resulting in a more accurate wax removal.

For a diagnostic technique to be translatable into routine clinical use it has to be affordable, and reliable. Effective digital subtraction of glass contribution from spectra means that glass could be used for FFPP or cytological samples, making vibrational spectroscopy techniques more affordable. The digital subtraction of wax using a matrix, decreases the processing time and involves less modification of the samples resulting in more reliable results.

References

1. Diem M, Mazur A, Lenau K, Schubert J, Bird B, Miljkovic M, Krafft C, Popp J. Molecular pathology via IR and Raman spectral imaging. *Journal of Biophotonics* 2013;6:855-886.

2. Baker MJ, Trevisan J, Bassan P, Bhargava R, Butler HJ, Dorling KM, Fielden PR, Fogarty SW, Fullwood NJ, Heys KA, Hughes C, Lasch P, Martin-Hirsch PL, Obinaju B, Sockalingum GD, Sule-Suso J, Strong RJ, Walsh MJ, Wood BR, Gardner P, Martin FL. Using Fourier transform IR spectroscopy to analyze biological materials. *Nature Protocols* 2014;9:1771-1791.

3. Faolain EO, Hunter MB, Byrne JM, Kelehan P, Lambkin HA, Byrne HJ, Lyng FM. Raman spectroscopic evaluation of efficacy of current paraffin wax section dewaxing agents. *Journal of Histochemistry & Cytochemistry* 2005;53:121-129.

4. Fullwood LM, Griffiths D, Ashton K, Dawson T, Lea RW, Davis C, Bonnier F, Byrne HJ, Baker MJ. Effect of substrate choice and tissue type on tissue preparation for spectral histopathology by Raman microspectroscopy. *Analyst* 2014;139:446-454.

5. O Faolain E, Hunter MB, Byrne JM, Kelehan P, McNamara M, Byrne HJ, Lyng FM. A study examining the effects of tissue processing on human tissue sections using vibrational spectroscopy. *Vibrational Spectroscopy* 2005;38:121-127.

6. Ali SM, Bonnier F, Tfayli A, Lambkin H, Flynn K, McDonagh V, Healy C, Lee TC, Lyng FM, Byrne HJ. Raman spectroscopic analysis of human skin tissue sections ex-vivo: evaluation of the effects of tissue processing and dewaxing. *Journal of Biomedical Optics* 2013;18.

7. Huang ZW, McWilliams A, Lam S, English J, McLean DI, Lui H, Zeng H. Effect of formalin fixation on the near-infrared Raman spectroscopy of normal and cancerous human bronchial tissues. *International Journal of Oncology* 2003;23:649-655.

8. Vrabie V, Gobinet C, Piot O, Tfayli A, Bernard P, Huez R, Manfait M. Independent component analysis of Raman spectra: Application on paraffin-embedded skin biopsies. *Biomedical Signal Processing and Control* 2007;2:40-50.

9. Tfayli A, Gobinet C, Vrabie V, Huez R, Manfait M, Piot O. Digital Dewaxing of Raman Signals: Discrimination Between Nevi and Melanoma Spectra Obtained from Paraffin-Embedded Skin Biopsies. *Applied Spectroscopy* 2009;63:564-570.

10. Mikoliunaite L, Rodriguez RD, Sheremet E, Kolchuzhin V, Mehner J, Ramanavicius A, Zahn DRT. The substrate matters in the Raman spectroscopy analysis of cells. *Scientific Reports* 2015;5.

11. Kerr LT, Byrne HJ, Hennelly BM. Optimal Choice Of Sample Substrate And Laser Wavelength For Raman Spectroscopic Analysis Of Biological Specimen. *Anal Methods* 2015;7:5041-5052.

12. Bonnier F, Traynor D, Kearney P, Clarke C, Knief P, Martin C, O'Leary JJ, Byrne HJ, Lyng F. Processing ThinPrep cervical cytological samples for Raman spectroscopic analysis. *Analytical Methods* 2014;6:7831-7841.

13. Kerr LT, Hennelly BM. A multivariate statistical investigation of background subtraction algorithms for Raman spectra of cytology samples recorded on glass slides. *Chemometrics and Intelligent Laboratory Systems* 2016;158:61-68.

14. Beier BD, Berger AJ. Method for automated background subtraction from Raman spectra containing known contaminants. *Analyst* 2009;134:1198-1202.

15. Liland KH, Kohler A, Afseth NK. Model-based pre-processing in Raman spectroscopy of biological samples. *Journal of Raman Spectroscopy* 2016;47:643-650.

16. Wittekind D. Traditional staining for routine diagnostic pathology including the role of tannic acid. 1. Value and limitations of the hematoxylin-eosin stain. *Biotechnic & Histochemistry* 2003;78:261-270.

17. Bassan P, Kohler A, Martens H, Lee J, Byrne HJ, Dumas P, Gazi E, Brown M, Clarke N, Gardner P. Resonant Mie Scattering (RMieS) correction of infrared spectra from highly scattering biological samples. *Analyst* 2010;135:268-277.

18. Trevisan J, Angelov PP, Carmichael PL, Scott AD, Martin FL. Extracting biological information with computational analysis of Fourier-transform infrared (FTIR) biospectroscopy datasets: current practices to future perspectives. *Analyst* 2012;137:3202-3215.

19. Wold S, Esbensen K, Geladi P.Principal Component Analysis. *Chemometrics and Intelligent Laboratory Systems* 1987;2:37-52.

20. Mark H, Workman J. Chemometrics in Spectroscopy Classical Least Squares , Part I : Mathematical Theory, 2010.

21. Rencher ACC, William F. Methods of Multivariate Analysis. John Wiley and Sons, 2012.
22. Chen D, Plemmons RJ. Nonnegativity constraints in numerical analysis. In: Bultheel A, Cools R, eds. *The Birth of Numerical Analysis*. Singapore: World Scientific, 2010.

23. Keating ME, Bonnier F, Byrne HJ. Spectral cross-correlation as a supervised approach for the analysis of complex Raman datasets: the case of nanoparticles in biological cells. *Analyst* 2012;137:5792-5802.

24. Notingher L, Jell G, Notingher PL, Bisson I, Tsigkou O, Polak JM, Stevens MM, Hench LL. Multivariate analysis of Raman spectra for in vitro non-invasive studies of living cells. *Journal of Molecular Structure* 2005;744:179-185.

25. Nguyen TT, Gobinet C, Feru J, Brassart-Pasco S, Manfait M, Piot O. Characterization of Type I and IV Collagens by Raman Microspectroscopy: Identification of Spectral Markers of the Dermo-Epidermal Junction. *Spectroscopy-an International Journal* 2012;27:421-427.

26. Squier C, Brogden K. Human Oral Mucosa: Development, Structure and Function. New Jersey: John Wiley & Sons, 2010:176.

27. Bonnier F, Mehmood A, Knief P, Meade AD, Hornebeck W, Lambkin H, Flynn K, McDonagh V, Healy C, Lee TC, Lyng FM, Byrne HJ. In vitro analysis of immersed human tissues by Raman microspectroscopy. *Journal of Raman Spectroscopy* 2011;42:888-896.

28. Zbik M, Horn RG, Shaw N. AFM study of paraffin wax surfaces. *Colloids and Surfaces a-Physicochemical and Engineering Aspects* 2006;287:139-146.

29. Byrne HJ, Baranska M, Puppels GJ, Stone N, Wood B, Gough KM, Lasch P, Heraud P, Sule-Suso J, Sockalingum GD. Spectropathology for the next generation: Quo vadis? *Analyst* 2015;140:2066-2073.

30. Nallala J, Lloyd GR, Stone N. Evaluation of different tissue de-paraffinization procedures for infrared spectral imaging. *Analyst* 2015;140:2369-2375.

31. Davey AP, Howard RG, Blau WJ, Byrne HJ. Polarized Photoluminescence and Measurement of Degree of Order in Mixed Oriented Polymer Liquid Crystal Films. *International Journal of Polymeric Materials and Polymeric Biomaterials* 1999;44:241-258.

32. Makowski AJ, Patil CA, Mahadevan-Jansen A, Nyman JS. Polarization control of Raman spectroscopy optimizes the assessment of bone tissue. *Journal of Biomedical Optics* 2013;18.

33. Smith ZJ, Berger AJ. Surface-sensitive polarized Raman spectroscopy of biological tissue. *Optics Letters* 2005;30:1363-1365.

Chapter 5: Raman spectroscopy for the identification of dysplastic changes in FFPP oral tissues (an intra-patient study)

5.1 Introduction

OSCC is commonly preceded by a range of cell and tissue alterations, described in Table 5-2, which are similar to the changes seen in carcinoma, but restricted to the surface epithelium. These changes, termed dysplasia, have been classified by the World Health Organisation (WHO), according to their severity, as[1];

Table 5-1 WHO classification of oral dysplasia

Degree of dysplasia	**Features**
Mild dysplasia	Architectural (tissue) changes limited to the lower third of the epithelium with minimum cellular atypia
Moderate dysplasia	Architectural changes extend to the middle third of the epithelium with cellular atypia
Severe dysplasia	Architectural changes that cover more than two thirds of the epithelium with marked cellular atypia
Carcinoma in situ	Architectural changes that extend to the full thickness of the epithelium with marked cellular atypia. The difference between

	carcinoma in situ and OSCC is the presence of invasion in OSCC.

The WHO classification system is the most widely used, although other classification systems have been devised, such as the one by Smith and Pindborg which classifies dysplasia as; none, present, or marked[2]. The oral intraepithelial neoplasia (OIN) System classifies dysplasia as none, OIN 1 and 2 which correspond to mild and moderate dysplasia respectively and OIN 3 which corresponds to severe and/or carcinoma in situ[3].

Table 5-2 Cellular and tissue features of oral epithelial dysplasia[4]

Cellular changes	**Tissue changes**
Increased nuclear/cytoplasmic ratio	Loss of polarity of the basal cells
Increased number and size of nucleoli	Drop shaped rete ridges
Cellular pleomorphism (variations in size and shape)	Disordered maturation from basal to squamous cells
Nuclear pleomorphism	Increased cellular density
Increased number of mitotic figures	Basal cell hyperplasia
Abnormal mitotic figures (abnormal in shape or location)	Dyskeratosis (premature keratinization and keratin pearls deep in epithelium)
Hyperchromatic nuclei	Loss of intercellular adherence

However, as mentioned in section 1.3.5 , histopathological classification is prone to inter- and intra- observer errors and the progression of dysplasia is not a linear process, so the degree of dysplasia is not necessarily a predictor for malignant transformation[5,6]. A previous *ex-vivo* study used Raman spectroscopy to classify oral lesions as normal, benign, premalignant and OSCC[7]. An *in-vivo* study was able to discriminate between normal, premalignant and malignant oral mucosa with an accuracy of 85%[8]. Another *in-vivo* study discriminating between premalignant lesions, normal mucosa and the mucosa of habitual tobacco users could classify the premalignant lesions with an accuracy of 80% using LOOCV and only 50% using an independent test set[9]. However, none of these studies took into account the presence or degree of dysplasia in the premalignant lesions.

The aim of the current study is to use Raman spectroscopy to discriminate between mild, moderate and severe dysplasia in FFPP tissues from biopsies of 4 patients who had undergone multiple biopsies over time. Studying the range and progression of dysplasia in the same patients reduces the differences due to genetic variability and can help understand the progression of the disease. Two methods were trailed for classification purposes, PCA-LDA which has been described in section 3.3.5 and partial least squares regression discriminate analysis (PLSDA). Data for progression in one patient is shown below.

5.2 Methodology

5.2.1 Sample preparation

Ethical approval from the Research Ethics Committee, St James' Hospital, Dublin, Ireland, and informed consent was obtained from a patient who had undergone multiple oral biopsies. 10µm sections were cut from the FFPP biopsies and mounted on glass slides. On the slide, the regions with the different pathologies (such as mild or moderate dysplasia) were marked by the pathologist.

5.2.2 Instrumentation

A confocal Horiba Jobin Yvon LabRam HR 800 Raman (upright) spectroscopic microscope with a 532 nm wavelength laser was used. The properties of the spectroscope and mapping details were described in chapter 4, section 4.3.3 . Two maps were taken for each pathology, one of epithelium and one of connective tissue. Each consisted of 200 spectral points taken at 10μm intervals.

5.2.3 Data Analysis

All the data analysis was carried out using Matlab (Mathworks, US) with the PLS-Toolbox (Eigenvector Research Inc.) and in-house algorithms. Two quality control steps were employed. In the first, before processing, spectra with excess scatter/background were eliminated by setting a maximum intensity. Processing involved smoothing with a Savitsky Golay filter (5th order, 13 points) then correcting the baseline with a rubberband function, and finally vector normalisation. The second quality control step involved removing the spectra with excess wax and low biological content. This was achieved using k-means clustering which is used to partition data into groups such that variation is minimized within groups but maximized between groups. Most of the current versions are based on the algorithm developed by Hartigan and Wong in 1979[10]. It assigns data points to their closest centre points which are updated (changed) with each iteration until optimal convergence is met[10]. The next step was subtracting the wax and glass backgrounds; which was done using the NNLS method described in section4.3.3 . Figure 5.1illustrates the spectral preprocessing steps.

PCA of the data was performed to elucidate whether there is discrimination between the different pathologies and the basis for that discrimination.

PCA-LDA: Information from the first 10 principal components was used to build an LDA model with LOOCV.

PLSDA: mean centering (dividing all the variables by the mean) was performed on the processed spectra before PLSDA modelling. This serves to adjust for the variance between large and small unit variables, leaving only the relevant variance (that between the samples) for analysis. Partial least squares regression (PLSR) is a generalization of multiple linear regression (MLR) in which a set of dependent variables y is regressed against independent predictor variables X[11]. PLSDA is a supervised form of multivariate analysis which works as a linear classifier that aims to separate the data into groups using a hyperplane, similar to LDA; it aims to maximise the variance between groups and minimise the variance within groups. It is based on PLSR. Whereas, in classic PLSR, y is a matrix of continuous variables, in PLSDA it is categorical and used to assign the observations into classes. The loadings of the discriminate hyperplanes or latent variables (LV)s can be plotted to give more information on the source of the variance[12]. The data was divided into y classes from 1 to 3, corresponding to mild, moderate and severe dysplasia.

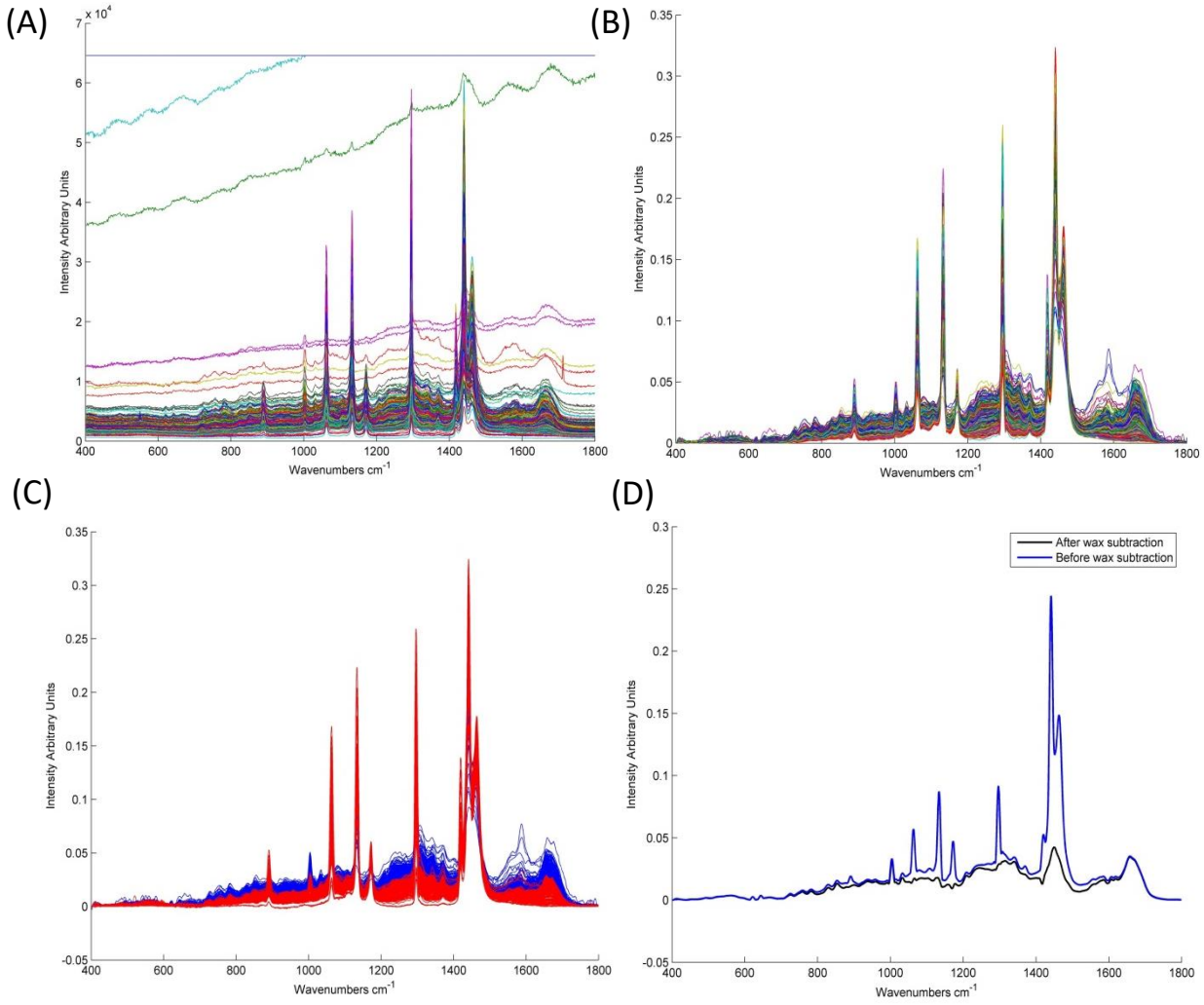

Figure 5.1 Spectral processing steps (A) Raw spectra. (B) Spectra after first quality control step, smoothing, baseline correction and normalization. (C) Spectra after k-means grouping; the spectra in red have high wax and low biological content while those in blue have higher biological content and less wax. (D) Spectra after glass and wax subtraction.

Table 5-3 Raman peak assignments, adapted from Movasaghi et al.[13].

Wavenumber (cm^{-1})	**Assignment**
484-90	Glycogen
599/600	Nucleotide conformation
666	G,T (ring breathing modes in DNA bases)
752	Symmetric breathing mode of tryptophan
782	DNA
811/12	RNA O-P-O stretch
814	C-C stretching (collagen assignment)
838	Deformative vibrations of amine groups
855	Ring breathing in tyrosine/C-C stretching in proline
919	C-C stretch of Proline ring/ glucose lactic acid C-C, proline ring (collagen assignment)
934/935	Protein/C-C backbone (collagen assignment)
937/8	Proline, hydroxyproline (C-C) skeletal of collagen backbone
1001/2	Phenylalanine ring breathing
1030-34	Phenylalanine of collagen
1128/9	Skeletal C-C stretch in lipids
1131	Fatty acid
1237	Amide III
1245-8	Amide III of collagen
1265	Amide III
1278	Proteins including collagen I
1285	Differences in collagen
1315-17	Guanine
1333	Guanine
1336	Polynucleotide chain (DNA purine bases)
1368	Guanine TRP protein, porphrin, lipids
1373	T,A,G (ring breathing modes of the DNA/RNA bases)
1437	CH_2 deformation (lipid)
1441	Wax
1449/50	C-H vibration lipids
1460	CH_2/CH_3 deformation in Lipids
1554	Amide II
1572-78	Guanine adenine
1650	Amide I
1652-55	Lipid C=C (lipids) / Amide I
1666-8	Protein / collagen
1674	C=C stretch in cholesterol
1700-50	Amino acids aspartic and glutamic acid

5.3 Results

According to their mean spectra, mild, moderate and severe dysplasia appear similar (Figure 5.2), which is why multivariate methods are employed to better observe the differences.

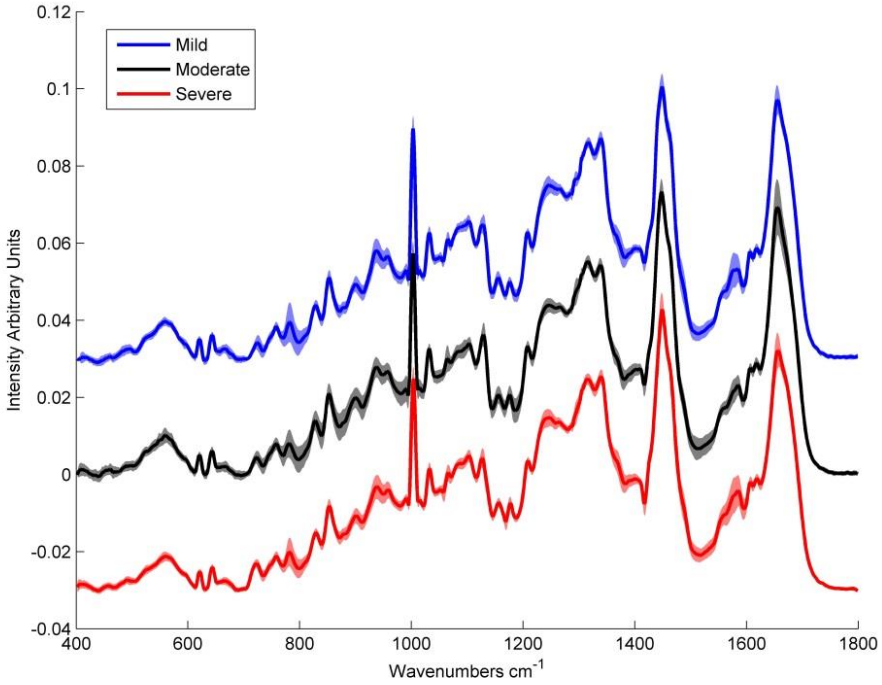

Figure 5.2 Mean Raman spectra of mild, moderate and severely dysplastic epithelial tissue. Shading denotes standard deviation.

PCA showed a good discrimination between mild and severe dysplasia according to PC1 (Figure 5.3 (A) (B)). Negative peaks in PC1 relating to the mild dysplasia are attributed to lipid (1128) and protein (935, 1652 cm^{-1}, 1462 cm^{-1}) contributions (Figure 5.3 (B)). On the positive side of the PC loading, relating to severe dysplasia, the most prominent peaks are attributed to nucleic acids (666, 1375 cm^{-1}) and protein (1555, 1709 cm^{-1}). Similar results were obtained in discriminating moderate and severe dysplasia (Figure 5.3 (C) (D)). Negative peaks in PC1 at

666, 1375 cm^{-1}, 1555, and 1709 cm^{-1} relate to the severely dysplastic epithelium. Positive peaks at 715, 934, 1129, 1296, 1445 and 1655 cm^{-1} relate to the moderately dysplastic epithelium. The peak at 1296 cm^{-1} is a paraffin wax feature whose variance, although reduced, is not eliminated. No discrimination was found between mild and moderate dysplasia in PCA (Figure 5.3 (E) (F)). This suggests that lipids and proteins are more prominent in the mildly and moderately dysplastic tissue, while nucleic acids and proteins are more prominent in the severely dysplastic tissue.

According to their mean spectra, differences between mild / moderate and severe connective tissue are observable, especially in the regions 800-1000 cm^{-1} and 1200-1400 cm^{-1} (Figure 5.4).

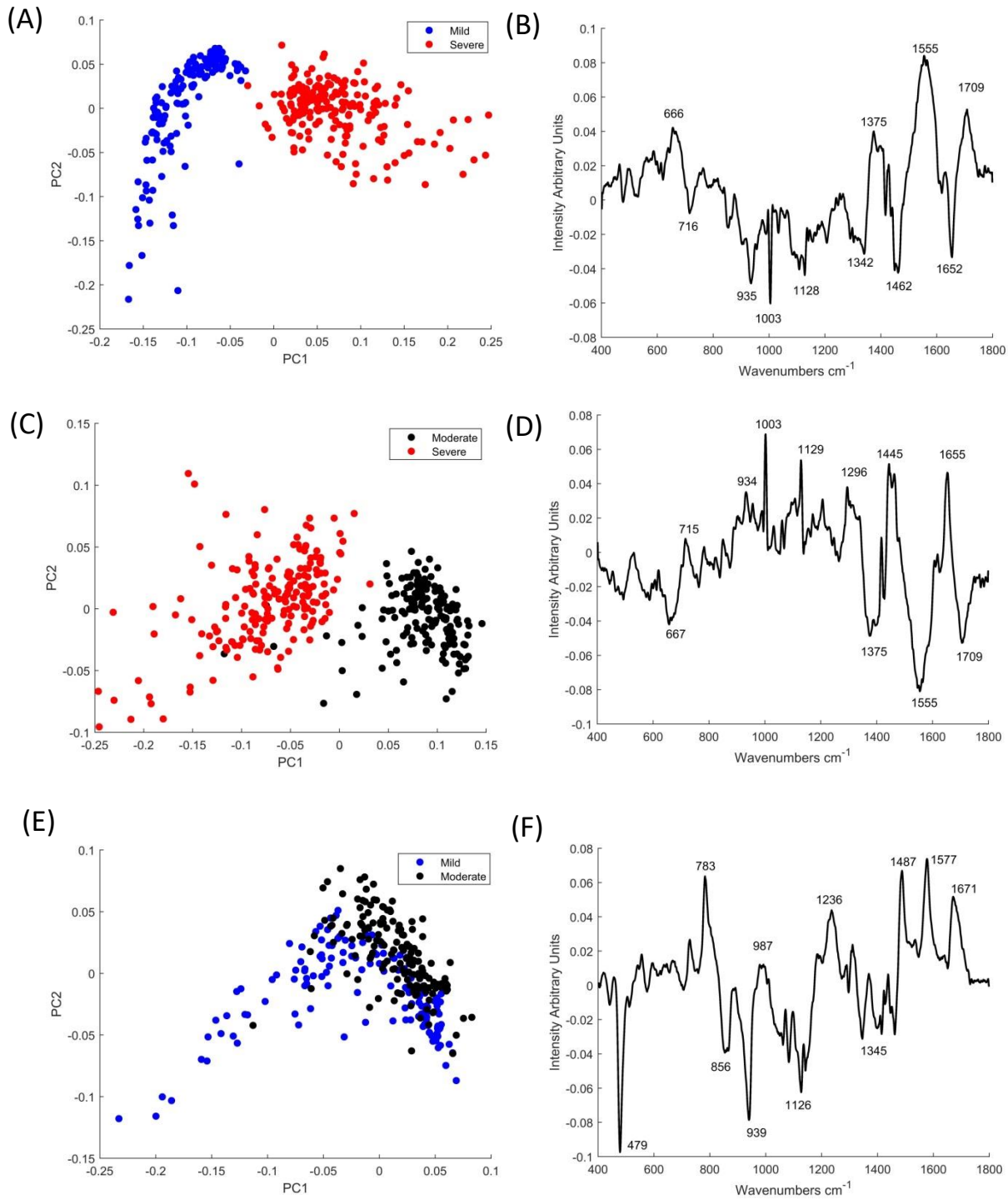

Figure 5.3 Results of PCA in epithelium (A) PCA scatter plot of mild vs severe dysplasia (B) Loading of PC1 which explains 42% of the variance (C) PCA scatter plot of moderate vs severe dysplasia (D) PC1 which explains 42% of the variance (E) PCA scatter plot of mild vs moderate dysplasia (F) PC1 which explains 31% of the variance.

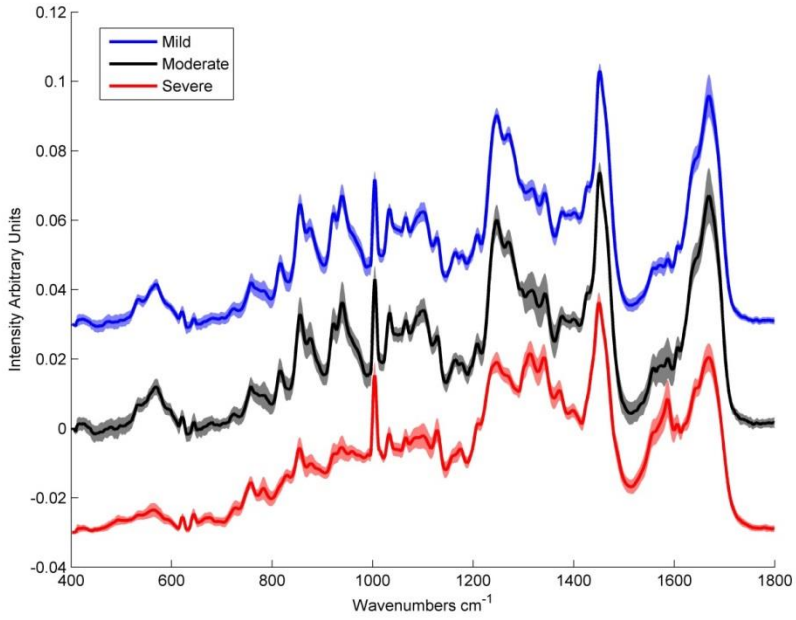

Figure 5.4 Mean Raman spectra of Mild, Moderate and severely dysplastic connective tissue. Shading denotes standard deviation.

A good discrimination between mild and severly dysplastic connective tissue was demonstrated with PCA (Figure 5.5 (A)). The negative side of PC1, which relates to the mildy dysplastic connective tissue, was dominated by collagen related peaks at (814, 856, 939, 1034, 1243 and 1667 cm^{-1}), while, the positive side, relating to severe dysplasia, was dominated by nucleic acid contributions (1314, 1335 and 1365 cm^{-1}) (Figure 5.5 (B)). Similar results were found on discriminating moderate and severe dysplasia (Figure 5.5 (C)(D)). PCA showed no discrimination between the mild and moderately dysplastic connective tissue.

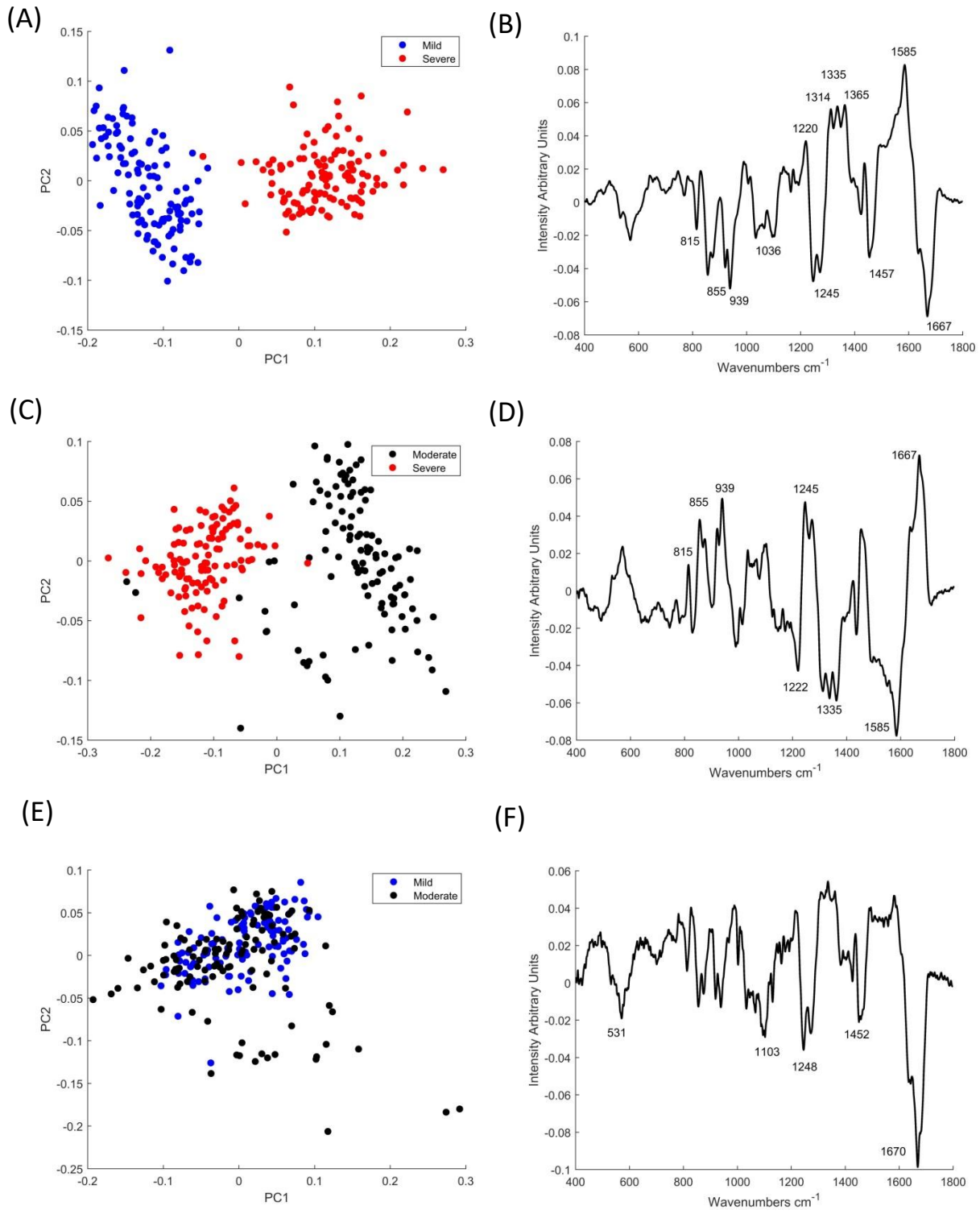

Figure 5.5 Results of PCA in connective tissue (A) PCA scatter plot of mild vs severe dysplasia (B) Loading of PC1 which explains 75% of the variance (C) PCA scatter plot of moderate vs severe dysplasia (D) PC1 which explains 73% of the variance (E) PCA scatter plot of mild vs moderate dysplasia (F) PC1 which explains 41% of the variance.

Table 5-4 summarises the sensitivity and specificity values obtained from the PCA-LDA classification with LOOCV. For both epithelium and connective tissue, severe dysplasia has the highest accuracy of discrimination in Raman followed by mild then moderate dysplasia. The discrimination in epithelium is better overall than that in connective tissue. Table 5-4 displays the sensitivity and specificity values obtained from the PLSDA classification with LOOCV. It follows the same trend as the PCA-LDA classification although the sensitivity and specificity values are higher overall.

Table 5-4 Sensitivity and specificity values obtained for the PCA-LDA classification model

	Epithelium		**Connective Tissue**	
	Sensitivity (%)	Specificity (%)	Sensitivity (%)	Specificity (%)
Severe	100	99	98	98
Moderate	88	95	63	89
Mild	92	95	79	82

Table 5-5 Sensitivity and specificity values obtained for the PLSDA classification model

	Epithelium		**Connective Tissue**	
	Sensitivity (%)	Specificity (%)	Sensitivity (%)	Specificity (%)
Severe	100	99	98	98
Moderate	96	95	78	84
Mild	97	95	91	71

5.4 Discussion

Discriminating between low grade dysplasia (mild and moderate) and high grade (severe and CIS) is important, as it determines both the management course and patient prognosis. High grade dysplasia have a higher risk of transformation and thus are treated more radically, while low grade dysplasia, depending on location and extent, may just be monitored. In this study, of interest are the changes taking place in epithelium and connective tissue during mild, moderate

and severe dysplasia, as identified by Raman spectroscopy. The choice to study each part of the tissue (epithelium and connective tissue) independently was made in order to better understand/identify the changes taking place in each. While it was expected to find discrimination between severe, mild and moderate in the epithelium, as the epithelial cells are undergoing morphological and biochemical changes, significant differences in connective tissue between the pathologies was not expected.

In the epithelium, the most prominent feature in the severely dysplastic epithelium was an increase in the nucleic acid related peak at 1375 cm^{-1} and a reduction in the peaks at 1128 and 1462 cm^{-1}, which relate to skeletal C-C stretch and CH_2/CH_3 deformation in lipids, respectively, in comparison to the mild and moderately dysplastic tissue. This has previously been reported in relation to OSCC[14] and can be explained by the higher replication rate and the relative increase in nuclear to cytoplasmic ratio in the more severe dysplasia. The spectral profile of the tissues in relation to proteins, however, is more complex, as peaks at 934 and 1650 cm^{-1}, which relate to protein C-C backbone and Amide I/lipids respectively, were higher in the mild and moderately dysplastic epithelium compared to severely dysplastic. Similar results were found by Cals et al. when comparing OSCC to surrounding normal squamous epithelium, as these peaks were higher in the normal epithelium[15]. On the other hand, severely dysplastic epithelium had higher peaks at 752 cm^{-1} (tryptophan) and 1555 cm^{-1} (Amide II). This suggests fewer proteins in the α helix conformation[16] in severely dysplastic epithelium, which may be due to disordered protein structure resulting from weakened bonds or a change in the amino acid microenvironment[17]. Increased Amide II may be due to upregulation of some proteins in the dysplastic progression, while increased tryptophan, an important amino acid in metabolic activities, has been reported previously in malignant cells[17-19].

The most significant change in connective tissue is in the collagen related bands (Table 5-3), which is reduced in the more severely dysplastic tissue. This has previously been described in

gastric dysplasia and ascribed to changes in matrix metalloproteinases which cleave collagen[20]. It may also be relative to an increase in cellularity in the severely dysplastic tissue. Mild and moderately dysplastic tissue did not show a good discrimination on PCA which is not very surprising as the categories are sometimes confused by the pathologists especially in borderline cases. More supervised classifiers, in this case LDA, and PLSDA were required to find the variance.

Overall, these results suggest that Raman spectroscopy can identify differences in mild, moderate, and severely dysplastic tissue which relate to relative changes in nucleic acid, lipid and protein content. By analysing these changes in a single patient, any differences due to genetic variability have been reduced. In Figure 5.6 the loading of LV-1 from the PLSDA of epithelium in each of the 4 patients (A-D) shows the progression from mild through moderate and severe. From the loadings it is apparent that while A and B have similar signatures, C and D are different.

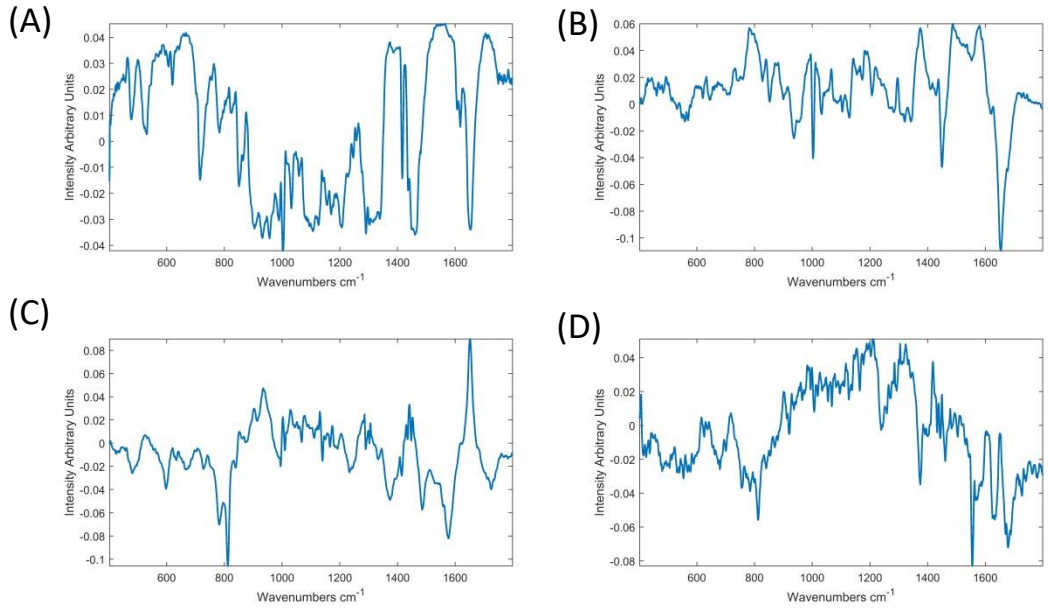

Figure 5.6 Loading of LV-1 from the PLSDA model for 4 patients A-D

This suggests that there may be some interpatient variability when it comes to progression from mild, through moderate to severe dysplasia. Hence doing an interpatient study, where the patients are grouped according to class (pathology) can be more informative, this is presented in chapter 6.

References

1. Leon B, W. EJ, Peter R, David S. World Health Organization Classification of Tumours Pathology and Genetics of Head and Neck Tumours. Lyon, France: IARC Press, 2005.

2. Manchanda A, Shetty DC. Reproducibility of grading systems in oral epithelial dysplasia. *Medicina Oral Patologia Oral Y Cirugia Bucal* 2012;17:E935-E942.

3. Bouquot JE, Speight PM, Farthing PM. Epithelial dysplasia of the oral mucosa—Diagnostic problems and prognostic features. *Current Diagnostic Pathology* 2006;12:11-21.

4. Nag R, Das RK. Analysis of images for detection of oral epithelial dysplasia: A review. *Oral Oncology* 2018;78:8-15.

5. Warnakulasuriya S, Reibel J, Bouquot J, Dabelsteen E. Oral epithelial dysplasia classification systems: predictive value, utility, weaknesses and scope for improvement. *Journal of Oral Pathology & Medicine* 2008;37:127-133.

6. Scully C. Challenges in predicting which oral mucosal potentially malignant disease will progress to neoplasia. *Oral Diseases* 2014;20:1-5.

7. Malini R, Venkatakrishna K, Kurien J, Pai KM, Rao L, Kartha VB, Krishna CM. Discrimination of normal, inflammatory, premalignant, and malignant oral tissue: A Raman spectroscopy study. *Biopolymers* 2006;81:179-193.

8. Krishna H, Majumder SK, Chaturvedi P, Sidramesh M, Gupta PK. In vivo Raman spectroscopy for detection of oral neoplasia: A pilot clinical study. *Journal of Biophotonics* 2014;7:690-702.

9. Singh SP, Deshmukh A, Chaturvedi P, Krishna CM. In vivo Raman spectroscopic identification of premalignant lesions in oral buccal mucosa. *Journal of Biomedical Optics* 2012;17.

10. Aggarwal CC, Reddy CK. Data Clustering Algorithms and Applications. Florida: Taylor and Francis, 2013:652.

11. Wold S, Sjöström M, Eriksson L. PLS-regression: a basic tool of chemometrics. *Chemometrics and Intelligent Laboratory Systems* 2001;58:109-130.

12. Brereton RG, Lloyd GR. Partial least squares discriminant analysis: taking the magic away. *Journal of Chemometrics* 2014;28:213-225.

13. Movasaghi Z, Rehman S, Rehman IU. Raman spectroscopy of biological tissues. *Applied Spectroscopy Reviews* 2007;42:493-541.

14. Singh SP, Krishna CM. Raman spectroscopic studies of oral cancers: correlation of spectral and biochemical markers. *Analytical Methods* 2014;6:8613-8620.

15. Cals FLJ, Schut TCB, Hardillo JA, de Jong RJB, Koljenovic S, Puppels GJ. Investigation of the potential of Raman spectroscopy for oral cancer detection in surgical margins. *Laboratory Investigation* 2015;95:1186-1196.

16. Rygula A, Majzner K, Marzec KM, Kaczor A, Pilarczyk M, Baranska M. Raman spectroscopy of proteins: a review. *Journal of Raman Spectroscopy* 2013;44:1061-1076.

17. Chen Y, Dai JH, Zhou XQ, Liu YJ, Zhang W, Peng GY. Raman Spectroscopy Analysis of the Biochemical Characteristics of Molecules Associated with the Malignant Transformation of Gastric Mucosa. *Plos One* 2014;9.4:e93906

18. Tankiewicz A, Dziemianczyk D Fau - Buczko P, Buczko P Fau - Szarmach IJ, Szarmach Ij Fau - Grabowska SZ, Grabowska Sz Fau - Pawlak D, Pawlak D. Tryptophan and its metabolites in patients with oral squamous cell carcinoma: preliminary study.

19. Huang ZW, McWilliams A, Lui H, McLean DI, Lam S, Zeng HS. Near-infrared Raman spectroscopy for optical diagnosis of lung cancer. *International Journal of Cancer* 2003;107:1047-1052.

20. Teh SK, Zheng W, Ho KY, Teh M, Yeoh KG, Huang Z. Diagnostic potential of near-infrared Raman spectroscopy in the stomach: differentiating dysplasia from normal tissue. *British Journal of Cancer* 2008;98:457-465.

Chapter 6: Raman spectroscopy for the identification of dysplastic and malignant FFPP oral tissues (inter-patient study).

6.1 Introduction

In this study, the work from the previous chapter is expanded on by studying the differences between benign, mild, moderate, severely dysplastic and OSCC FFPP tissue in a cohort of patients. The archival FFPP patient samples were obtained from St James' Hospital, Dublin. The benign category was made up of benign lesions, such as fibroepithelial polyp, squamous papilloma and benign hyperplasia. Fibroepithelial polyps are reactive lesions with an underlying aetiology of trauma or irritation. They are characterised by a small growth which can occur anywhere in the oral cavity, although they are most commonly found in the gingiva, tongue and lip[1]. Similarly, squamous papillomas are exophytic asymptomatic growths, although their pathogenesis is assumed to be viral, as they have been tentatively linked to HPV types 6 and 11[2]. Hyperplastic lesions are benign lesions that are keratotic but show no cellular atypia. Raman spectroscopic measurements were taken of the tissues and partial least squares regression discriminate analysis (PLSDA) was used to classify the tissue samples into classes of benign, mild, moderate, severe dysplasia and OSCC. PLSDA was chosen over other multivariate techniques, such as PCA-LDA and support vector machine (SVM), for a number of reasons. Firstly, the results of chapter 5 revealed that it was better at discriminating between mild, moderate and severe oral dysplasia. Furthermore, unlike LDA, it can analyse data with numerous x variables, and it works well with data that is noisy or has highly collinear x variables[3]. A study comparing PCA-LDA and PLSDA models for colorectal cancer diagnosis found that PLSDA could discriminate between normal and cancerous tissue with a higher

accuracy than PCA-LDA[4]. PLSDA is not without its limitations, however, as it can tend to overfit the model, meaning it can classify training data well but not new data[5]. This can be overcome by using a validation data set or, as in this case where there are a small number of samples, by using cross validation.

6.2 Methodology

6.2.1 Sample Preparation

Archival oral FFPP tissues for each cohort were obtained following ethical approval from St James' Hospital Ethics Committee and informed written consent from patients. In total, 57 patients were included, from which 72 pathologies were identified. 17 were benign lesions, 20 mildly dysplastic, 20 moderately dysplastic, 10 severely dysplastic and 5 invasive SCC. The H&E stained sections from the different pathologies were examined by a consultant oral and maxillofacial pathologist in St James' Hospital, who then edited the images to mark the areas of pathology (Figure 6.1). The FFPP tissue blocks and corresponding images were then taken to the RESC laboratory where10μm sections were cut from the FFPP tissues and mounted on glass slides. One of the sections from each sample was dewaxed, stained with haematoxylin and eosin, and a parallel unstained section (which was not dewaxed) was used for Raman spectroscopy measurement.

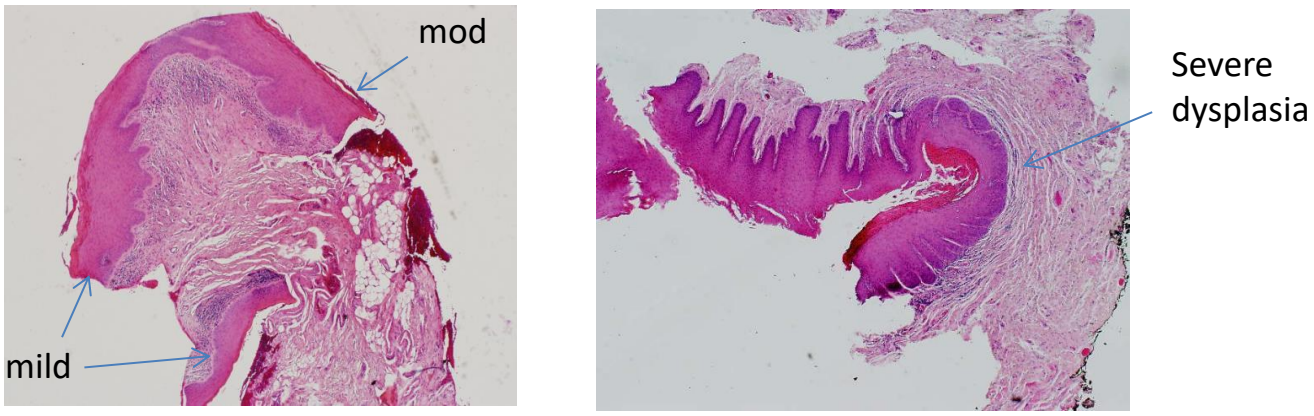

Figure 6.1 Representative H&E images showing the regions of dysplasia marked by the pathologist.

6.2.2 Instrumentation

A confocal Horiba Jobin Yvon LabRam HR 800 Raman (upright) spectroscopic microscope with a 532 nm laser was used. The instrument and mapping properties are described in section 4.3.2. For every pathology section, 200 spectral points were taken from epithelium and the same from connective tissue at 10 µm intervals.

6.2.3 Data Analysis

All the data analysis was carried out using Matlab (Mathworks, US) with the PLS-Toolbox (Eigenvector Research Inc.) and in-house algorithms. The spectral pre-processing steps are described in section 5.2.3.

PLSDA with leave one patient out cross validation (LOPOCV) was used to build the classifier. LOPOCV is similar to LOOCV except, in this instance, in place of leaving one spectrum out, one patient is left out so that all the spectra of the patient are left out and predicted.

Receiver operating characteristic (ROC) curves were graphed for each class. ROCs are a plot of the true positive rate (sensitivity) against the false positive rate (1-specificity) over a continuous range (from 0 to 1) of cut-points of a classifier. Each point on the ROC curve represents a sensitivity/specificity pair corresponding to a particular decision threshold. Accuracy is measured by the area under the ROC curve (AUC), so that, the closer the curve tends to the left and top borders, the more accurate the classifier. Conversely, the closer the curve is to the diagonal (baseline), the higher the misclassification rate and the lower the accuracy[6].The baseline is at 0.5, while a perfect classifier would have an AUC of 1.In general, an AUC of 0.5 is considered to have no discrimination, while 0.7 to 0.8 is considered acceptable. 0.8 to 0.9 is considered excellent while over 0.9 is considered outstanding[7]. A schematic of an ROC curve is shown in Figure 6.2.

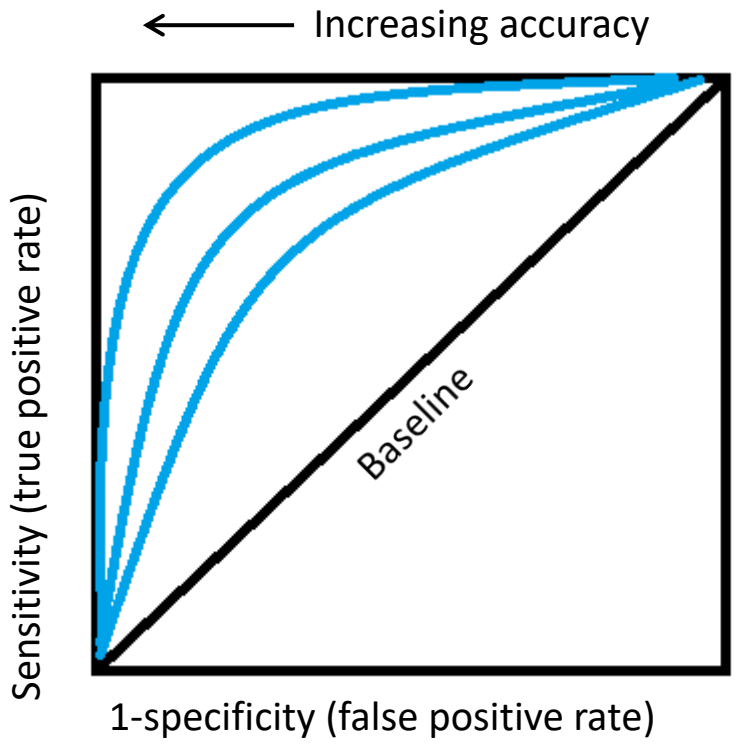

Figure 6.2 Schematic of an ROC curve. Sensitivity is plot on the y axis and 1-specificity on the x axis. Accuracy is increased as the curve goes towards the left and top borders (increasing the AUC) and decreases as the curve goes inwards towards the baseline (decreasing the AUC).

6.3 Results

6.3.1 Epithelial tissue

The mean spectra of the benign, mild, moderate and malignant epithelial tissues all appear similar (Figure 6.3), demonstrating the need for more sophisticated multivariate analytical techniques, such as PLSDA, to differentiate the tissue pathologies based on the spectral signatures of their differing biochemical constituents.

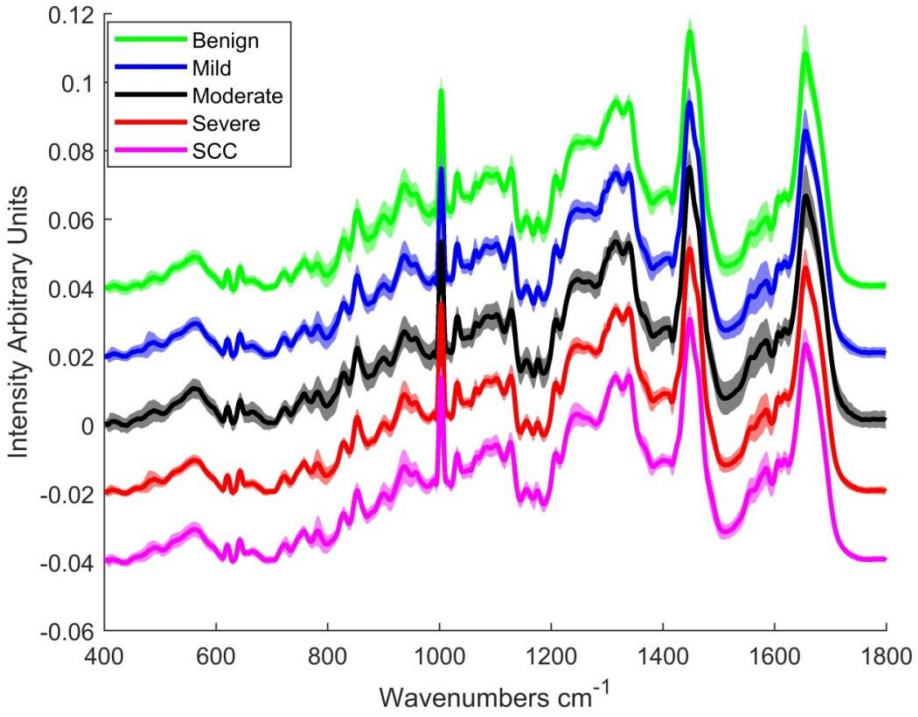

Figure 6.3 Mean Raman spectra of benign, mild, moderate and severely dysplastic epithelial tissue. The spectra have been offset for clarity and shading denotes standard deviation.

The results of the PLSDA classification do not show a very good discrimination across the groups (Table 6-1). The estimated ROC curves are based on predicted class for each spectrum. Sensitivity is calculated from the fraction of in class spectra while the specificity is calculated from the fraction not in class for a given threshold. The cross validated ROC curves follow the same method except the class predicted when the spectra are left out during cross validation is used. From the ROC curves (Figure 6.4) it appears that the classifier has the highest accuracy for SCC (AUC=0.71) and lowest for mildly dysplastic epithelium (AUC=0.46).

Table 6-1 Sensitivity and specificity values obtained from PLSDA classification with LOPOCV of epithelial tissue.

	Benign	Mild	Moderate	Severe	OSCC
Sensitivity (%)	74	67	39	69	65
Specificity (%)	49	38	86	57	76

To assess whether it affects the classification, different combinations of the pathologies were assessed. Combining the severely dysplastic and SCC group did not have much effect on the overall model (Table 6-2). However, combining the mild and moderate groups leads to an improved classification in the other groups (benign, severe and SCC), but a low classification in the mild/moderate group (Table 6-3).

Table 6-2 PLSDA classification combining the severe and SCC groups

	Benign	Mild	Moderate	Severe/SCC
Sensitivity (%)	75	67	39	66
Specificity (%)	49	38	86	75

Table 6-3 PLSDA classification combining the mild and moderate groups

	Benign	Mild/Moderate	Severe	SCC
Sensitivity (%)	77	38	74	71
Specificity (%)	49	86	52	72

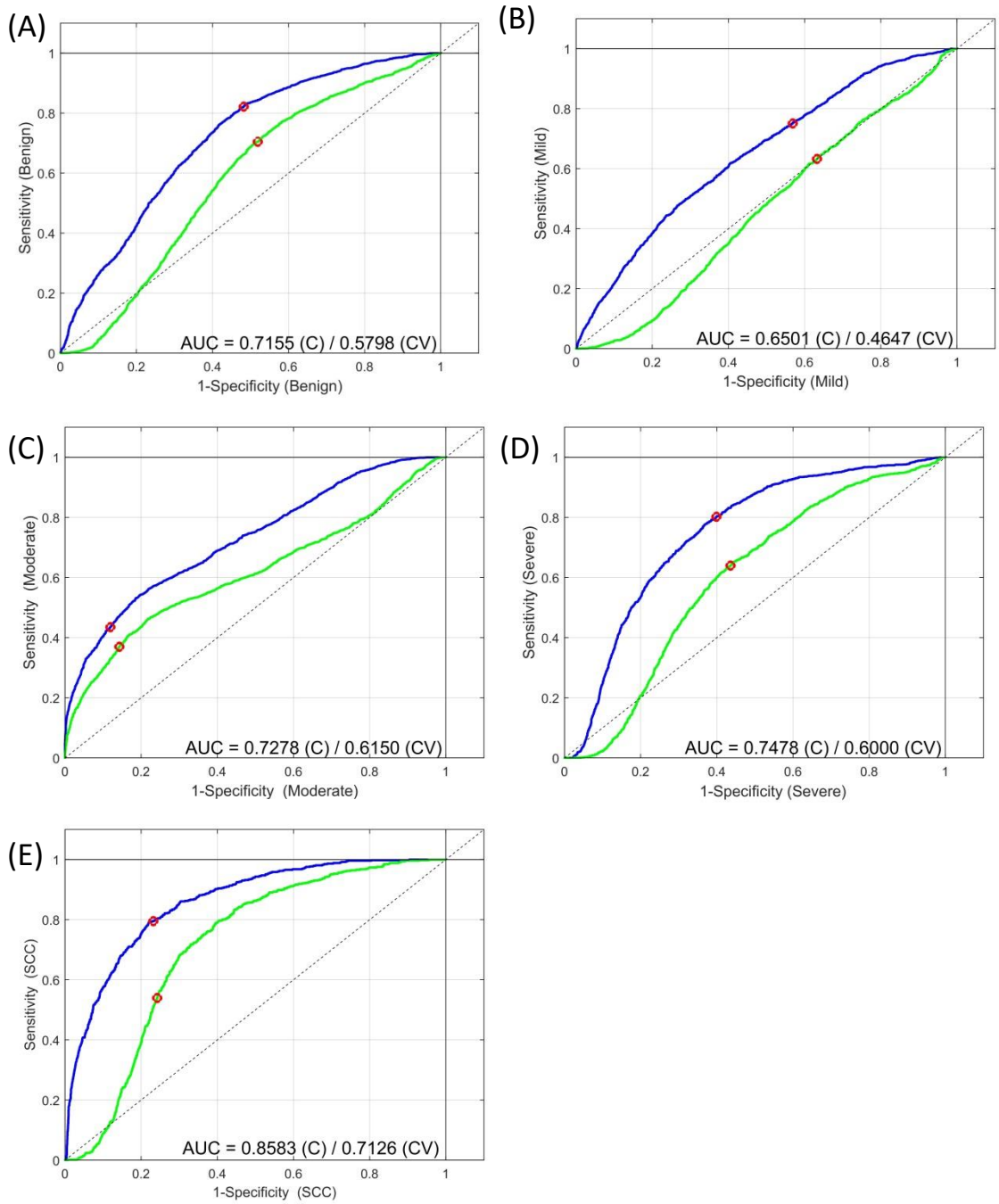

Figure 6.4 ROC curves for (A) Benign (B) Mild (C) Moderate (D) Severe and (E) SCC epithelial tisssues. The blue line is the estimated and the green the cross validated ROC curve. AUC is a measure of the accuracy of the classifier, (C) is the calibrated and (CV) is the crossvalidated AUC. The red dot(s) represents the calculated sensitivity and 1-specificty on the y and x axis respectively. So for eaxample for (A) sensitivity is 0.74 (CV) and 1-specificity = (1-0.49)=0.51.

To better elucidate the variability between the different classes, their scores on the first latent variable (LV-1) were plotted. This shows a large intra-class spread, the greatest spread being observed in the moderate group and the smallest in the SCC (Figure 6.5).

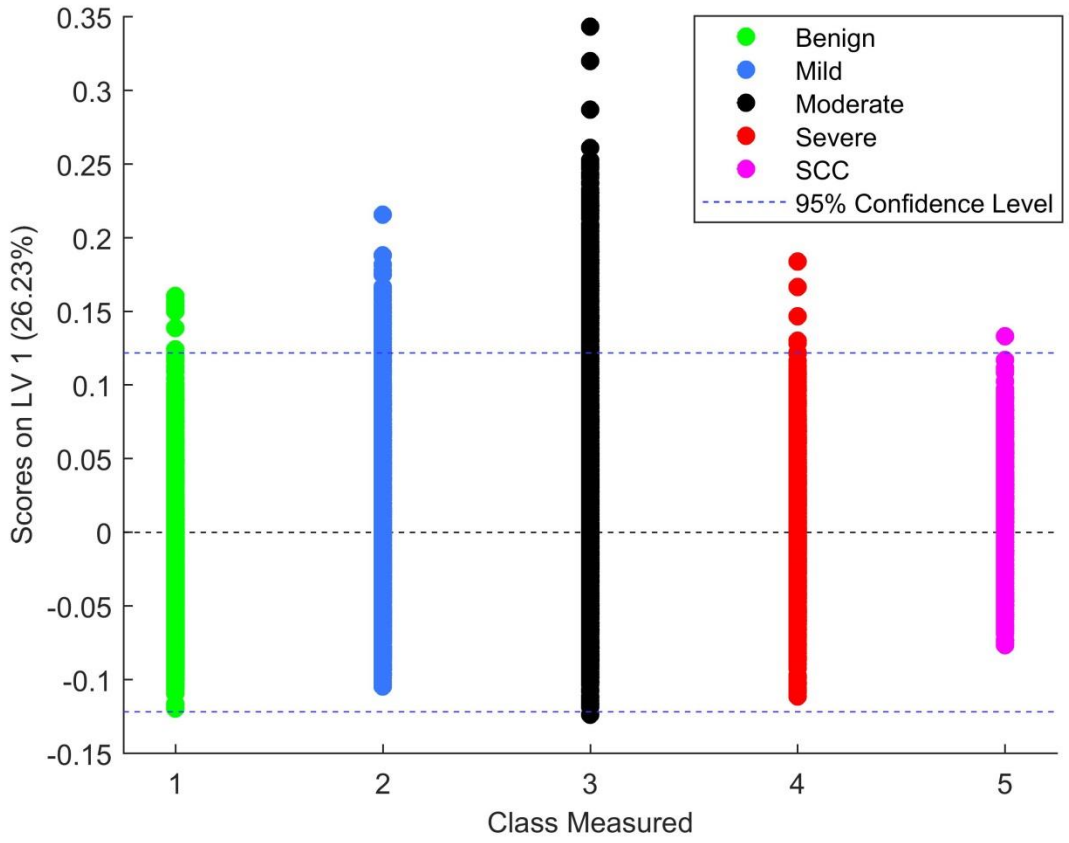

Figure 6.5 A plot of the PLSDA scores according to LV-1

Plotting the means and standard deviations of the scores on LV-1 (Figure 6.6) does not show an obvious progression, but it can be assumed from their means that the benign and mild are mostly negative for LV-1 while moderate, severe and SCC are mostly positive.

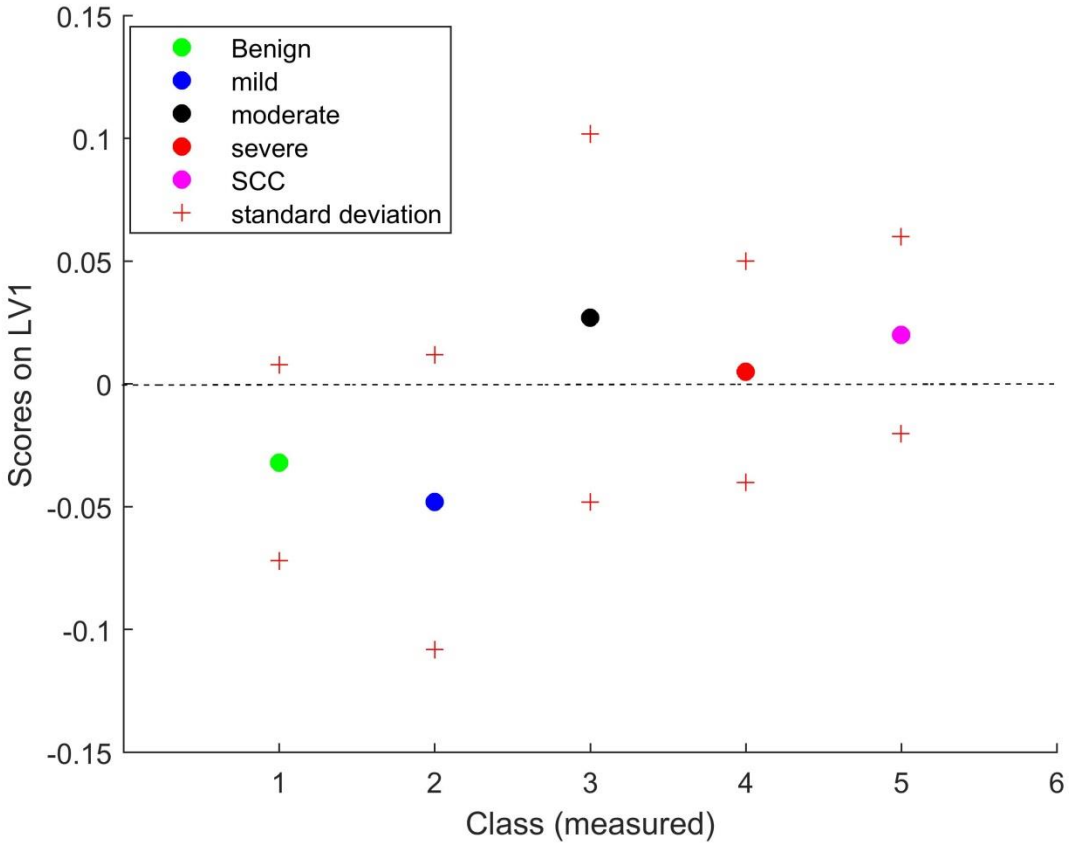

Figure 6.6 Mean and standard deviation of PLSDA scores of LV-1

LV-1 (Figure 6.7), which is reponsible for 26.23% of the variance, has positive peaks at 783, 1371 and 1576 cm^{-1}, which relate to nucleic acids (Table 5-3). Negative peaks are observed at 934, and 1282 cm^{-1} (relating to protein/collagen) and the amide 1 band at 1650 cm^{-1}.

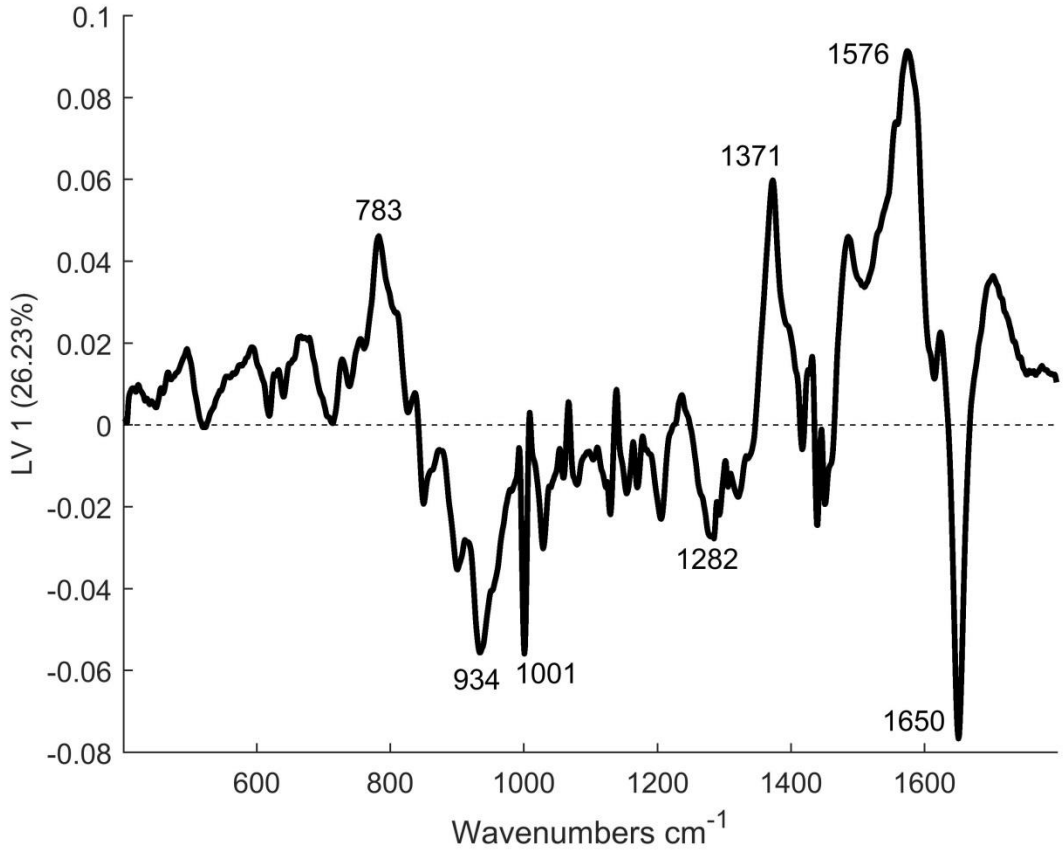

Figure 6.7 LV-1 of the PLSDA model which included all the classes

Connective tissue

From their mean spectra, (Figure 6.8) the most notable difference between benign, mild, moderate, severe and SCC connective tissue appears to be in the regions (800-1000 cm^{-1}) and (1200-1400 cm^{-1}), similar to the findings of chapter 5 (Figure 5.5).

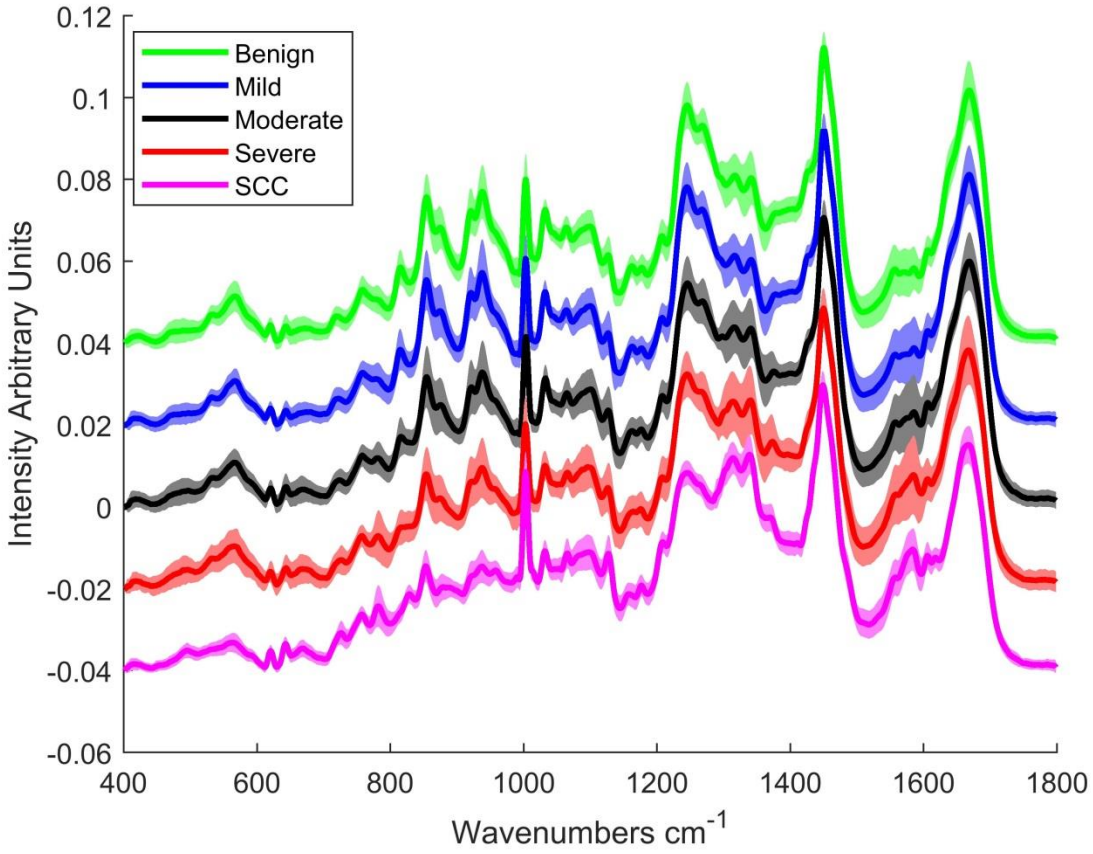

Figure 6.8 Mean Raman spectra of benign, mild, moderate severely dysplastic and SCC connective tissue. The spectra have been offset for clarity and shading denotes standard deviation.

The results of the PLSDA classification (Table 6-4) show high sensitivities for benign and SCC compared to the dysplasia classes. However, the specificity for benign was low, indicating a high false positive rate. The classifier has the best accuracy among the classes for SCC according to the ROC curve (Figure 6.9).

Table 6-4 Sensitivity and specificity values obtained from PLSDA classification with LOPOCV of connective tissue

	Benign	Mild	Moderate	Severe	SCC
Sensitivity (%)	81	67	42	59	88
Specificity (%)	44	46	61	67	72

Plotting the scores of LV-1 shows the greatest intra-class spread in the mild group and the smallest in the SCC (Figure 6.10). Plotting the means and standard deviations of the scores of LV-1 (Figure 6.11) shows a progression from benign to SCC on LV-1. The means of the benign and mild are negative in LV-1 while those of moderate, severe and SCC are positive.

Positive peaks of LV-1 can be observed at 1005, 1131, 1218, 1337, 1435 and 1581 cm^{-1} LV-1(Figure 6.12). The peaks at 1005 and 1581 cm^{-1} relate to phenylalanine, while those at 1131, 1218 and 1435 cm^{-1} relate to lipids and that at 1337 cm^{-1} relates to nucleic acids. On the other hand, negative peaks can be observed; at 811, 855, 938, 1241, 1453 and 1672 cm^{-1}. The peaks at (855, 938 and 1241 cm^{-1}) relate to collagen while 1453 and 1672 relate to lipid contributions.

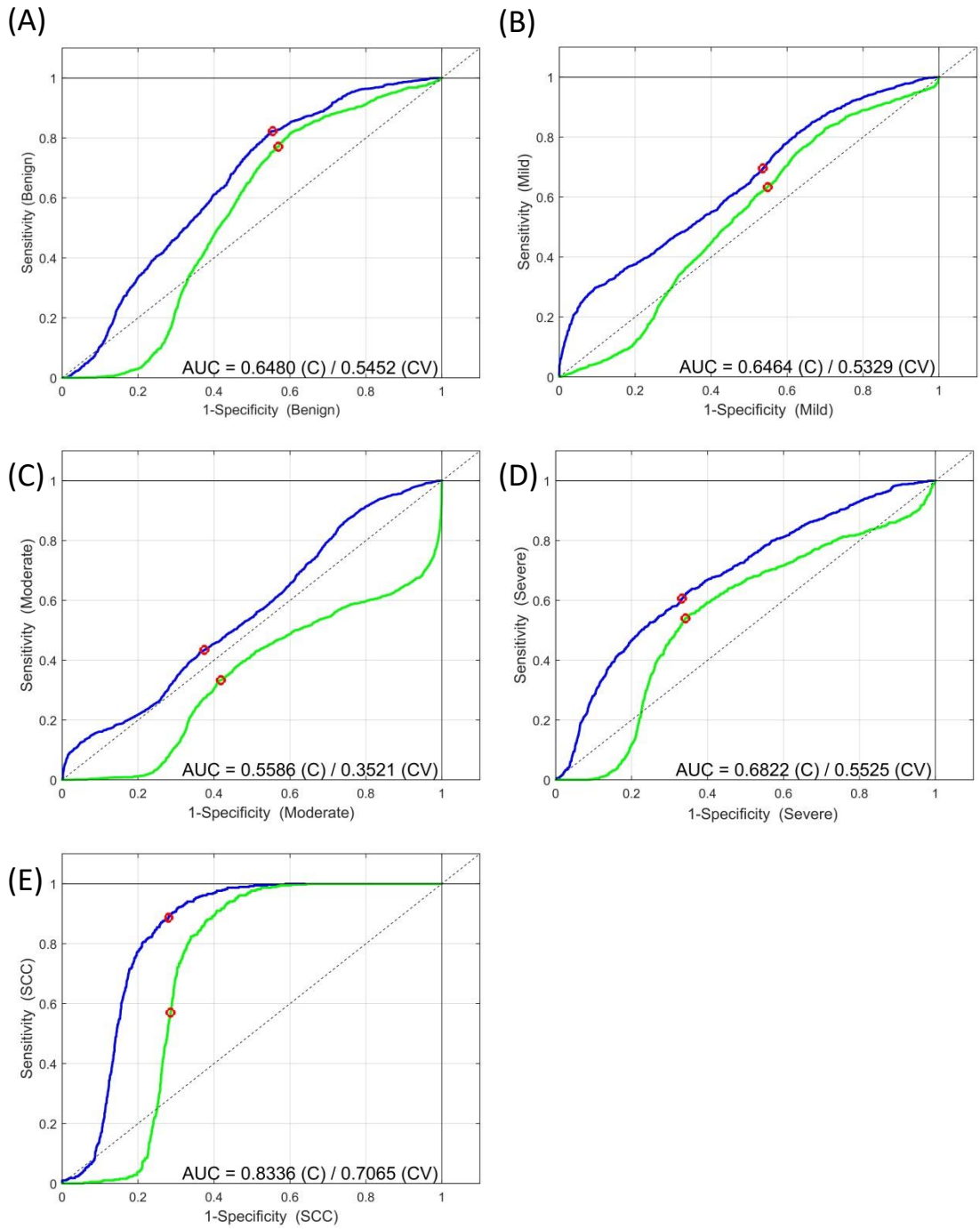

Figure 6.9 ROC curves for (A) Benign (B) Mild (C) Moderate (D) Severe and (E) SCC connective tisssues. The blue line is the estimated and the green is the cross validated ROC curve. AUC is a measure of the accuracy of the classifier.

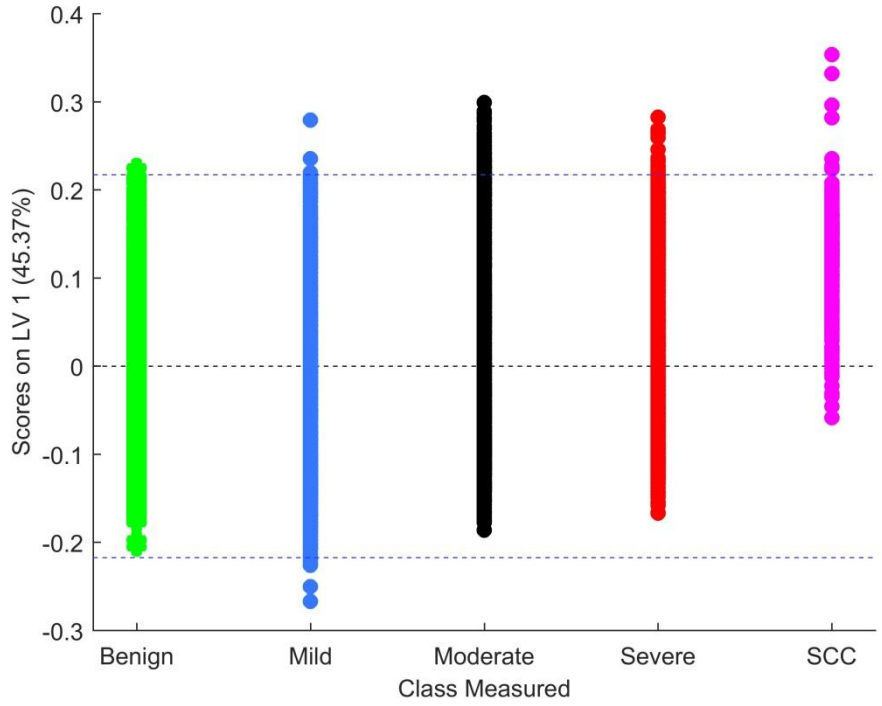

Figure 6.10 A plot of the PLSDA scores of LV-1

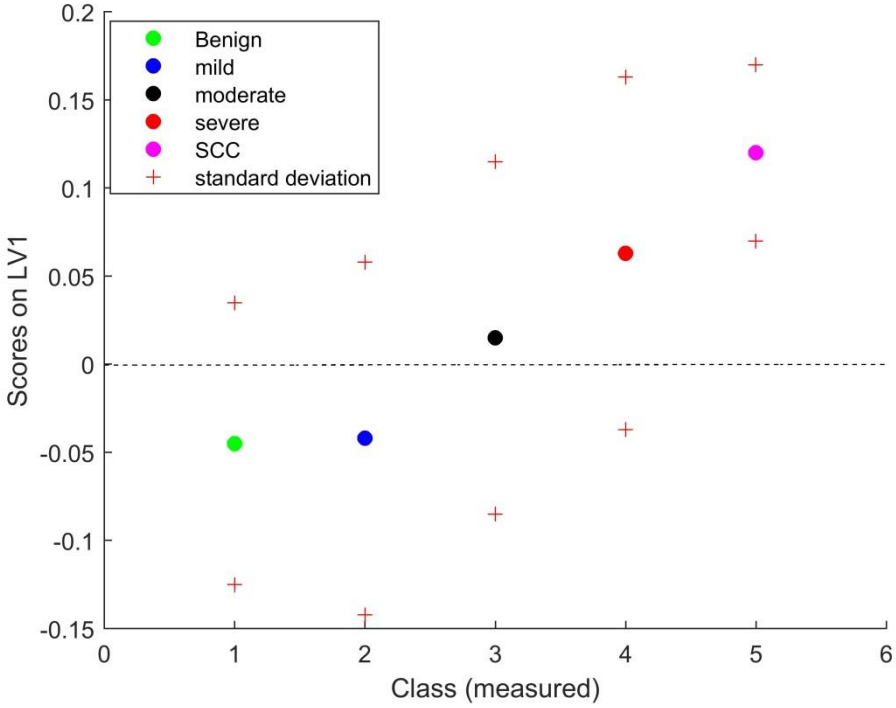

Figure 6.11 Mean and standard deviation of PLSDA scores of LV-1

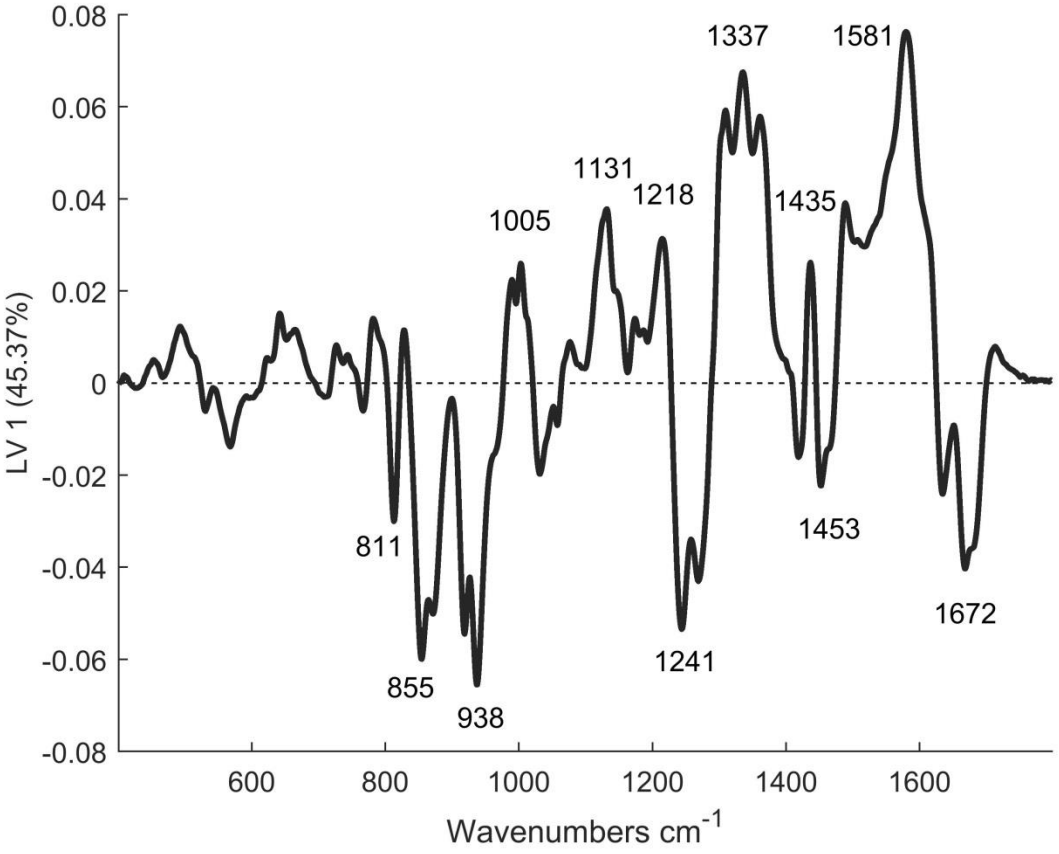

Figure 6.12 Loading of LV-1 of the PLSDA model which included all the classes

6.4 Discussion

The use of benign lesions as a control category was for logistical reasons (as it is difficult to get archival FFPP samples of patients with normal pathology). Besides, since clinicians do not usually biopsy normal looking mucosa, it is important to differentiate dysplasia or cancer from benign lesions. It was elected not to use the normal areas of dysplastic or SCC tissues because previous studies have shown that the cells at the periphery of a malignant lesion may be subject to cancer field effects, meaning that they appear histologically normal but have undergone molecular changes[8,9]. LOOCV can tend to overfit the model and overestimate the accuracy of

the classifier. Hence LOPOCV, which is better at evaluating classifier performance on new samples, was used.

Results from the PLSDA show a similar trend to the results of chapter 5, indicating increasing nucleic acid contributions and lower protein and lipid contributions as dysplasia progresses in the epithelium. According to the ROC curves, the accuracy of the classifier was highest for the SCC class (AUC=0.71), intermediate (~0.6 AUC) for the benign, moderate and severe classes, and lowest (AUC=0.46) for the mild. This is likely due to the fact that the mild is not a very well defined category for the classifier leading it to misclassify with benign and moderate. Moreover, the fact that combining the mild and moderate categories improves the classification in the other categories reinforces that fact that there is considerable overlap between these categories. The moderate group had the lowest sensitivity in the PLSDA classification and the greatest spread in LV-1, suggesting a higher variability in this group compared to the others.

In connective tissue, nucleic acid peaks were more prominent with progressive dysplasia and collagen peaks were less prominent. Connective tissue associated with SCC could be classified from that associated with dysplasia and benign with a high sensitivity and specificity. This is to be expected as, due to epithelial mesenchymal transition[10]; the boundary between epithelium and connective tissue in SCC is often lost as a result of islands of epithelium invading the connective tissue[11].

When building a machine learning system or classifier, it is expected to be better than or match the current state of the art, which in this case is histopathological diagnosis. The findings of this study do not fulfil this standard which may be due to a number of factors. Firstly, the small sample size makes it harder to build a representative model[12], especially when the differences between categories is small, as in this case with different degrees of dysplasia. Secondly, this model is based on histopathological diagnosis but, as discussed in sections 1.3.5 and 5.1 ;

morphological changes are not necessarily predictive of malignant transformation[13]. In fact, it is now emerging that genetic alterations such as abnormalities in the number of chromosomes (aneuploidy), losses at 3p, 9p and 17p and mutations in the P-53 gene can be a more important prognostic marker[14,15]. Finally, factors other than the degree of dysplasia can have an influence on the Raman spectrum and hence classification. These factors are investigated in chapter 7.

References

1. Zain RB, Fei YJ. Fibrous lesions of the Gingiva- A histopathologic analysis of 204 cases. *Oral Surgery Oral Medicine Oral Pathology Oral Radiology and Endodontics* 1990;70:466-470.

2. Babaji P, Singh V, Chaurasia VR, Masamatti VS, Sharma AM. Squamous papilloma of the hard palate. *Indian Journal of Dentistry* 2014;5:211-213.

3. Wold S, Sjöström M, Eriksson L. PLS-regression: a basic tool of chemometrics. *Chemometrics and Intelligent Laboratory Systems* 2001;58:109-130.

4. Liu WJ, Sun ZT, Chen JY, Jing CB. Raman Spectroscopy in Colorectal Cancer Diagnostics: Comparison of PCA-LDA and PLS-DA Models. *Journal of Spectroscopy* 2016.

5. Westerhuis JA, Hoefsloot HCJ, Smit S, Vis DJ, Smilde AK, van Velzen EJJ, van Duijnhoven JPM, van Dorsten FA. Assessment of PLSDA cross validation. *Metabolomics* 2008;4:81-89.

6. Zweig MH, Campbell G. Receiver-operating characteristic (ROC) plots – a fundamental evaluation tool in clinical medicine. *Clinical Chemistry* 1993;39:561-577.

7. Mandrekar JN. Receiver Operating Characteristic Curve in Diagnostic Test Assessment. *Journal of Thoracic Oncology* 2010;5:1315-1316.

8. Chai H, Brown RE. Field Effect in Cancer-An Update. *Annals of Clinical and Laboratory Science* 2009;39:331-337.

9. Rashid N, Nawaz H, Poon KWC, Bonnier F, Bakhiet S, Martin C, O'Leary JJ, Byrne HJ, Lyng FM. Raman microspectroscopy for the early detection of pre-malignant changes in cervical tissue. *Experimental and Molecular Pathology* 2014;97:554-564.

10. Kalluri R, Weinberg RA. The basics of epithelial-mesenchymal transition. *Journal of Clinical Investigation* 2009;119:1420-1428.

11. Speight PM. Update on Oral Epithelial Dysplasia and Progression to Cancer. *Head and Neck Pathology* 2007;1:61-66.

12. Beleites C, Neugebauer U, Bocklitz T, Krafft C, Popp J. Sample size planning for classification models. *Analytica Chimica Acta* 2013;760:25-33.

13. Scully C. Challenges in predicting which oral mucosal potentially malignant disease will progress to neoplasia. *Oral Diseases* 2014;20:1-5.

14. Curfman GD, Morrissey S, Drazen JM. DNA content as a prognostic marker in patients with oral leukoplakia (Retraction of vol 344, pg 1270, 2001). *New England Journal of Medicine* 2006;355:1927-1927.

15. Braakhuis BJM, Leemans CR, Brakenhoff RH. A genetic progression model of oral cancer: current evidence and clinical implications. *Journal of Oral Pathology & Medicine* 2004;33:317-322.

Chapter 7: Influence of patient factors and clinical features on Raman classification

7.1 Introduction

Following on from the work of chapter 6, patient factors and clinical features that may have an influence on the classification using Raman spectroscopy are explored. Tobacco smoke contains carcinogens and has a well-studied connection with the development of both dysplastic[1] and malignant[2] oral lesions, as has been discussed in detail in section 1.2.3.1 . Similarly, alcohol consumption has been associated with the development of both oral dysplasia[1] and cancer[2], as detailed in section 1.2.3.2 . The incidence of oral cancer is higher in males than females[3,4], which is likely due to habits such as smoking and alcohol consumption rather than a genetic predisposition, although the prognosis is the same[5]. Gender was not found to have an association with the development of oral dysplastic lesions[1]. Further variability can arise because of the different sites of anatomical origin of the lesion. Oral cancer refers to any cancer in the oral cavity proper which includes; the tongue, labial and buccal mucosa, hard and soft palate, gingiva, alveolar ridges and floor of the mouth. These areas vary in degree of keratinization, vascularity and lymphatic drainage[5] and thus anatomic site may also influence the spectroscopic signatures upon which a classification is to be based. As the interpatient study was based on a heterogeneous group of patients with different gender, age, habits, medical histories and lesion clinical features, the aim of this chapter was to discern whether these factors have an influence on the classification using Raman spectroscopy.

7.2 Methodology

7.2.1 Sample Preparation

The archival FFPP tissue samples detailed in section 6.2.1 were used in this study.

7.2.2 Instrumentation

Instrument and mapping properties were described in section 4.3.2 . The maps taken for section 6.2.2 were used in this study.

7.2.3 Data analysis

Metadata on the patients included in chapter 6 is provided in Table 7-1. This was used to divide all the patients, regardless of histopathological diagnosis, into groups according to gender, smoking habits, alcohol consumption and site of lesion. The spectral maps, acquired for the study of chapter 6, were analysed using PLSDA with LOPOCV, as described in section 6.2.3

Table 7-1 Information on patient factors and clinical features

Patient	Gender	Age	Smoking	Alcohol Consumption	Site of Lesion
1	M	59	No	Yes	Retromolar area
2	F	38	n/a	n/a	Tongue
3	M	86	No	Yes	Tongue
4	F	75	No	Yes/rarely	Buccal mucosa
5	M	50	n/a	n/a	Tongue
6	F	66	No	Yes	Hard palate
7	F	45	N/A	n/a	Premolar ridge
8	F	32	Ex-smoker	No	Tongue
9	F	59	No	Yes/2-3 units/fortnight	Buccal mucosa
10	F	61	Yes 8-10 cpd/week	No	Hard palate
11	F	62	15-20 cpd	No	Soft palate
12	M	71	Ex-smoker	n/a	Gingiva
13	F	62	No	Yes/occasionally	Labial mucosa
14	M	21	n/a	n/a	Tongue

15	F	62	Ex-smoker	No	Floor of the mouth
16	F	69	Yes 10 cpd	Yes	Tuberosity
17	M	67	Ex-smoker	Yes	Tongue
18	M	37	Yes	No	Buccal mucosa
19	M	57	1-2 cpw	10 units/week	Soft palate
20	F	65	n/a	1-2 units/week	Buccal mucosa
21	M	60	Ex-smoker	n/a	Hard palate
22	M	81	Ex-smoker	2-3 units/week	Tongue
23	M	69	30 cpd	4 units/day	Floor of the mouth
24	M	55	No	n/a	Maxilla
25	F	77	No	6 units/week	Gingiva
26	F	47	15 cpd	10-12 units/week	Tongue
27	F	63	Ex-smoker	2 units/week	Tongue
28	F	55	n/a	n/a	Labial mucosa
29	F	44	No	5-6 units/week	Tongue
30	M	74	n/a	n/a	
31	M	68	Ex-smoker	5 units/week	Tongue
32	M	66	n/a	n/a	Soft palate
33	M	58	15 cpd	15 units/week	Labial mucosa
34	M	56	20 cpd	5-6 units/week	Buccal mucosa
35	F	53	n/a	n/a	Buccal mucosa
36	F	53	15 cpd	Yes 3 units/week	Floor of the mouth
37	M	38	Ex-smoker	Yes	Buccal mucosa
38	F	63	No	n/a	Tongue
40	F	71	No	No	Tongue
41	F	61	No	Yes	Labial mucosa
42	F	66	Ex-smoker	Yes	Soft palate
43	M	54	Yes 30 cpd	No	Alveolus
44	F	51	Ex-smoker	Yes	Buccal mucosa
45	F	41	n/a	Yes 1 unit/week	Buccal mucosa
46	F	73	n/a	Yes	Tongue
47	M		n/a	n/a	Tongue
48	M	30	Yes 1 cpd	Yes 20-30 units/week	Tongue
49	F	61	Ex-smoker	Yes	Tongue
50	F	71	No	No	Buccal mucosa
51	F	64	Ex-smoker	Yes	Tongue
52	M	47	Yes	Yes	Buccal mucosa
53	F	76	Ex-smoker	Yes	Alveolus
54	M	53	Ex-smoker	Yes	Labial mucosa
55	M	31	Yes	No	Tongue
56	F	50	Ex-smoker	No	Tongue
57	F	56	Ex-smoker	No	Tongue

n/a, information was not available
cpd, cigarettes per day
cpw, cigarettes per week

7.3 Results

7.3.1 Gender

The data of all the patients (Table 7-1) was split according to gender into females and males. PLSDA results, expressed in terms of ROC curves, of epithelium (AUC =0.43) and connective tissue (AUC=0.47) (figure 7.1) show no discrimination based on gender. The female vs male sensitivity and specificity values were 22% and 77% respectively in epithelium. In connective tissue the sensitivity was 62% and specificity was 44%.

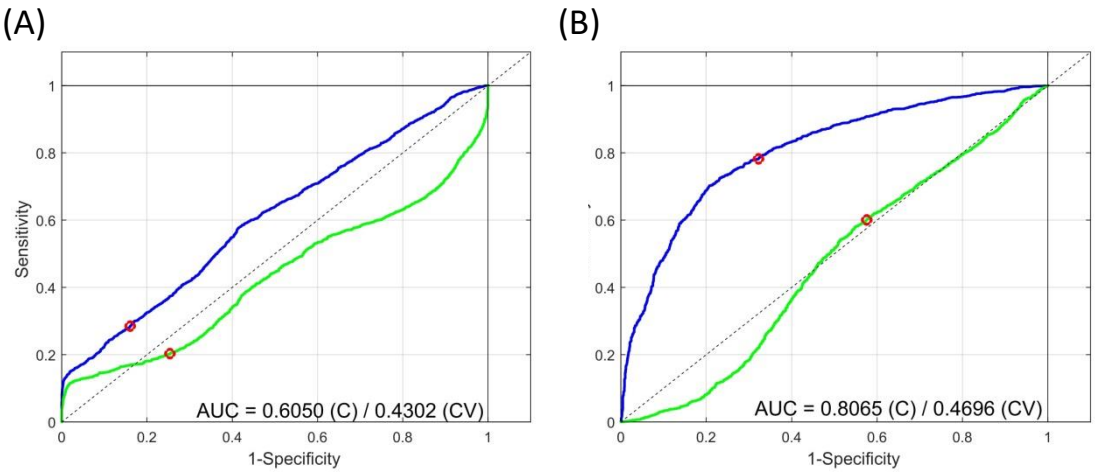

Figure 7.1 ROC curves for (A) Epithelium and (B) Connective tissue of Female vs Male. The blue line is the estimated and the green the cross validated ROC curve. AUC is a measure of the accuracy of the classifier, (C) is the calibrated and (CV) is the crossvalidated AUC.

7.3.2 Smoking

According to smoking status, the patients in table 7-1 were divided into 3 groups; non-smoker, ex-smokers (previous smokers) and smokers.

Table 7-2 Sensitivity and specificity values from PLSDA with LOPOCV for smoking status in epithelium

	Non smoker	Ex-smoker	Smoker
Sensitivity (%)	83	81	52
Specificity (%)	46	38	88

The PLSDA results showed high classification sensitivity for Non-smokers and Ex-smokers but lower specificities. On the other hand, the classification sensitivity was lower for smokers but the specificity was higher (Table 7-2). The ROC curve (Figure 7.2) shows a significant accuracy (AUC=0.76) of the classifier for smokers. To further understand the source of the variance, non-smoker and ex-smokers were combined and the scores of LV-1 and LV-2 were plotted against smokers (Figure 7.3). While there is some overlap, smokers are mainly negative in LV-1 while non-smoker/ex-smokers are mainly positive. According to LV-1, negative bands at 667, 784, 1372, and 1573 cm^{-1} suggest higher nucleic acids in the epithelium of smokers. Non-smoker/ex-smokers had a more prominent amide I band at 1651 cm-1 and protein band at 934 cm^{-1} (Figure 7.4).

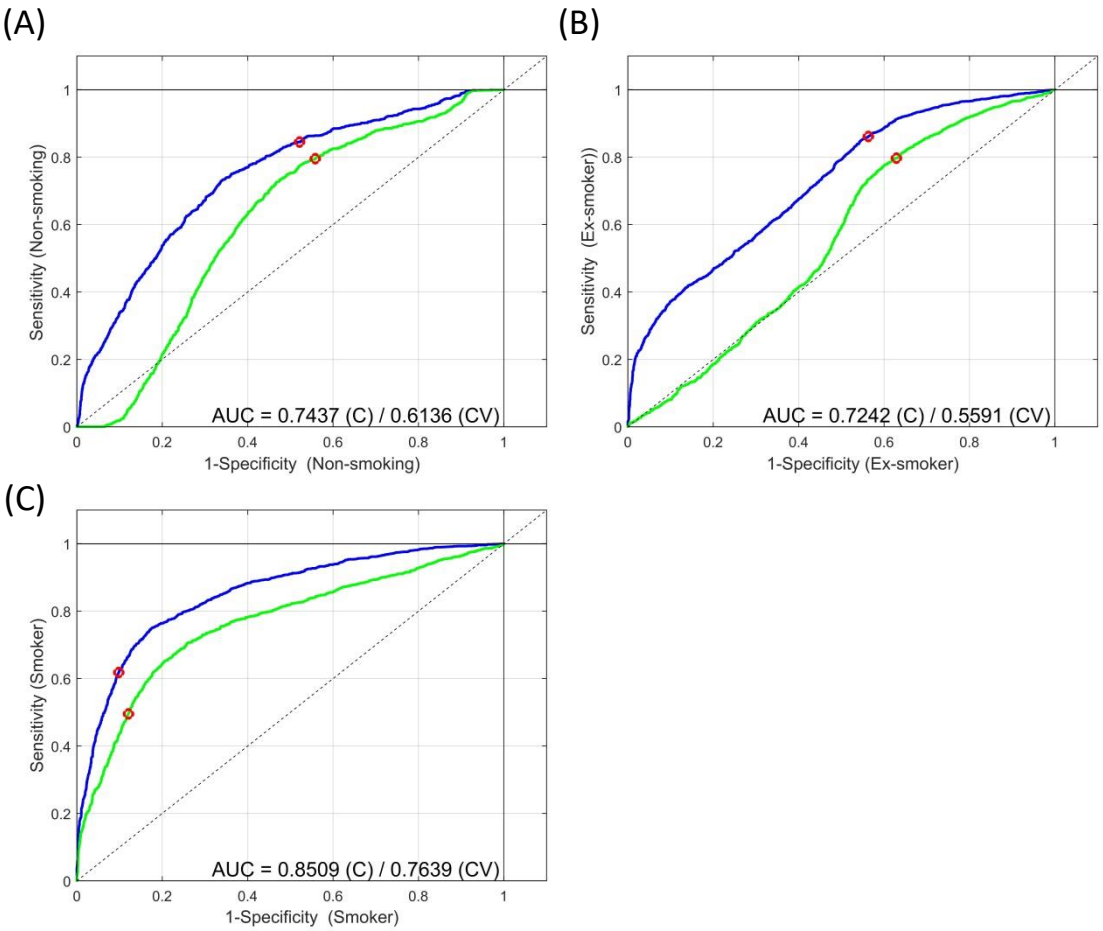

Figure 7.2 ROC curves for (A) Non-smoker (B) Ex-smokers and (C) Smokers epithelium. The blue line is the estimated and the green the cross validated ROC curve. AUC is a measure of the accuracy of the classifier, (C) is the calibrated and (CV) is the crossvalidated AUC.

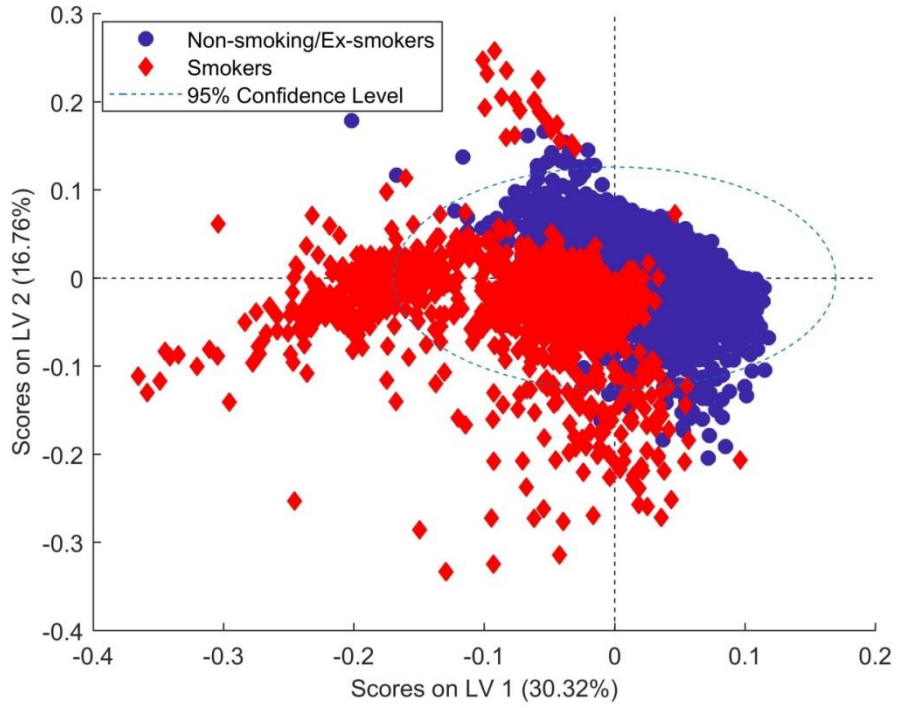

Figure 7.3 Scores of Smokers and Non-smoker/Ex-smokers on the latent variables from the PLSDA model.

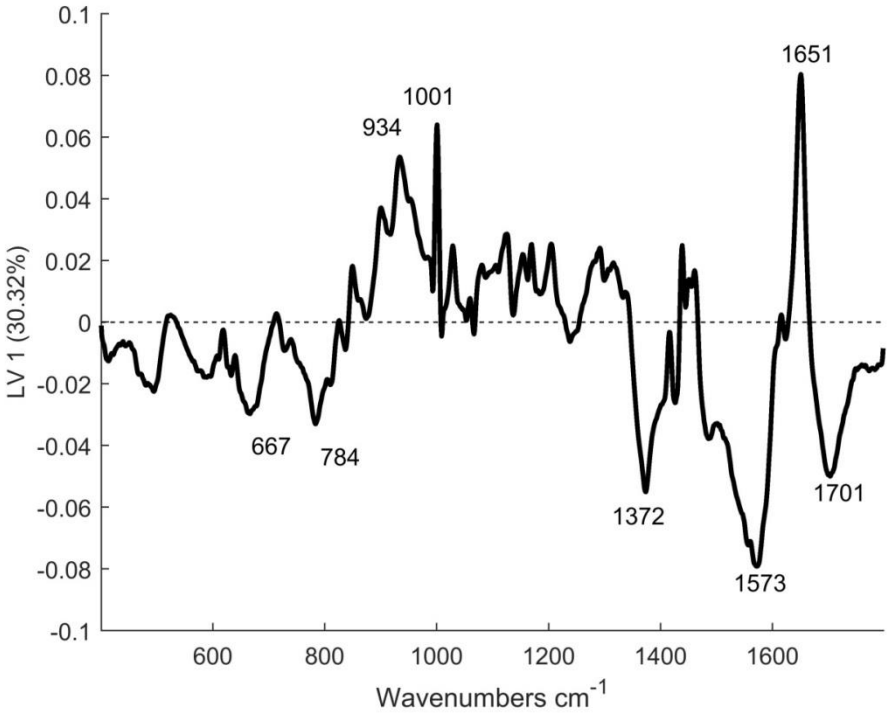

Figure 7.4 Loading of LV-1 from PLSDA of Smokers vs Non-smoker and Ex-smokers in epithelial tissue.

In connective tissue, while there is some degree of classification (

Table 7-3), according to the ROC curves for non-smoker (AUC=0.43) ex-smokers (AUC=0.51) and smokers (AUC=0.64), the accuracy is not significant (Figure 7.2).

Table 7-3 Sensitivity and specificity values from PLSDA with LOPOCV for smoking status in connective tissue

	Non smoker	Ex-smoker	Smoker
Sensitivity (%)	**70**	**39**	**54**
Specificity (%)	**39**	**69**	**71**

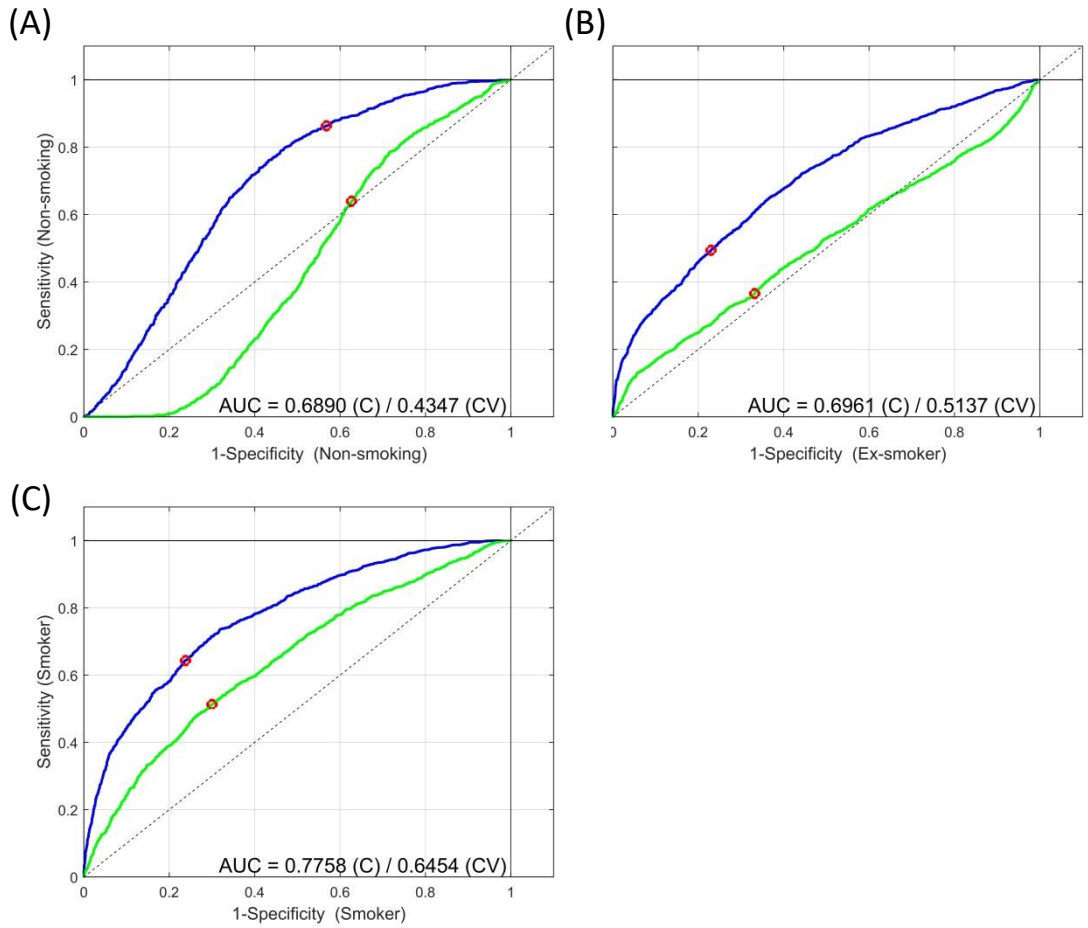

Figure 7.5 ROC curves for connective tissue of (A) Non-smoker (B) Ex-smokers and (C) Smokers. The blue line is the estimated and the green the cross validated ROC curve. AUC is a measure of the accuracy of the classifier, (C) is the calibrated and (CV) is the crossvalidated AUC.

7.3.3 Alcohol

Alcohol consumption in the patient group was varied (Table 7-1). For the sake of simplicity, as the patient numbers were not large, they were divided into 2 main groups; alcohol consuming and non-alcohol consuming. According to this grouping, PLSDA was performed on epithelium (AUC=0.57) and connective tissue (AUC=0.63). No significant discrimination was found in either based on alcohol consumption (Figure 7.6).

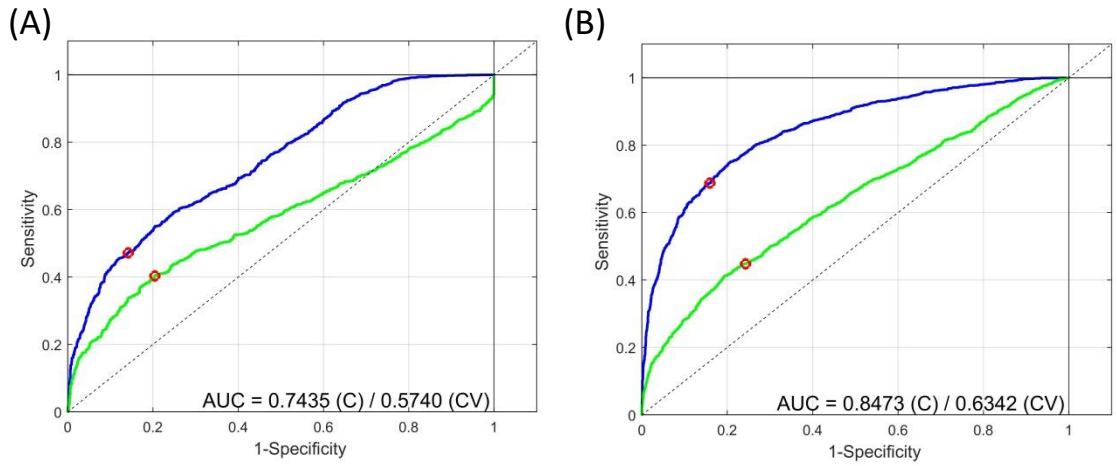

Figure 7.6 ROC curves for (A) Epithelium and (B) Connective tissue of Alcohol consuming vs Non-alcohol consuming. The blue line is the estimated and the green the cross validated ROC curve. AUC is a measure of the accuracy of the classifier, (C) is the calibrated and (CV) is the crossvalidated AUC.

7.3.4 Anatomical Site of lesion

The lesions come from different anatomical sites in the oral cavity, as detailed in Table 7-1. Raman spectra of lesions from the tongue, buccal mucosa, soft palate, hard palate and labial mucosa were assessed using PLSDA with LOPOCV.

Table 7-4 Sensitivity and specificity values from PLSDA with LOPOCV for oral site in epithelium

	Tongue	**Buccal mucosa**	**Soft palate**	**Hard palate**	**Labial mucosa**
Sensitivity (%)	**81**	**50**	**32**	**40**	**72**
Specificity (%)	**31**	**83**	**72**	**41**	**27**

While the sensitivity values for tongue and labial mucosa were high, 81 and 72% respectively, (Table 7-4), the ROC curves (Figure 7.7) were not significant for any of the oral sites (all AUC

values were less than 0.7). Similarly, in connective tissue the hard palate and the labial and buccal mucosa could be classified with a high sensitivity (Table 7-5) but again AUC values were not significant (Figure 7.8). Note that, in Figure 7.7(C) (D) and (E), there is a large difference between the cross validated and estimated ROCs. This is likely due to the small number of patients with lesions in these sites hence when one patients spectra are taken out this is equivalent to a quarter of the dataset of that site which results in an unstable model[6].

Table 7-5 Sensitivity and specificity values from PLSDA with LOPOCV for oral site in connective tissue

	Tongue	**Buccal mucosa**	**Soft palate**	**Hard palate**	**Labial mucosa**
Sensitivity (%)	**47**	**75**	**51**	**83**	**87**
Specificity (%)	**78**	**27**	**25**	**54**	**56**

Grouping according to keratinised (Tongue and hard palate) and non ketatinised (soft palate, buccal and labial mucosa) did not show a good discrimination, sensitivity of 33% and specificity of 88% in epithelium and 35 and 75% sensitivity and specificity in connective tissue respectively.

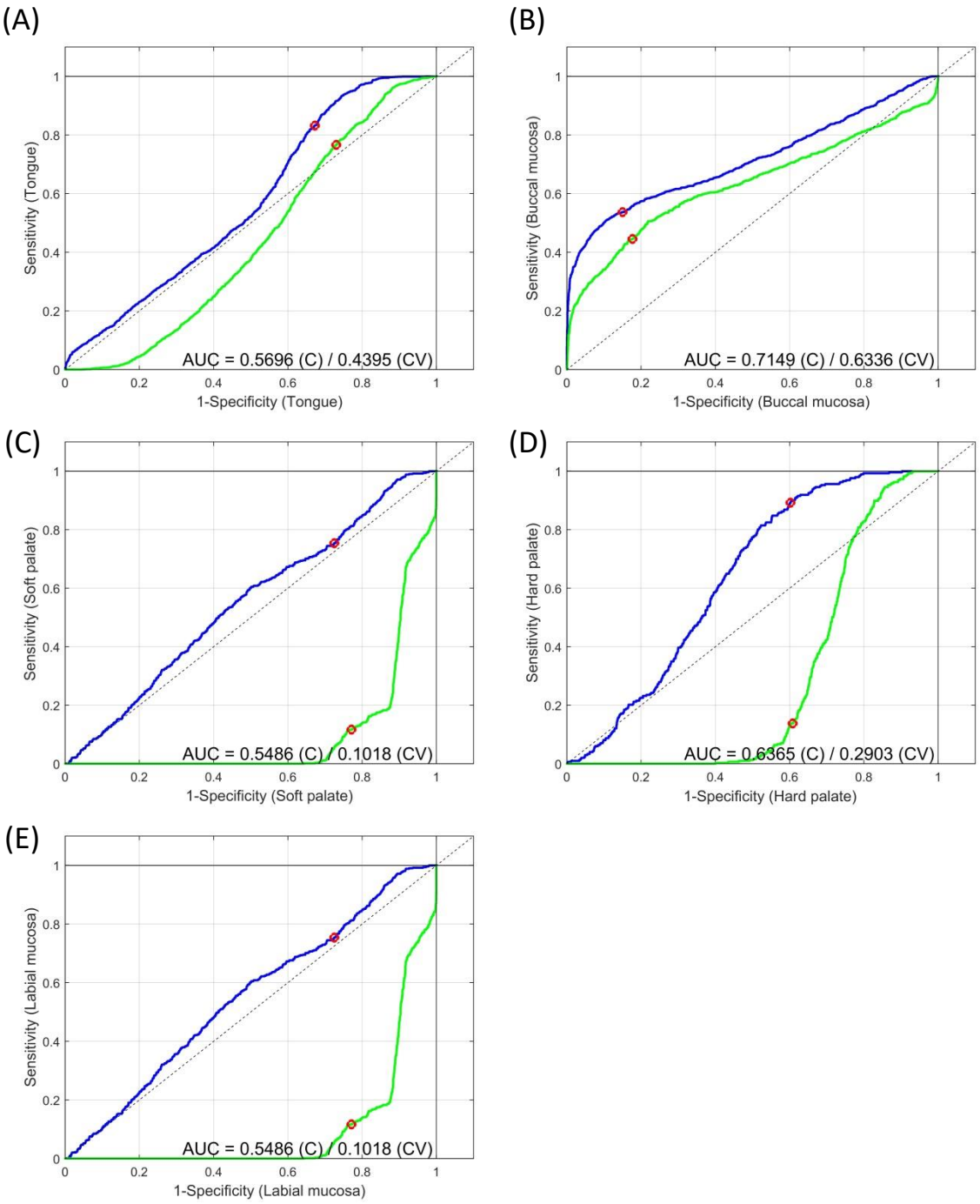

Figure 7.7 ROC curves for (A) Tongue (B) Buccal mucosa (C) Soft palate (D) Hard palate and (E) Labial mucosa of epithelial tissue. The blue line is the estimated and the green is the cross validated ROC curve. AUC is a measure of the accuracy of the classifier, (C) is the calibrated and (CV) is the crossvalidated AUC.

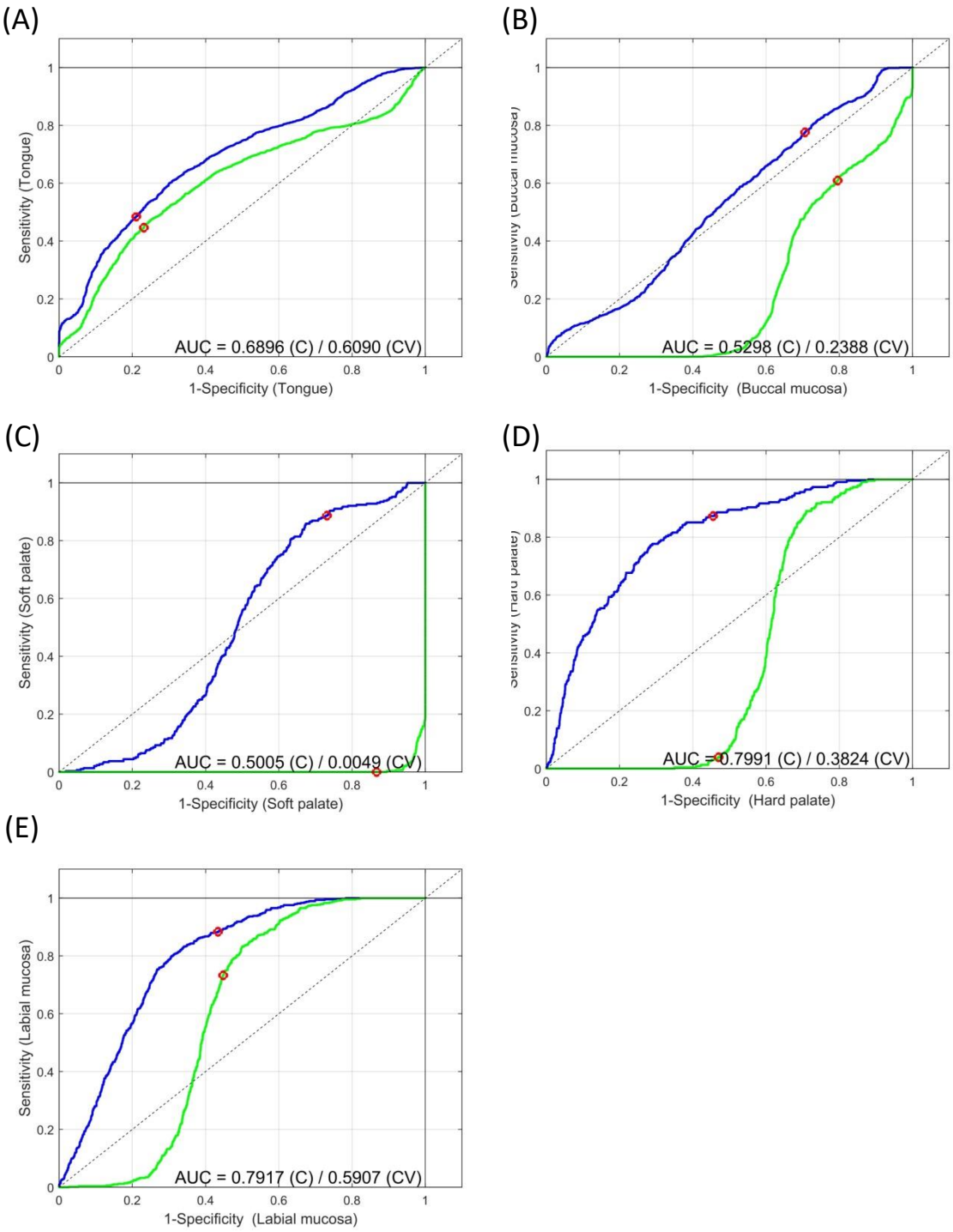

Figure 7.8 ROC curves for (A) Tongue (B) Buccal mucosa (C) Soft palate (D) Hard palate and (E) Labial mucosa of connective tissue. The blue line is the estimated and the green is the cross validated ROC curve. AUC is a measure of the accuracy of the classifier, (C) is the calibrated and (CV) is the crossvalidated AUC.

7.3.5 Presence of inflammation

All the pathologies were evaluated for the presence of inflammation (H&E stained slides were evaluated under a bright-field microscope by the investigator). Table 7-6 shows the number of inflamed samples per class. PLSDA was used to classify inflamed vs non-inflamed for all the pathologies combined. The results show that inflamed tissue can be classified from non-inflamed tissue with sensitivity and specificity values of 68% and 70%, respectively, in epithelium and 77% and 86%, respectively, in connective tissue. The AUCs were significant, at 0.72 for epithelium and 0.84 for connective tissue (Figure 7.9).

Table 7-6 Number of inflamed samples per class

Class	**Benign (n=17)**	**Mild (n=20)**	**Moderate (n=20)**	**Severe (n=10)**	**SCC (n=5)**
Number Inflamed	2	3	9	7	5

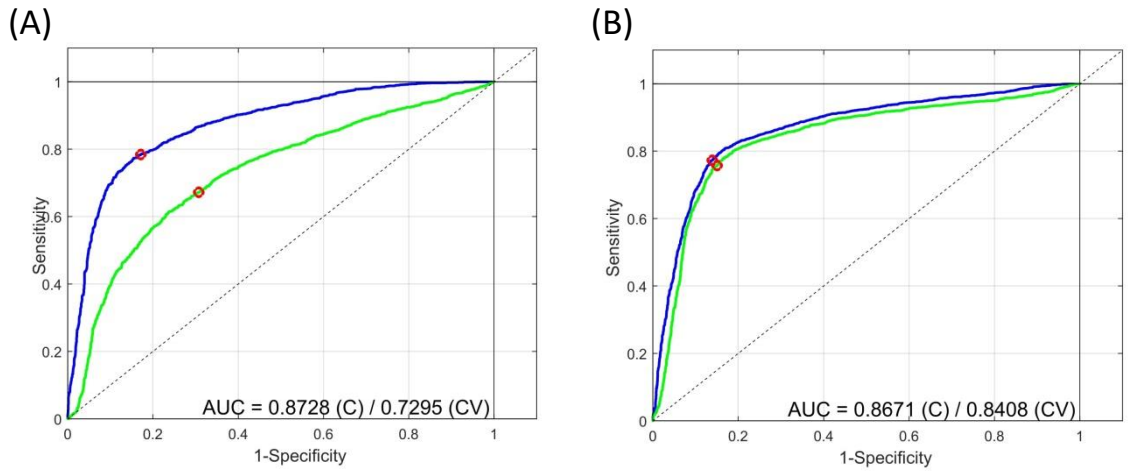

Figure 7.9 ROC curves for (A) Epithelium and (B) Connective tissue of Inflamed vs Non-inflamed in all classes. The blue line is the estimated and the green the cross validated ROC curve. AUC is a measure of the accuracy of the classifier, (C) is the calibrated and (CV) is the crossvalidated AUC.

To ensure that the results obtained are due to the presence of inflammation rather than the pathology (as most of the severe and SCC samples were inflamed which could skew the results), inflamed vs non-inflamed was assessed in the moderate category. The results show a very high accuracy in connective tissue (AUC=0.94) and, to a lesser extent, in epithelium (AUC=0.69) (Figure 7.10). Plotting the scores of the latent variables shows a good separation based on LV-1, the majority of inflamed spectra having negative scores while the majority of non-inflamed spectra have positive scores on LV-1 (Figure 7.11). Note, the group of non-inflamed that are outside the 95% confidence interval are likely from one patient who was misclassified due to increased variability from the rest of the non-inflamed group. The loading of LV-1 (Figure 7.12) shows positive peaks at 813, 855, 939, 1031, and 1245 cm^{-1} which relate to collagen (Table 5-3), while the negative peaks relate to nucleic (1334, 1580 cm^{-1}) and fatty acids (1132, 1438 cm^{-1}).

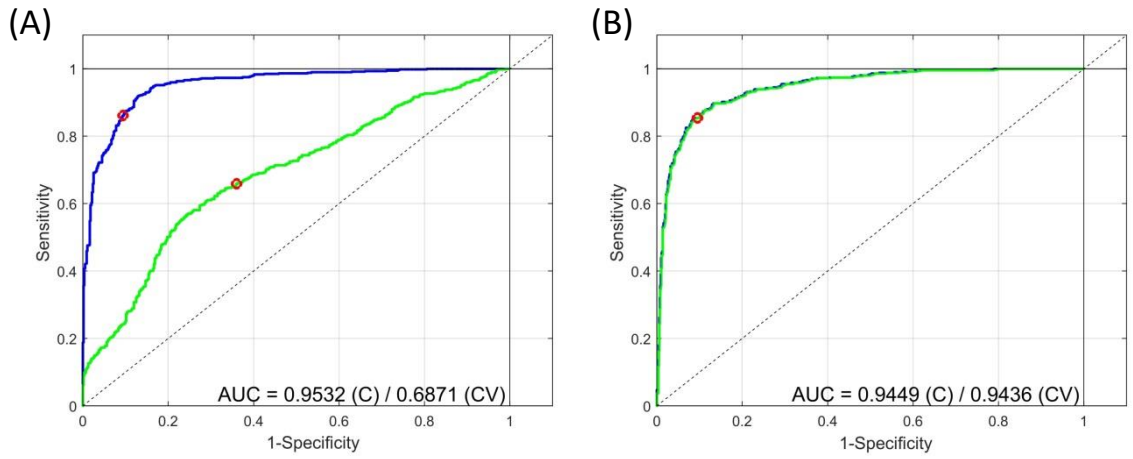

Figure 7.10 ROC curves for (A) epithelium and (B) connective tissue of inflamed vs non-inflamed in the moderately dysplastic lesions. The blue line is the estimated and the green the cross validated ROC curve. AUC is a measure of the accuracy of the classifier, (C) is the calibrated and (CV) is the crossvalidated AUC.

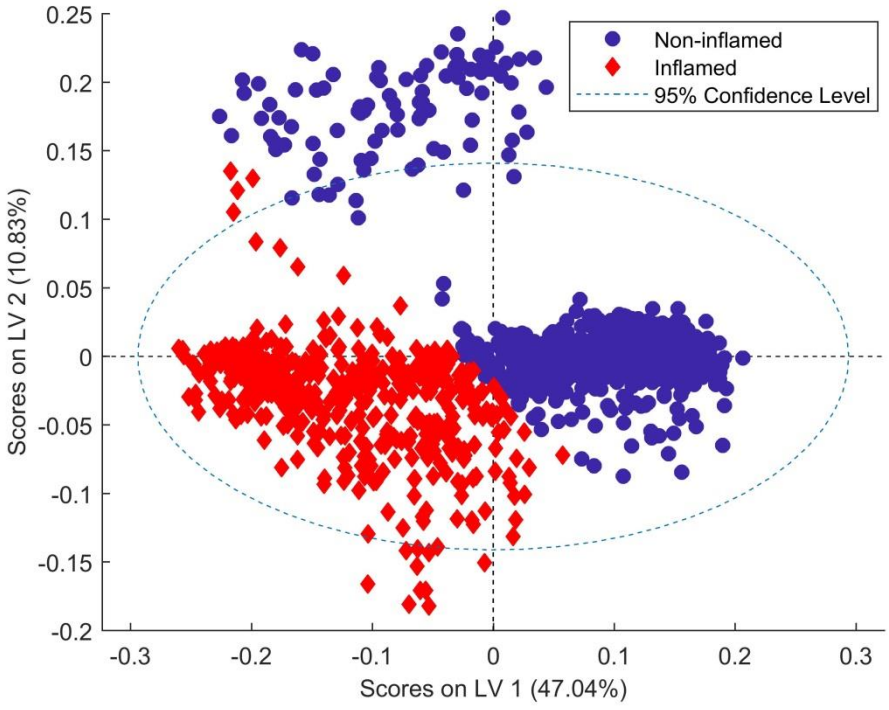

Figure 7.11 Scores obtained from the PLSDA model of inflamed and non-inflamed moderately dysplastic connective tissue on the latent variables.

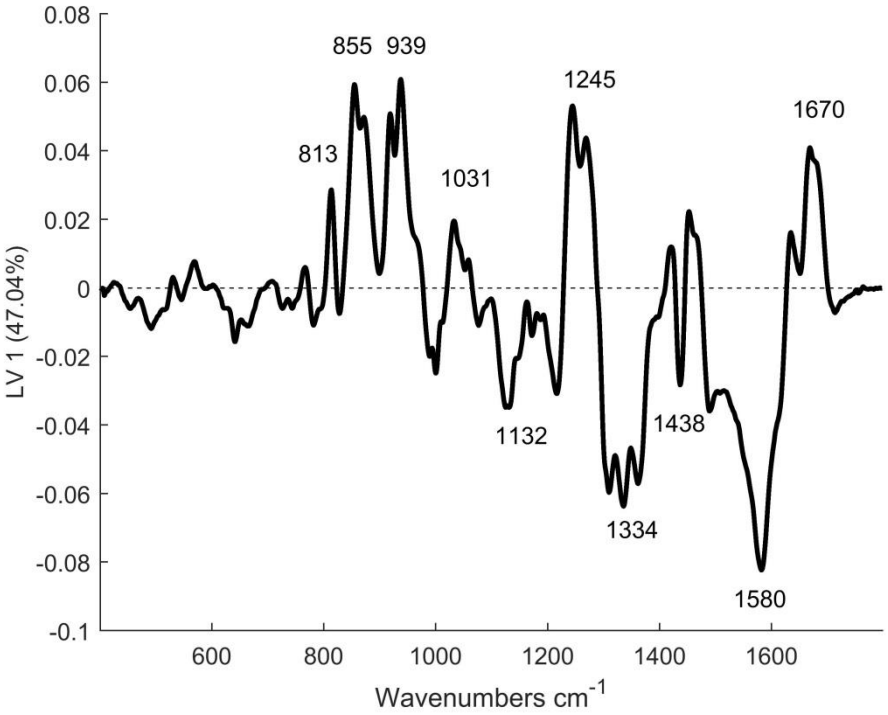

Figure 7.12 Loading of LV-1 from the PLSDA model of inflamed vs non-inflamed connective tissue

7.4 Discussion

The findings of the current study suggest that no clear Raman classification could be made based on gender, alcohol consumption or site of lesion. The link between alcohol consumption and carcinogenesis is not well understood, for, while alcohol can act as a synergistic agent for other carcinogens, its main metabolite, acetaldehyde, is believed to have a role in DNA damage[9]. Previous studies suggest that the risk of developing oral cancer increases with quantity of alcohol intake[10]. Unfortunately this study was limited in that information on alcohol intake quantities was not available for all patients. To date, no studies have looked at the effect of alcohol on the oral mucosa using Raman spectroscopy. Previous studies have investigated Raman classification of oral mucosal sites. Bergholt et al. found that the sites in normal/healthy oral mucosa can be clustered into three groups; (1) buccal, inner lip, and soft palate; (2) dorsal, ventral tongue, and floor; (3) gingiva and hard palate[7]. Sahu et al., studying normal, and

malignant oral mucosa found that while the tongue and buccal mucosa could be classified by Raman spectroscopy in healthy mucosa with some degree of accuracy, classification could not be achieved in malignancy[8].

From the results, it is apparent that some factors other than the degree of dysplasia can influence the Raman classification. Smoking status was seen to impact on the classification of epithelial tissue (AUC=0.76). This is consistent with previous work by Singh et al., who have shown that the oral buccal mucosa of smokers is more likely to misclassify with that of premalignant lesions than that of non-smokers[11,12]. This is likely due to the fact that smoking is an aetiological factor in developing oral dysplasia, and hence biochemical changes occurring in the mucosa of smokers are similar to those occurring in dysplastic lesions.

What was found to have a significant influence on the Raman classification, however, was the presence of inflammation in connective tissue (AUC=0.94). Reduced collagen features and increased nucleic acid features in the Raman spectra of inflamed connective tissue were the main findings. The nucleic acid features may be due to increased cellularity caused by the inflammatory cells infiltrating the tissue. The reduction of collagen features is likely due to the breakdown of collagen by matrix metalloproteinases (especially MMP-8) which are upregulated in inflammation[13]. In this study, most of the severely dysplastic and SCC tissue was found to be inflamed, which is consistent with a previous study that has shown increasing inflammatory cell infiltration with increasing severity of oral dysplasia and SCC[14]. The presence of inflammation in the tumour microenvironment has been well documented[15,16] and is due to multiple factors. The environmental factors that prompt carcinogenesis, such as alcohol and smoking, have been shown to trigger an inflammatory response[17]. Furthermore, the tumour cells release inflammatory mediators which generate an inflammatory microenvironment that promotes cancer growth, invasion and metastasis[18]. A study looking at OSCC surgical margins found that inflamed connective tissue was more likely to misclassify

with SCC than non-inflamed connective tissue[19]. Of note is the fact that the FFPP tissue from chapter 5 (Figure 5.5) also showed inflammation which would explain the similar signature in connective tissue.

While it has been reported that age related physiological changes can be discriminated with Raman spectroscopy[11], most of the patients in this cohort were between 50-60 years, and hence there was not enough variation to study age related factors. Other patient factors and clinical features which have not been considered, due to lack of metadata, can still have an influence on the Raman classification. These include HPV and candida status of the patients, the size of the lesions, and the degree of differentiation in the SCC lesions.

To sum up, these findings suggest that it is important when studying tissue pathologies to consider them in the context of patient factors and clinical features which emphasises the need for large scale studies with more representative patient samples.

References

1. Jaber MA, Porter SR, Gilthorpe MS, Bedi R, Scully C. Risk factors for oral epithelial dysplasia - the role of smoking and alcohol. *Oral Oncology* 1999;35:151-156.

2. Hashibe M, Brennan P, Benhamou S, Castellsague X, Chu C, Paula Curado M, Dal Maso L, Dauct AW, Fabianova E, Wunsch-Filho V, Franceschi S, Hayes RB, Herrero R, Koifman S, La Vecchia C, Lazarus P, Levi F, Mates D, Matos E, Menezes A, Muscat J, Eluf-Neto J, Olshan AF, Rudnai P, Schwartz SM, Smith E, Sturgis EM, Szeszenia-Dabrowska N, Talamini R, Wei Q, Winn DM, Zaridze D, Zatonski W, Zhang Z-F, Berthiller J, Boffetta P. Alcohol drinking in never users of tobacco, cigarette smoking in never drinkers, and the risk of head and neck cancer: Pooled analysis in the international head and neck cancer epidemiology consortium. *Journal of the National Cancer Institute* 2007;99:777-789.

3. Chaturvedi AK, Anderson WF, Lortet-Tieulent J, Curado MP, Ferlay J, Franceschi S, Rosenberg PS, Bray F, Gillison ML. Worldwide Trends in Incidence Rates for Oral Cavity and Oropharyngeal Cancers. *Journal of Clinical Oncology* 2013;31:4550-4559.

4. Torre LA, Bray F, Siegel RL, Ferlay J, Lortet-Tieulent J, Jemal A. Global Cancer Statistics, 2012. *Ca-a Cancer Journal for Clinicians* 2015;65:87-108.

5. Massano J, Regateiro FS, Januario G, Ferreira A. Oral squamous cell carcinoma: Review of prognostic and predictive factors. *Oral Surgery Oral Medicine Oral Pathology Oral Radiology and Endodontics* 2006;102:67-76.

6. Eigenvector. PLS_Toolbox FAQ, 2017:How are the ROC curves calculated for PLSDA?

7. Bergholt MS, Zheng W, Huang ZW. Characterizing variability in in vivo Raman spectroscopic properties of different anatomical sites of normal tissue in the oral cavity. *Journal of Raman Spectroscopy* 2012;43:255-262.

8. Sahu A, Deshmukh A, Hole AR, Chaturvedi P, Krishna CM. In vivo subsite classification and diagnosis of oral cancers using Raman spectroscopy. *Journal of Innovative Optical Health Sciences* 2016;9.

9. Boffetta P, Hashibe M. Alcohol and cancer. *Lancet Oncology* 2006;7:149-156.

10. Bagnardi V, Blangiardo M, La Vecchia C, Corrao G. A meta-analysis of alcohol drinking and cancer risk. *British Journal of Cancer* 2001;85:1700-1705.

11. Sahu A, Deshmukh A, Ghanate AD, Singh SP, Chaturvedi P, Krishna CM. Raman Spectroscopy of Oral Buccal Mucosa: A Study on Age-Related Physiological Changes and Tobacco-Related Pathological Changes. *Technology in Cancer Research & Treatment* 2012;11:529-541.

12. Singh SP, Deshmukh A, Chaturvedi P, Krishna CM. In vivo Raman spectroscopic identification of premalignant lesions in oral buccal mucosa. *Journal of Biomedical Optics* 2012;17.

13. Sorsa T, Tjaderhane L, Salo T. Matrix metalloproteinases (MMPs) in oral diseases. *Oral Diseases* 2004;10:311-318.

14. Mashhadiabbas F, Fayazi-Boroujeni M. Correlation of vascularization and inflammation with severity of oral leukoplakia. *Iranian Journal of Pathology* 2017;12:225-230.

15. Negus RPM, Stamp GWH, Hadley J, Balkwill FR. Quantitative assessment of the leukocyte infiltrate in ovarian cancer and its relationship to the expression of C-C chemokines. *American Journal of Pathology* 1997;150:1723-1734.

16. Talmadge JE. Immune cell infiltration of primary and metastatic lesions: Mechanisms and clinical impact. *Seminars in Cancer Biology* 2011;21:131-138.

17. Takahashi H, Ogata H, Nishigaki R, Broide DH, Karin M. Tobacco Smoke Promotes Lung Tumorigenesis by Triggering IKK beta- and JNK1-Dependent Inflammation. *Cancer Cell* 2010;17:89-97.

18. Feller L, Altini M, Lemmer J. Inflammation in the context of oral cancer. *Oral Oncology* 2013;49:887-892.

19. Cals FLJ, Schut TCB, Hardillo JA, de Jong RJB, Koljenovic S, Puppels GJ. Investigation of the potential of Raman spectroscopy for oral cancer detection in surgical margins. *Laboratory Investigation* 2015;95:1186-1196.

Chapter 8: Conclusions and future work

8.1 Conclusions

8.1.1 Summary of findings

The primary objective of this thesis was to evaluate the potential of Raman spectroscopy in diagnosing premalignant oral lesions. The first two chapters act as an introduction to the thesis, Chapter 1:introducing clinical aspects of OSCC and dysplasia, while Chapter 2: places the emphasis on diagnostic techniques. In Chapter 3: the aim was to establish whether Raman spectroscopy can differentiate the different phases of the cell cycle in an oral squamous cell carcinoma cell line and how that correlates with biomarker expression levels. The findings were that Raman spectroscopy could differentiate the different phases of the cell cycle based on nucleic acid, protein and lipid content. However it was not possible to correlate the expression levels of cyclin D1 and PCNA to the Raman profiles. This may be due to the fact that a Raman profile of a cell carries a great deal of information and, as many molecular processes take place inside the cell, it is difficult to extract information on one particular biomarker. This demonstrates both the strengths and weaknesses of Raman spectroscopy for biological samples as it is sensitive in that it can detect small changes in the cell as it moves through the cell cycle, but because it is a label free technique, distinguishing information on one variable is more difficult. In Chapter 4:the aim was to optimise the FFPP tissue processing for Raman spectroscopy. One of the main difficulties in performing Raman spectroscopy on FFPP tissues is that the paraffin wax, in which the tissues are embedded, has a very intense Raman signal and is hard to remove with the routine chemical dewaxing techniques which change the composition of the tissue. The same is true of glass, which is generally used in histopathology laboratories as a substrate for FFPP tissues .To solve the issues with the glass and wax background; a novel method was developed whereby cell components were used as inputs for NNLS subtraction and glass and wax matrices were digitally subtracted from the

spectra. The use of matrices captures the variability in the wax or substrate spectra which improves the subtraction. In Chapter 5:, the different levels of dysplasia; mild, moderate and severe were assessed in the FFPP tissue sections within the same patients. This was done in order to gain insight into the differences between the different levels of dysplasia without influence from other patient variables. Using PCA-LDA with LOOCV, it was found that Raman spectroscopy could classify the different levels of dysplasia with an accuracy of over 90% in epithelium and over 76% in connective tissue. In Chapter 6: benign, mild, moderate, and severely dysplastic and SCC FFPP tissues were assessed in a cohort of patients using Raman spectroscopy. PLSDA with LOPOCV was used for classification. The results showed that SCC could be classified from the other pathologies with over 70% accuracy in epithelium and connective tissue. However, the accuracy of Raman spectroscopy for differentiating between different levels of dysplasia was lower. In Chapter 7: other variables which could have an influence on classification based on the Raman spectra were assessed. From the results, it was clear that smoking had the greatest influence in epithelium while the presence of inflammation had the greatest influence in connective tissue.

8.1.2 Clinical relevance

Currently, there is a lot of interest in using Raman spectroscopy as a diagnostic aid. However, a number of factors need to be evaluated before it can be translated into clinical use. For ex-vivo studies, using inexpensive substrates is of paramount importance. The novel method developed in Chapter 4: for removing the substrate background has been used for a number of varied studies[1-4]. The method is both reproducible and adaptable, as the pure components can be selected based on the constituents of the cells/tissues/fluid under study. Furthermore, the method of validation of the classifier is very important in determining how well it can classify future (unseen) samples. For the interpatient studies, chapters 6 and 7, it was elected to use LOPOCV as, although it has been shown to give lower accuracies than LOOCV[5], due to the

presence of biochemical differences between patients, it is better at evaluating classifier performance on new samples as it avoids overtraining the model. While this study used *ex-vivo* samples, the results can guide the development of the technique for *in-vivo* use. Having a diagnostic aid such as Raman spectroscopy that can be developed for use chairside, would not only aid in selecting the region to biopsy in large lesions, but can also reduce the number of biopsies needed for monitoring. Important factors to consider in clinical translation include instrument properties. The Raman instrument should be; small, easily transportable, inexpensive, easily aligned and calibrated, and have an optical probe that is sterilisable[6]. The finding that Raman spectroscopy can differentiate between cancer and dysplasia is very important, as the management and prognosis is different for both. Dysplasia is a common finding in tumour borders and regenerative changes which mimic dysplasia can often be found in the margins of resected tumours[7]. The balance between being conservative and maintaining as much of the tissue as possible, which is important both aesthetically and functionally, and removing enough of the tumour to prohibit recurrence is a difficult one in oral cancer surgery. Hence the ability of Raman spectroscopy to discriminate between cancerous and dysplastic and/or healthy tissue can be important in striking that balance[8].

8.2 Future perspectives

A more comprehensive study with a larger sample size[9] which takes into account inherent patient variability in addition to other variables such as age, smoking, alcohol consumption, site of lesion, presence of inflammation etc. may result in a better classifier. The use of a larger sample size would also allow for an independent validation set which can better evaluate the performance of the classifier. The dataset in the current study did not include any dysplastic lesions that had transformed into OSCC. However, a study looking at such lesions and comparing them with dysplastic lesions that did not progress to OSCC in a given time period, for example in a 5 year period, can be more informative, as morphology is not a predictor of

malignant transformation. Hence, a study of transformed lesions could be of more value. As Raman spectroscopy identifies molecular bonds that are common to many different biomolecules as opposed to identifying individual biomolecules, changes with dysplasia/cancer are often subtle and spectrally distributed, requiring full spectral scanning[10]. However, if biomolecules are identified that both have an enhanced Raman signal and vary with increasing dysplasia they can act as label free spectral markers which could make the Raman classification faster and more accurate. Additionally, the Raman spectrum can be open to different interpretations as to the source of the peaks. Although previous studies have explored the biochemistry behind the various peak assignments there is still no accepted standardised database for Raman peak assignments. Finally, it is difficult to compare Raman spectroscopic studies of the oral mucosa as the sample collection, spectral processing and data analysis techniques differ between laboratories, an international standardisation of protocols would go a long way to taking Raman spectroscopy closer to clinical translation.

References

1. Kearney P, Traynor D, Bonnier F, Lyng FM, O'Leary JJ, Martin CM. Raman spectral signatures of cervical exfoliated cells from liquid-based cytology samples. *Journal of Biomedical Optics* 2017;22.

2. Behl I, Calado G, Ibrahim O, Malkin A, Flint S, Byrne HJ, Lyng FM. Development of methodology for Raman microspectroscopic analysis of oral exfoliated cells. *Analytical Methods* 2017;9:937-948.

3. Nawaz H, Rashid N, Saleem M, Hanif MA, Majeed MI, Amin I, Iqbal M, Rahman M, Ibrahim O, Baig SM, Ahmed M, Bonnier F, Byrne HJ. Prediction of viral loads for diagnosis of Hepatitis C infection in human plasma samples using Raman spectroscopy coupled with partial least squares regression analysis. *Journal of Raman Spectroscopy* 2017;48:697-704.

4. Ramos I, Meade AD, Ibrahim O, Byrne H, McMenamin M, McKenna M, Malkin A, Lyng F. FDVIBSPC16: Raman spectroscopy for cytopathology of exfoliated cervical cells. *Faraday Discussions* 2015.

5. Petersen D, Naveed P, Ragheb A, Niedieker D, El-Mashtoly SF, Brechmann T, Kotting C, Schmiegel WH, Freier E, Pox C, Gerwert K. Raman fiber-optical method for colon cancer detection: Cross-validation and outlier identification approach. *Spectrochimica Acta Part a-Molecular and Biomolecular Spectroscopy* 2017;181:270-275.

6. Pence I, Mahadevan-Jansen A. Clinical instrumentation and applications of Raman spectroscopy. *Chemical Society Reviews* 2016;45:1958-1979.

7. Cankovic M, Ilic MP, Vuckovic N, Bokor-Bratic M. The histological characteristics of clinically normal mucosa adjacent to oral cancer. *Journal of Cancer Research and Therapeutics* 2013;9:240-244.

8. Santos IP, Barroso EM, Schut TCB, Caspers PJ, van Lanschot CGF, Choi DH, van der Kamp MF, Smits RWH, van Doorn R, Verdijk RM, Hegt VN, von der Thusen JH, van Deurzen CHM, Koppert LB, van Leenders G, Ewing-Graham PC, van Doorn HC, Dirven CMF, Busstra MB, Hardillo J, Sewnaik A, ten Hove I, Mast H, Monserez DA, Meeuwis C, Nijsten T, Wolvius EB, de Jong RJB, Puppels GJ, Koljenovic S. Raman spectroscopy for cancer detection and cancer surgery guidance: translation to the clinics. *Analyst* 2017;142:3025-3047.

9. Beleites C, Neugebauer U, Bocklitz T, Krafft C, Popp J. Sample size planning for classification models. *Analytica Chimica Acta* 2013;760:25-33.

10. Jermyn M, Desroches J, Aubertin K, St-Arnaud K, Madore WJ, De Montigny E, Guiot MC, Trudel D, Wilson BC, Petrecca K, Leblond F. A review of Raman spectroscopy advances with an emphasis on clinical translation challenges in oncology. *Physics in Medicine and Biology* 2016;61:R370-R400.

Appendices

Appendix 1 Cell protocols

Cell Passaging

Cells were cultured in sterile vented culture flasks of size (25, 75 or 125cm^2) depending on the experiment. For passaging;

1. 3 ml of trypsin/EDTA solution are added to the flask to detach the adherent cells and incubated for 3-5 minutes.
2. Once the cells have detached 7 ml of media are added to stop the trypsin and the cell suspension is then transferred onto a sterile universal tube and centrifuged for 5 minutes at 1200 rpm.
3. After centrifugation the supernatant is discarded carefully without disturbing the cell pellet.
4. For a 1:10 split 10 ml of media is added to the cells which are then carefully resuspended in the media.
5. In a new sterile cell culture flask 20 ml of media is added together with 1 ml of the cell suspension from step 4.

Cell Counting

A Z series Coulter counter (Beckman Coulter Life Sciences) was used for cell counting. To count the cells;

1. Cells are trypsinised and media added as in steps 1-2 of passaging.
2. 1 ml of the cell suspension is added to 20 ml of Isoton electrolyte solution in a vial

3. Following set-up the vial is placed on the stage of the coulter counter and the stage is moved up to the probe
4. To do the cell count press set up then start
5. A reading is displayed showing the number of cells/ml

Appendix 2

Dewaxing protocol

1. Place slides in 1st xylene for 5 minutes
2. Transfer slides to 2nd xylene and leave for 4 minutes
3. Transfer slides to 1st ethanol and leave for 3 minutes
4. Transfer slides to 2nd ethanol and leave for 2 minutes
5. Transfer slides to IMS and leave for 1 minute
6. Transfer to water for 1 minute

H&E protocol

After step 6 of dewaxing;

1. Add a few drops of haematoxilyn to the tissue section (enough to cover the tissue) and leave for 3 minutes
2. Rinse in running tap water for 5 minutes
3. Add a few drops of eosin and leave for 3 minutes
4. Rinse in tap running tap water for 2 minutes

   Rehydrate and clear by passing through;
5. IMS for 3 minutes
6. Transfer to 1st ethanol for 3 minutes
7. Transfer to 2nd ethanol for 3 minutes
8. Transfer to 1st xylene for 3 minutes
9. Transfer to 2nd xylene for 3 minutes
10. Add a few drops of dpx mountant to the cover slip
11. Carefully place the slide over the cover slip

List of Publications

Ibrahim O, Maguire A, Meade AD, Flint S, Toner M, Byrne HJ, Lyng FM. Improved protocols for pre-processing Raman spectra of formalin fixed paraffin preserved tissue sections. *Analytical Methods* 2017;9:4709-4717.

Nawaz H, Rashid N, Saleem M, Hanif MA, Majeed MI, Amin I, Iqbal M, Rahman M, **Ibrahim O**, Baig SM, Ahmed M, Bonnier F, Byrne HJ. Prediction of viral loads for diagnosis of Hepatitis C infection in human plasma samples using Raman spectroscopy coupled with partial least squares regression analysis. *Journal of Raman Spectroscopy* 2017;48:697-704.

Behl I, Calado G, **Ibrahim O**, Malkin A, Flint S, Byrne HJ, Lyng FM. Development of methodology for Raman microspectroscopic analysis of oral exfoliated cells. *Analytical Methods* 2017;9:937-948.

Singh SP, **Ibrahim O**, Byrne HJ, Mikkonen JW, Koistinen AP, Kullaa AM, Lyng FM. Recent advances in optical diagnosis of oral cancers: Review and future perspectives. *Head and Neck-Journal for the Sciences and Specialties of the Head and Neck* 2016;38:E2403-E2411.

Ramos I, Meade AD, **Ibrahim O**, Byrne H, McMenamin M, McKenna M, Malkin A, Lyng F. FDVIBSPC16: Raman spectroscopy for cytopathology of exfoliated cervical cells. *Faraday Discussions* 2015.

Lyng FM, Ramos IRM, **Ibrahim O**, Byrne HJ. Vibrational Microspectroscopy for Cancer Screening. *Applied Sciences-Basel* 2015;5:23-35.

List of Conferences

- British Society of Oral Medicine (BSOM) -Dublin, April 2017- Oral presentation (Prize for best oral presentation)
- European Association of Oral Medicine (EAOM) -Turin, September 2016 -Oral presentation
- Microscopy Society of Ireland symposium (MSI) -Dublin, June 2016 -Oral presentation (Prize for best student oral presentation in life sciences)
- Raman 4 Clinics -Dublin, March 2016 -Oral presentation
- Advanced Vibrational Spectroscopy for Biomedical Applications: Faraday Discussion -Cambridge, March 2016 -Poster presentation
- The International Society for Clinical Spectroscopy (CLIRSPEC) -Exeter, April 2015 -Poster presentation
- PITTCON -New Orleans, March 2015 -Poster presentation
- Microscopy Society of Ireland and Scottish Microscopy Group symposium MSI_SMG -Glasgow, November 2014 -Poster presentation
- SPEC Shedding new light on disease -Krakow, August 2014 -Poster presentation